# Trace Element Variability in Clay Sediments as a Function of Environmental Conditions within the Fluvial to Marine Water Transition Zone

by

Calla Jeannette Helen Knudson

A thesis submitted in partial fulfillment of the requirements for the degree of

Master of Science

Department of Earth and Atmospheric Sciences
University of Alberta

# ABSTRACT

Estuaries are marginal marine environments of considerable complexity, due to their spatial and temporal variations in hydrodynamic energy, water chemistry, and sediment source and composition. This complexity hinders geologists' ability to accurately reconstruct paleoenvironments and geological histories from the rock record. In particular, the geochemical evolution of sediments in the transition from freshwater to marine environments remains poorly understood. Determining the location of the freshwater to brackish-water transition zone in sedimentary rock successions is essential to accurate paleoenvironmental reconstructions and detailed facies models. The interpretation of estuarine depositional environments is currently predicated on ichnological and micropaleontological analyses. However, the utility of these methods is limited by the preservation potential and subjectivity of trace fossil and microfossil assemblages. Geochemical techniques have the potential to enhance and refine these interpretations in intervals where ichnological and micropaleontological datasets are inconclusive. Other researchers have made attempts to correlate specific trace element abundances and ratios in mudstones to paleosalinity conditions. However, these studies do not provide sufficient direct evidence for the relationship between these specific geochemical signatures and their inferred environmental salinity conditions. In an effort to refine the relationship between environmental salinity and trace element signatures in mudstones, I use quantitative geochemical methods to make observations of trace element enrichment in clay minerals under controlled conditions. Laboratory experiments

were conducted with three common clay minerals that contribute to mudstones: illite, kaolinite, and montmorillonite. The adsorption of caesium cations to each clay at a range of ionic strength conditions was measured to evaluate the efficacy of caesium as a potential proxy for paleosalinity in mud deposits. Each clay sample was also equilibrated with North Saskatchewan River water and English Bay sea water samples to make empirical observations of element partitioning between aqueous and particulate clay phases under fluvial and marine conditions. The results of the ionic strength-dependent adsorption experiments suggest that there is an inverse proportional relationship between solution ionic strength and the proportion of caesium that is sorbed to clay. Caesium shows promise as a salinity indicator and further work on this element in that context is recommended. The partitioning of elements between the aqueous and particulate clay phases differed significantly between the fluvial and marine systems, as well as between discrete suspended sediment load conditions. This discrepancy suggests that it may be feasible to determine whether fine-grained sediments were deposited in fluvial or marine settings based upon their geochemical signatures, although the effects of climate, suspended sediment load, mineralogy, and organic matter should be considered. Sediment and surface water samples were collected from the wave-dominated Arcachon Bay and the tidal-fluvial Gironde Estuary, southwestern France. The geochemical signatures of these two modern, marginal marine environments are defined and compared in an effort to develop an analogue for controls on geochemical signatures in the rock record. I determined the chemical indices of alteration, distribution coefficients of trace elements

between the surface waters and sediments, sum totals of rare earth element (REE) abundances, and various critical element ratios (Eu/Eu*, Th/Co, La/Sc, $La_N/Yb_N$, Th/Sc, Zr/Sc). These parameters were compared at various locations to infer relationships between sediment geochemistry and locations within each modern coastal environment. The sediments of Arcachon Bay and the Gironde Estuary are interpreted as the early to intermediate weathering products of a source rock with mixed felsic and mafic composition derived from an active continental margin. The results of this study further indicate that the composition of the sediment source rock is the primary control on the availability of REEs and trace elements in sediment deposits. However, the spatial variation and preservation of REEs and trace elements in sediments are dictated by organic matter distributions. These observations suggest that the use of trace elements to infer the syn-depositional conditions of sedimentary rocks is problematic, and that other parameters such as sediment source compositions, sedimentary processes, and organic matter content need to be incorporated into these models.

# PREFACE

This thesis is an original work by Calla Knudson. No part of this thesis has been previously published.

# ACKNOWLEDGMENTS

This project was made possible through the generous financial support of BP Canada, Cenovus Energy, Husky Energy, Nexen-CNOOC, Woodside Energy, the Alberta Graduate Student Scholarship (2018), the Canadian Association of Petroleum Producers Graduate Scholarship in Geology (2017), the Queen Elizabeth II Scholarship (2016), and the Department of Earth and Atmospheric Sciences at the University of Alberta.

I am incredibly grateful to all of the people who have contributed to this thesis and enriched my graduate school experience over the last three years.

Firstly, I must thank my supervisor Dr. Murray Gingras, who sparked my interest in research by supervising my undergraduate thesis project, encouraged me to pursue graduate studies, and entrusted me with an interesting and challenging project. Thank you, Murray, for providing so much valuable mentorship, guidance, and advice along the way. Thanks as well to my supervisory committee, Dr. Daniel Alessi and Dr. Kurt Konhauser, for many valuable discussions about geochemistry. I learned so much from both of their classes and have gained a new perspective on geology as a result. Their knowledge and insight has contributed to making this thesis project what it is, and for that I am grateful. I would also like to thank Dr. Bruce Sutherland and Dr. John-Paul Zonneveld for their many words of encouragement, which have helped more than they know.

Members of the Environmental Geochemistry Research Group (Dr. Shannon Flynn, Dr. Salman Safarimohsenabad, Katherine Snihur, and Konstantin Von Gunten), the Geomicrobiology Research Group (Weiduo Hao, Tiffany Playter, and Dr. Jamie Robbins), and the Quaternary Geoscience Research Group (Sasiri Bandara), were very helpful with instrumentation and analyses. I truly appreciate all of their generosity and time. Thank you to the very talented staff at the University of Alberta: Diane Caird, for X-ray diffraction analyses, Guangcheng Chen, for ICP-MS analyses, Nathan Gerein, for scanning electron microscope imaging, and Mark Labbe, for sample processing.

Undoubtedly, one of the highlights of my graduate studies was my field work in France; I had the opportunity to meet many talented scientists whose enthusiasm for research was incredibly inspiring. Thank you to Dr. Rafaël Bourillot for your interest in my project and several interesting discussions, Dr. Hugues Féniès, for your hospitality, Dr. Stefan Lalonde for your ideas and input in the development of the project, and Marie Thoby, for all of your assistance with the laboratory analyses of my samples.

Thank you to my fellow McMurray Consortium members, especially Chloe Chateau, Qi Chen, Dr. Shahin Dashtgard, Derek Hayes, and Lucian Rinke-

Hardekopf, for many enjoyable discussions during field trips, Consortium meetings, and conferences. Thank you as well to everyone in the Ichnology Research Group, past and present, for all of their helpful advice, camaraderie, and for organizing some truly memorable field trips to Willapa Bay and Normandy.

I feel privileged to have participated in the 2017 U of A Imperial Barrel Award Team alongside the best team mates that one could ask for. Sean Bettac , Jared Kugler, Matthew Sommers, and Kim Wagner, thank you for your brilliance, hard work, enthusiasm, and, of course, the old fashioneds.

I was very fortunate in having Benjamin Neil, Sophie Norris, and Joseph Young to share an exceptionally small office space with. Thank you for all of the distractions, laughs, and coffee. I would also like to thank my wonderful friends Maggie Jensen and Emily Wadge, for always being there for me.

The last people that I have to acknowledge are those to whom I owe the most. My family cannot be thanked enough for all of the love, support and encouragement they have given me over the years. I would especially like to thank my mother, Deanna Dixon, for everything. She has always inspired me to work hard and pursue my passions, and I couldn't have done this without her. My stepfather, Terence Owens, and my sister, Jasia Knudson, have been incredibly encouraging; I feel very lucky to have them in my life, and appreciate all of the times that they patiently listened to my ramblings on all things clay- and trace element-related. I would also like to thank my father, Allan Knudson, for giving me a sense of urgency and asking what the practical applications of my research were. And of course, thank you to Dr. Eric Timmer, who believed in me when I couldn't believe in myself and who was willing to trudge through mud flats with me in the pouring rain. Thank you for your boundless optimism, sense of adventure, and for always being able to make me smile.

# Table of Contents

# List of Figures

# List of Tables

# CHAPTER I

# INTRODUCTION

## 1.0 SIGNIFICANCE AND RATIONALE

In clastic sedimentary systems, the transition zone between continental and marine environments is notoriously complex. Marginal marine environments are shaped by myriad sediment sources, hydrological regimes, ecological communities, and geochemical conditions, all of which vary both spatially and temporally. The variegated nature of these depositional settings impedes efforts to precisely identify the freshwater to brackish-water transition zone, which is essential for accurate paleoenvironmental reconstructions. These interpretations enable the development of detailed facies models and realistic subsurface maps, both of which are highly relevant to both Earth history research and resource management and development. High-resolution sedimentological and stratigraphic analyses of this nature can be applied to the identification of targets for hydrocarbon exploration, as well as to the documentation of changes in sea level and river flux throughout geological time for integration in paleoclimate models.

Defining the freshwater to brackish-water transition zone in sedimentary successions hinges upon interpretations of paleosalinity. The current techniques available for estimating paleosalinity are largely based on biological evidence, which can sometimes yield uncertain results. Palynological datasets are problematic due to the difficulty to distinguish between brackish and freshwater pollen assemblages. It is also nearly impossible to guarantee that the microfossils

are in situ rather than transported from distal regions that may have very different environmental conditions (e.g. Matthiessen, 1995). Furthermore, analytical methods in palynology tend to be expensive and highly labour-intensive, and it is not uncommon for errors to be introduced by over- or under-processing samples. Interpretation of ichnofossil assemblages can provide qualitative information on paleosalinity, but this method is only applicable to intervals in which traces are preserved, and can be inconclusive in cases in which the trace fossil assemblages are non-diagnostic of a particular environment, such as *Planolites*. The development of a new method to estimate paleosalinity is invaluable for the characterization of intervals where reliable, diagnostic trace fossil or palynological assemblages and sedimentary structures are lacking or of uncertain quality.

The Cretaceous McMurray Formation in northeastern Alberta, Canada is a classic example of an interval with a highly contentious debate surrounding its depositional environment. The McMurray Formation comprises interbedded sand and mud deposited during the Lower Cretaceous in the Western Canada Sedimentary Basin. This formation is the primary host of the Athabasca Oil Sands, one of the world's largest deposits of bitumen, and as such is of considerable economic and research interest (Hubbard *et al.*, 2011). Bitumen distribution in the McMurray Formation is controlled by the sedimentary facies, and the stratigraphic complexity of the McMurray Formation makes the location and extent of good reservoir units difficult to predict (Ranger & Pemberton, 1997). Therefore, the paleogeographic reconstructions and facies models available

for the McMurray Formation have significant economic implications. Many researchers interpret the McMurray Formation as an estuary with a salinity gradient that can be estimated using trace fossils (e.g. Gingras *et al.*, 2016; Pemberton *et al.*, 1982). Researchers have interpreted this ichnological dataset to reflect an increasing marine influence over time, progressing from fluvial to estuarine settings (Musial *et al.*, 2012; Crerar & Arnott, 2007; Ranger & Pemberton, 1988). An alternate model for the depositional environment of this sedimentary succession has been proposed. Trends in the lithology, physical sedimentary structures, stratigraphy, and bed thicknesses of the McMurray Formation have been attributed to deposition in a fluvial system with intermittent periods of tidal influence (e.g. Jablonski & Dalrymple, 2016; Hubbard *et al.*, 2011). The integration of an independent dataset into existing and future McMurray research has the potential to resolve the debate surrounding the depositional setting of the McMurray formation, thereby increasing predictability of facies distributions and adding economic efficiency to the development of this petroleum resource.

In marginal marine settings, where freshwater rivers laden with dispersed clay particles debouche into saline oceans, the process of clay flocculation is an important mechanism for mud sedimentation. A prominent feature of the freshwater to brackish-water transition zone is the turbidity maximum zone (TMZ), where the flocculation and resuspension of suspended sediment particles in the water column create the highest turbidity level in the depositional system. The TMZ is associated with the thickest and most extensive mud deposits in an

estuarine system (La Croix & Dashtgard, 2014). The increased salinity of the ambient waters in the freshwater to brackish-water transition zone promotes clay particles to flocculate and settle out of the water column. Differential flocculation tendencies between clay minerals have been quantified experimentally. For example, illite and kaolinite, both of which are non-swelling clays, begin to flocculate at salinities of 2 psu (Whitehouse *et al.*, 1960). In contrast, montmorillonite is a swelling clay and flocculates across an approximate salinity range of 3 psu to over 18 psu (Whitehouse *et al.*, 1960).

Fine-grained sediments, and clay minerals in particular, are volumetrically important sinks for trace elements (Taylor & McLennan, 1985). Trace elements can accumulate in multiple different phases of the sediments with which they are associated: pore water (e.g. Boulegue *et al.*, 1982), carbonate minerals (e.g. Allen *et al.*, 2016), clay minerals (e.g. Sposito *et al*., 1999), organics (e.g. Algeo & Lyons, 2006), hydrous Fe/Mn oxide minerals (e.g. Jenne, 1968), sulphide minerals (e.g. Large *et al.*, 2014), and silicate minerals (Jones & Bowser, 1978). Trace elements most frequently become associated with clay minerals via adsorption, in which dissolved chemical species are removed from solution and held on the exterior of the clay particles by surface complexation sites (Smith, 1999; Horowitz, 1985). The identity and relative proportions of the dissolved chemical species available for sorption vary along the spectrum of fluvial-tidal influences, and thus the trace elements that are adsorbed by clay minerals and transferred to the rock record are dependent on location within a depositional system. Consequently, the trace element assemblages in fine-grained sediment

deposits can be used to infer the syn-depositional geochemical conditions of their environments.

## 2.0 PREVIOUS WORK

There is a strong linear relationship between the concentrations of many trace elements, including Cr, Mo, U, and V, in seawater and in shale successions. This relationship indicates that shale intervals source these elements from the ambient seawater (Brumsack & Gieskes, 1983). Several researchers have already used the relative enrichment and depletion of various trace elements in pelagic sediments to determine the oxidation states of ancient oceans and thus constrain the timing of the Great Oxidation Event (Kendall *et al.*, 2010; Kump, 2008; Scott *et al.*, 2008; Slack *et al.*, 2007; Tribovillard *et al.*, 2006; Canfield *et al.*, 1998). Enrichment of both Mo and Re in pelagic sediments is indicative of syn-depositional euxinia, while enrichment of Re and depletion of Mo correlates to syn-depositional anoxic or oxic conditions (Kendall *et al.*, 2010; Scott *et al.*, 2008).

Several researchers have successfully correlated measured concentrations of B (e.g. Stewart & Parker, 1979; Couch, 1971; Bohor & Gluskoter, 1967; Goldschmidt *et al.*, 1932), as well as Ga and Rb (e.g. Landergren & Joensuu, 1963; Degens *et al.*, 1958, 1957) in clay minerals to the paleosalinity of their depositional environment. Adams *et al.* (1965) demonstrated a quantitative relationship between boron concentration and salinity in the Dovey Estuary by means of a linear regression equation. In a study on modern sediments and waters

from multiple localities, Landergren & Carvajal (1969) used a Freundlich adsorption isotherm to correlate the concentration of boron in clay sediments with the salinity of the depositional waters, suggesting that adsorption is the mechanism by which boron becomes associated with clay, illite in particular. Empirical adsorption models such as these have been widely used to characterize trace element sorption to clay minerals. However, these models are generally simplistic, heavily rely on fitting parameters, and are often not predictive.

Degens *et al.* (1957) investigated the trace element content and proportions of clay minerals in shales of Pennsylvanian age from the Allegheny series of the Eastern bituminous coal basin and found that these attributes were somewhat diagnostic of the depositional environment of the shales: marine or non-marine. Findings from this study indicate that marine shales are characterized by trace element assemblages that are enriched in B, Ni, and Rb. By contrast, non-marine shales are characterized by trace element assemblages that are enriched in Cr and Ga. In addition, the authors constructed ternary diagrams on which marine and non-marine shales were plotted according to their composition with respect to B, Ga, Rb, and their illite:kaolinite ratio. Degens *et al.* (1958) expanded upon this work by adding Pennsylvanian-age sandstones, "underclays", and limestones to their sample database and plotting them on ternary diagrams as in the previous study. The classification of these rocks as freshwater or marine based upon their composition with respect to B, Ga, Rb, and their illite:kaolinite ratio was in good agreement with that derived from fossil data.

Recent studies (e.g. Fu *et al.*, 2016) have made use of B/Ga and Th/U ratios in Jurassic-age black shales to determine the paleosalinity of their respective depositional environments. Marine waters contain relatively high concentrations of Bo, which then becomes adsorbed by coastal and pelagic illite deposits (Couch, 1971). In the continental realm, the weathering of soils and paleosols mobilizes Ga, which is then absorbed by terrestrial smectite deposits (Fu *et al.*, 2016). As such, B/Ga ratios could be paleosalinity proxies, based on the premise that the B/Ga ratio increases in proportion with salinity: less than 3.0 in freshwater deposits, between 3.0 and 5.0 in brackish water deposits, and greater than 5.0 in marine deposits (Zhang *et al.*, 2013; Hu *et al.*, 2012).

These studies utilize trace element abundances and ratios in mudstones to interpret syn-depositional salinity conditions. However, the proposed mechanisms from which these geochemical signatures arise have not been reproduced and observed. In addition, these methods are not sufficiently specific for precise orientation of facies within the transition zone between continental and marine environments. Furthermore, Earth surface-level geochemical conditions and processes at the time of deposition are not the only influences on the trace element assemblages and trace element variability in fine-grained sedimentary rocks. Biological activity, sediment source composition, tectonic setting, depositional age, climate, sediment mineralogy, diagenesis, and weathering may all significantly redistribute trace elements throughout sedimentary systems. These additional factors are often not considered when making interpretations of relative marine and fluvial influence on a sedimentary deposit. Therefore, whether these

geochemical techniques for estimating depositional sub-environments are truly "universally" applicable to a variety of sedimentary successions is uncertain. Researchers need to be able to make direct observations of the interactions between the sedimentary and aqueous phases of systems in order to infer geochemical cause and effect relationships to constrain the effect of different environmental conditions on trace element signatures in mudstones. In this way, we will be able to ascertain whether it is reasonable to correlate trace element geochemistry of sedimentary rocks to depositional environmental conditions, and locations within a depositional system.

## 3.0 THESIS OBJECTIVES AND ORGANIZATION

In this thesis, I investigated the geochemical characteristics of fine-grained sediments and surface waters from a sedimentological perspective The large-scale objective is to examine the relationships between water chemistry, sediment composition, and partitioning of trace metals. These primary observations are used to evaluate the feasibility of using trace element geochemistry of fine-grained sediment deposits to interpret paleosalinity, as well as to characterize the interactions of trace elements and fine sediments under different environmental conditions and to predict whether evidence of these reactions is preserved in the rock record. These research questions are approached through controlled laboratory experiments and a field study of modern depositional settings. This thesis is comprised of two main chapters and three appendices.

Chapter II of this thesis describes the methodology, results, and interpretations of two main phases of controlled laboratory experiments involving standard clay mineral samples. In this chapter, a new geochemical proxy for salinity is proposed and assessed by measuring the sorption of caesium to different clay minerals under a spectrum of ionic strength conditions. In addition, the partitioning of various elements between different clay minerals and either river water or sea water is measured experimentally to characterize riverine and marine environments.

Chapter III of this thesis presents the methodology, results, and interpretations of geochemical analyses for two modern sedimentary depositional systems encompassing the fluvial to marine transition: Arcachon Bay and the Gironde Estuary, in southwestern France. The major and trace elements in sediment and surface water samples from these two systems are analyzed and used to calculate chemical differentiation indices, chemical indices of alteration, element distribution coefficients, sums of rare earth elements (REEs), and element abundances relative to reference standards. These parameters are used to characterize the areas of interest in terms of sediment source composition and tectonic setting, extent of chemical weathering, and trace element distributions between particulate and dissolved phases. The potential of the observed trace element signatures to be preserved in the rock record is evaluated and discussed.

Chapter IV of this thesis synthesizes the findings from Chapter II and Chapter III and discusses their implications in the context of the scope and objectives of this thesis. Avenues for future research are proposed.

Appendix A presents the results of experiments in which the elements desorbed from each of the three standard clay mineral samples (used in Chapter II) at six different pH conditions are measured quantitatively. The results of these experiments supplement the discussion in Chapter II.

Appendix B presents models of the speciation of major elements in the river water and sea water samples (used in Chapter II). These models supplement the discussion in Chapter II.

Appendix C tabulates enrichment factors of the major and trace elements measured in the sediment and surface water samples of Arcachon Bay and the Gironde Estuary. These enrichment factors are calculated relative to the composition of upper continental crust and supplement the discussion in Chapter III.

# CHAPTER II

# EXPERIMENTAL EVALUATION OF POTENTIAL GEOCHEMICAL PROXIES FOR SALINITY IN CLAY SEDIMENTS

## 1.0 INTRODUCTION

Salinity is one of the most important parameters of any depositional environment and yet, the ability of researchers to accurately predict the paleosalinity of ancient depositional systems is hampered by a lack of currently available chemical methods. At present, micropaleontology and ichnology are used to infer syn-depositional salinity conditions. Clay-associated trace element ratios unique to specific aqueous environments have the potential to augment these methods. The determination of a suitable geochemical proxy would allow for the finer resolution of spatial distribution of paleoenvironments in units with complex stratigraphic architecture, such as estuaries.

There is a considerable body of work that investigates trace element assemblages associated with clay minerals and correlates them to depositional salinity (e.g. Adams *et al.*, 1965; Bohor & Gluskoter, 1967; Couch, 1971; Degens *et al.*, 1957, 1958; Fu *et al.*, 2016; Goldschmidt *et al.*, 1932; Hu *et al.*, 2012; Landergren & Joensuu, 1963; Landergren & Carvajal, 1969; Stewart & Parker, 1979; Zhang *et al.*, 2013). However, these paleosalinity interpretation methods have yet to be put into common, widespread practice by stratigraphers. This discrepancy suggests that further development and refinement of this technique is needed before it may be considered a viable geochemical tool for inferring paleosalinity.

The objective of this research is to establish general, empirical relationships between salinity, mineralogy, and trace element partitioning with respect to clays. The work presented here is intended as a preliminary step towards establishing a framework for using clay mineralogy in the rock record to predict salinity distributions of depositional environments.

## 1.1 BACKGROUND

### *1.1.1 CLAY PROPERTIES AND CLASSIFICATION*

Clays are hydrous aluminium phyllosilicate minerals, which may be divided into two groups based on the ratio of their aluminum octahedral sheets to their silica tetrahedral sheets (Fig. II-1). Clays with one tetrahedral sheet bound to an octahedral sheet are classified as 1:1 layer clays, while clays with two tetrahedral sheets bounding an octahedral sheet on either side are classified as 2:1 layer clays (Grim, 1968). Within each layer type, clays are further classified into groups by their type of cation substitution. This study focuses exclusively on clay minerals from the illite, kaolinite, and smectite groups, and so the other groups will not be discussed here. The kaolinite group comprises 1:1-layer clays with relatively low layer charges, low CECs, and low flocculation susceptibility. This group is represented here by the mineral kaolinite [$Al_2Si_2O_5(OH)_4$]. The illite group comprises 2:1-layer clays characterized by intermediate layer charges, intermediate CECs, and low to intermediate flocculation susceptibilities. This group is represented here by the mineral illite [$Al_2(Si_{4-x}Al_x)O_{10}(OH)_2 \cdot K_{1-x}$]. The smectite group of clay minerals are also 2:1-layer clays. However, their layer

charges, CECs, and flocculation susceptibilities are generally much higher than those of the illite group. The smectite group is represented in this study by montmorillonite [$(Na,Ca)_{0.33}(Al,Mg)_2(Si_4O_{10})(OH)_2 \cdot nH_2O$].

The two types of clay minerals – 1:1-layer and 2:1-layer – may behave differently when exposed to water. Clay minerals of the 2:1-layer type may form outer-sphere complexes in the inter-layer region, incorporating water molecules into their crystal structure between the aluminum octahedral sheets and expanding in volume. By contrast, when 1:1-layer clay minerals form outer-sphere complexes, these are located on the exterior of the clay particle surfaces, and therefore no corresponding increase in volume occurs. It should be noted that not all 2:1-layer clays are swelling clays. Whether a 2:1-layer clay expands when hydrated is dependent on the distribution of charges between the layers and the type of interlayer cations present (e.g. Hensen & Smit, 2002). Isomorphic cation substitution in the tetrahedral sheets imparts a negative charge that is localized near the interlayer. This localized negative charge results in a stronger electrostatic attraction between the clay surface and cations in the interlayer, thus increasing the likelihood that inner-sphere complexes form (Teich-McGoldrick *et al.*, 2015; Sposito, 1989). When isomorphic cation substitution occurs in the octahedral sheet, the resulting negative charge is distributed more evenly through the sheet, as the locus of charge is located further from the interlayer space. This diffuse negative charge results in weaker electrostatic attraction between the clay surface and interlayer cations, thereby increasing the likelihood that outer-sphere complexes form (Teich-McGoldrick *et al.*, 2015; Sposito, 1989). Smectite-group

clay minerals, such as montmorillonite, have a high swelling capacity. Montmorillonite typically contains Ca or Na cations in the interlayer space, both of which have a strong tendency to interact with water molecules, thereby expanding the interlayer space (e.g. Missana *et al.*, 2014a). By contrast, the interlayer space in illite crystals typically contains K cations, which have relatively low hydration energies (Ruiz Pestana *et al.*, 2017; Eberl, 1980). The resulting K inner-sphere complexes often instigate the dehydration and collapse of the illite interlayer, thus preventing interlayer expansion (Fuller, 2015; Cornell, 1993; Newman, 1987; Sawhney, 1972).

### *1.1.2 CLAY MINERALS AS SORBENTS IN THE ENVIRONMENT*

Within the abiotic component of a depositional environment, any trace metals present are distributed in three phases: dissolved metals, particulate metals and metals in sediment (Branica, 1990). In the case of most trace metals in fluvial environments, the suspended sediment component, rather than the dissolved aqueous component, is the dominant transport phase. This is exemplified by the Amazon and Yukon Rivers, in which the proportions of Cr, Mn, Fe, Co, Ni, and Cu that are transported in suspended sediment are far greater than those that are transported as ions in solution (Gibbs, 1977). Trace metal concentration values in bottom and suspended sediments tend to be significantly higher than those in aqueous solution; for example, the concentration of Pb that is sequestered in the bottom sediment of the Elbe River in Hamburg is $1.0 \times 10^5$ times greater than the

concentration of Pb that is dissolved within the water column (Förstner & Wittmann, 1979).

Adsorption, the adhesion of chemical species to a surface, is the primary means by which trace metals are collected on clay particles (Horowitz, 1985). In the case of clays, cations sorb to the negatively charged sites – deprotonated forms of the ≡SiOH, ≡$Al(OH)_2$, and ≡AlOH groups – as well as to the inter-layer regions of certain phyllosilicates. Reactive sites on clay minerals can be located at both the faces and edges of the crystals. The basal plane of a tetrahedral sheet is composed primarily of oxygen ions and is known as a siloxane surface (Sposito *et al.*, 1999). Within this surface, there are multiple reactive sites in the form of hexagonal siloxane cavities, some of which may contain hydroxyl groups. In addition to the face-centered siloxane surface reactive sites, there are also interstitial regions of cations between the tetrahedral and octahedral sheets, as well as hydroxyl groups around the edges of the clay particles.

A substance's capacity to sorb positively charged ions is referred to as its cation exchange capacity (CEC), which is a measure of the available negatively charged sites in the substance. The CEC of a clay mineral is increased by the presence of incomplete chemical bonds at grain edges, the substitution of $Al^{3+}$ for $Si^{4+}$ in the tetrahedral layers, the substitution of $Mg^{2+}$ for $Al^{3+}$ in the octahedral layers, and the presence of expandable lattices (Grim, 1968). Due to structural variations in their crystal lattices, different types of clay minerals have different cation exchange capacities, as well as different layer charges. These variations result in clays having differential abilities to sorb trace metals from their

environment. Montmorillonite has the greatest sorption ability, followed by illite and then by kaolinite (Hirst, 1962).

The charge of the sorbate species has a bearing on the type of sorption that occurs. Monovalent cations tend to become associated with clay surfaces via outer-sphere complexation, which results in relatively weak, transient bonds (e.g. Nagata *et al.*, 2009). By contrast, cations of higher valences tend to become associated with clay surfaces via inner-sphere complexation, which forms relatively strong bonds (e.g. Fernandes *et al.*, 2016). Both of these surface complexation behaviours are driven by electrostatic forces resulting from charge differences between the sorbate species and the clay surface sites. Inner-sphere and outer-sphere complexation are differentiated by their levels of hydration: the latter type includes interstitial water molecules which prevent electron sharing between the sorbate cation and the surface site on the clay, while the former type is not hydrated and thus may involve covalent bonds (Sposito, 1989).

Clays are ubiquitous in a variety of modern environments and throughout the rock record (e.g. Schieber, 1998). It is estimated that clay minerals amount to 50% of sediment particles, and that more than 95% of all sedimentary rocks contain clay minerals, whether these rocks are deposited in continental or marine environments (Weaver, 1958). Indeed, clays are significant components of such disparate environments as marine basins (e.g. Leontopoulou *et al.*, 2019), estuaries (e.g. Virolle *et al.*, 2018), riverine floodplains (e.g. Khan *et al.*, 2019), terrestrial soils (e.g. Andrade *et al.*, 2019), and coal swamps (e.g. Bohor & Gluskoter, 1967). Numerous studies have demonstrated that grain size is a

significant determining factor in the extent to which suspended sediment and bottom sediment are able to retain trace metals (Filipek & Owen, 1979; Gibbs, 1977; Jenne *et al.*, 1980; Jones & Bowser, 1977; Thorne & Nickless, 1981). Trace metal concentrations in sediments are inversely proportional to grain size, due to the larger available surface area of fine-grained particles (Grim, 1953; Jones & Bowser, 1977) available for reaction and adsorption with inorganic chemical species (Jenne *et al.*, 1980; Jenne, 1968; Jones & Bowser, 1977; Krauskopf, 1956). In fact, experiments have demonstrated that illite samples with large surface areas sorb significantly more Cs onto their particles than do illite samples with smaller surface areas (Rajec *et al.*, 1999). Therefore, in terms of volume and surface reactivity, clay minerals are important environmental sorbents.

### *1.1.3 CLAY FLOCCULATION DYNAMICS*

Clay particles typically remain dispersed in solutions as a result of repulsive electrostatic forces that arise due to the negative charges around the exterior of the particles. However, as the ionic strength of the solution (i.e. salinity) increases, clay particles increasingly flocculate to form relatively large cumulate masses that can settle out of suspension. Flocculation is driven by attractive electrostatic forces between the negatively charged faces and the positively charged edges of clay particles. Flocculation of clays can be instigated by salinity values as low as 0.5 – 1.0 psu, or practical salinity units (Gibbs, 1983). Clay sediments in modern, natural settings flocculate to the greatest extent in estuarine waters with salinities measuring ~10 psu (e.g. Allen & Posamentier,

1993; Guan, *et al.*, 2005; Hauck, *et al.*, 2009). These observations have been corroborated with controlled laboratory experiments (Sutherland *et al.*, 2015). Although a minimum level of salinity is generally required to induce clays to flocculate, there is an upper limit to the proportional relationship between salinity and flocculation. Beyond 20 psu, increasing salinity values do not correspond to increases in flocculation (Sutherland *et al.*, 2015).

Flocculated clay particles tend to pull other particles and trace elements out of suspension as they settle through the water column (Sutherland *et al.*, 2015). The rate at which flocs settle is dependent on the concentration of clay in suspension. Mud deposition slows in proportion to increasing clay concentration with the formation of a boundary layer (Sutherland *et al.*, 2015). Low concentrations of suspended clay particles in the water column allow salinity to promote flocculation, resulting in increased particle size and a corresponding increase in settling rates. By contrast, high concentrations of suspended clay particles in the water column interfere with flocculation, leading to decreased settling rates. One consequence of this relationship is that mud plumes, which contain dense suspensions of clay particles, can extend significantly into marine basins before the clay particles begin to flocculate and settle out of the water column. This can be seen in many modern estuaries that have very high suspended sediment loads and are therefore able to transport significant volumes of sediment to the shelf. Examples include: the Amazon River estuary (Geyer *et al.*, 1996); the Changjiang Estuary (Mitchell *et al.*, 2003); the Trent Estuary (Shi & Kirby, 2003); and the Gironde Estuary (Doxaran *et al.*, 2009). When

flocculation is precluded or delayed in this manner, there can be sufficient time for trace elements bound to the surfaces of clay particles equilibrate with ambient water chemistry. As such, it is reasonable to infer that mud beds would preserve the trace element signature of their deposition location (e.g. marine waters), rather than of their source location (e.g. upper fluvial waters), and could therefore be accurate paleosalinity indicators.

### *1.1.4 CAESIUM AS A POTENTIAL SALINITY INDICATOR*

Degens *et al.* (1957) defined suitable environmental indicators for marine and non-marine sedimentary units by the following characteristics:

i. Significantly respond to changes in environmental salinity.

(Alkali (Li, Na, K, Rb, Cs, Fr) and alkaline earth (Be, Ca, Sr, Ra, Mg, Ba) elements have strong affinities to $Cl^-$ ions. At high salinity conditions, these elements tend to form aqueous chloride complexes, thus reducing the proportion of free alkali and alkaline earth cations in solution (e.g. Sadiq, 1992). As a result, the amount of these elements that can be transferred to sediment deposits via adsorption is significantly decreased).

ii. Relatively ubiquitous in a variety of settings.

iii. Present in concentrations in excess of instrument detection limits, such that their measurement occurs within an acceptable range of error.

iv. Accumulate in rocks via authigenic precipitation or concentration.

v. Essentially unaltered by diagenetic processes.

Caesium, an alkali group metal that most commonly exists in the environment as the monovalent cation $Cs^+$, has many properties that render it suitable for use as a possible salinity indicator. This element is relatively rare, amounting to only 4.9 ppm in the Earth's crust (Rudnick & Gao, 2014), and does not form common detrital minerals. In seawater, caesium is classified as a conservative element, as its concentration does not vary significantly with depth from the typical value of $2.2 \times 10^{-9}$ mol/L (Brewer *et al.*, 1972). Caesium is also stable over relatively long time scales, having a residence time in ocean water of $3.0 \times 10^5$ years (Broecker & Peng, 1982). In contrast to cerium and many other elements, caesium is not redox-sensitive (e.g. Pattan *et al.*, 2005), and does not sorb significantly to iron hydroxides (e.g. Wang *et al*., 2000). Therefore, it is expected that caesium concentrations in sediments can be reliably attributed to the salinity of the depositional environment, rather than the redox state. Furthermore, unlike elements such as copper, iron, and zinc (e.g. Rutherford & Bird, 2004), caesium is not an essential nutrient, and is therefore not expected to be concentrated in sediments by metabolic activity of organisms.

## 1.2 OBJECTIVES AND APPROACH

Previous studies (e.g. Fu *et al.*, 2016; Ingri *et al.*, 2014; Couch, 1971) have correlated trace-element concentrations in mudstone units with inferred depositional salinities. However, these studies fail to adequately reproduce the mechanisms by which salinity-dependent trace element signatures develop. Other environmental parameters, such as organic matter, oxygenation, and source

sediment composition, have the potential to influence the chemistry of *in situ* sediment deposits. Experiments performed under controlled conditions are necessary in order to definitively attribute trace element distributions to salinity.

In an effort to refine the relationship between environmental salinity and trace element signatures in mudstones, we used laboratory-based experiments to measure trace element adsorption to clay minerals under controlled conditions. We tested three common clay minerals that contribute to mudstones: illite, kaolinite, and montmorillonite. To approximate the end members of freshwater and marine conditions, we used two natural water samples. The river water sample was collected from the North Saskatchewan River in Edmonton, Alberta, Canada. The sea water sample was collected from English Bay, Vancouver, British Columbia, Canada. This study comprises two phases of experiments: (i) adsorption experiments with $Cs^+$ and clay suspensions at various ionic strengths to define the relationship between the sorption behaviour of this element with respect to clay mineralogy and solution ionic strength, and (ii) equilibration experiments wherein the clay samples were mixed with natural seawater and river water samples to identify sorption signatures in marine and fluvial environments, respectively.

The objectives of this research are to: (1) characterize the sorbent properties of the three detrital clay minerals of interest in this study; (2); evaluate the suitability of a potential salinity indicator by establishing relationships between the sorption of caesium cations to selected clay minerals and solution

ionic strength; and (3) differentiate between the sorption behaviour of specific elements in river water and sea water with respect to selected clay minerals.

### *1.2.1 IONIC STRENGTH-DEPENDENT ADSORPTION EXPERIMENTS*

The ionic strength-dependent adsorption experiments presented in this study involve the combination of a fixed volume of clay stock solution and $Cs^+$ stock solution with variable volumes of NaCl stock solution and deionized water. The aim of these experiments is to observe the adsorption of $Cs^+$ cations to three different detrital clay minerals in solutions with a range of ionic strengths to determine the effects of ambient salinity on the partitioning of $Cs^+$ between solid and liquid phases of a system. The trends described here demonstrate a preliminary assessment of the suitability of Cs as a geochemical indicator of salinity.

### *1.2.2 EQUILIBRIUM EXPERIMENTS WITH NATURAL RIVER WATER AND SEA WATER SAMPLES*

The equilibrium experiments using natural river water and seawater samples were designed to characterize the sorption signature of each of the three clay samples under freshwater and marine water conditions in the environment. The partitioning of several elements in sea water and river water systems were examined by comparing their concentrations in natural water samples before and after the addition of clay minerals. For each clay-water pair, four clay concentrations were tested in order to quantify the effect of sediment load

conditions on trace metal removal from solution. To account for the effects of dilution of water chemistry upon the addition of an aliquot of concentrated clay suspension to each experimental system, matching control experiments were conducted. In these controls, an equivalent volume of deionized water, precisely matching the volume of the aliquot of clay stock suspension, was added to an equivalent amount of river water or seawater. The ion concentrations in the resulting mixture were measured and considered to be the initial concentrations in the corresponding experimental system.

The percent change in the concentration of an element was an indirect measure of how the partitioning of that element between the solid and liquid phases of a system has changed in response to the equilibration of the water sample with the clays. The relationships interpreted from these experiments are used to infer differences between trace element partitioning in fluvial systems and marine systems.

# 2.0 MATERIALS AND METHODS

## 2.1 MATERIALS

The sample material for this research comprises clay samples purchased from the Source Clay Repository at Purdue University, as well as natural river water and sea water samples. The clay samples used are illite (IMt-2), kaolinite (KGa-1b), and Na-rich montmorillonite (Swy-3), which were used to model the behaviour and properties of three detrital clay minerals (Table II-1). Each sediment sample was imaged using scanning electron microscopy (SEM) prior to

each experiment (Fig. II-2). The river water sample was collected from the North Saskatchewan River in Edmonton, Alberta, Canada (Fig. II-3), and the seawater sample was collected from English Bay in Vancouver, British Columbia, Canada (Fig. II-4).

## 2.2 PROCEDURES FOR CLAY WASHING

In each of three 50 mL polypropylene tubes, 3 g of each clay sample was suspended in 30 mL of deionized water, yielding a sediment concentration of 100 g/L. The initial pH of the suspension was measured and recorded. The pH of each suspension was adjusted to a value of 3 by adding small aliquots of concentrated HCl and NaOH. After a sufficient number of adjustments for the pH to remain stable at the target pH, each of the clay-water suspensions were mixed thoroughly using a Glas-Col Rugged Rotator for 24 hours, to ensure that equilibrium was reached. The polypropylene tubes were then centrifuged with a Thermo Scientific Sorvall Lynx 4000 Centrifuge for 20 minutes at 15,000 x g to separate the solid and liquid phases, and the resulting supernatant was removed. 30 mL of deionized water were added to each polypropylene tube and a Fisher Scientific vortex mixer was used to re-suspend the clay. The pH of each new clay-water suspension was measured and compared with the initial pH value. The pelleting and re-suspension process was repeated as many times as necessary for the pH of each clay-water suspension to reach equilibrium, thus ensuring the removal of chloride that was previously added to the system in the form of HCl.

## 2.3 PROCEDURES FOR IONIC STRENGTH-DEPENDENT ADSORPTION EXPERIMENTS WITH $Cs^+$

The 1.0 M NaCl stock solution was prepared by dissolving 58.4 g of $NaCl_{(s)}$ in 1000 mL of deionized water. The required volume of NaCl stock solution for the relevant ionic strength was added to each experimental tube. An aliquot of deionized water was then added to each experimental tube such that the total volume of liquid in each tube was 27 mL. Seven suspensions of different ionic strengths – 0 M, 0.01 M, 0.05 M, 0.1 M, 0.2 M, 0.4 M, and 0.7 M – were made for each clay mineral, for a total of 21 experimental suspensions. Each clay-water stock suspension was agitated with a Fisher Scientific vortex mixer to achieve an even distribution of clay particles, from which 3 mL were aliquoted and added to each experimental tube to achieve a final sediment concentration of 10 g/L. The 30 ppm Cs stock solution was made by dissolving 0.019 g of $CsCl_{(s)}$ in 500 mL of deionized water. An aliquot of 0.01 mL of the Cs stock solution was added to each experimental tube to achieve a final concentration of 0.01 ppm. A Fisher Scientific vortex mixer was used to thoroughly mix the contents of each experimental tube.

The pH of each experimental mixture was adjusted to a value of 7 using aliquots of concentrated HCl and NaOH. After a sufficient number of adjustments for the pH to remain stable at the target pH, each of the clay-water suspensions were mixed thoroughly using a Glas-Col Rugged Rotator for twenty-four hours, to ensure that equilibrium was reached. The samples were then prepared for ICP-MS analysis (described in Sec. II-2.5).

## 2.4 PROCEDURES FOR EQUILIBRIUM EXPERIMENTS WITH NATURAL RIVER WATER AND SEA WATER SAMPLES

After collection from their respective sources, each of the two natural water samples used in this study – river water from the North Saskatchewan River in Edmonton and seawater from English Bay in Vancouver – were sealed and stored in a refrigerator at 4º C. Prior to combination with the clay samples, each of the natural water samples was filtered with a 0.22 μm nylon membrane syringe filter to remove the majority of solid particles remaining in suspension.

Each clay-water stock suspension was agitated with a Fisher Scientific vortex mixer to achieve an even distribution of clay particles. The experimental suspensions were made by combining a small aliquot of this clay stock suspension with some volume of the water sample of interest, such that the total suspension volume was 30 mL. Four suspensions were made for each water type-clay mineral combination, with final sediment concentrations of 0.5 g/L, 1 g/L, 5 g/L, or 10 g/L.

Two control mixtures were made for each sediment concentration by combining each of the two water samples with the same volume of deionized water as the volume of clay stock required to make suspensions with sediment concentrations of 0.5 g/L, 1 g/L, 5 g/L, and 10 g/L. Each of the clay-water suspensions was mixed thoroughly using a Glas-Col Rugged Rotator for twenty-four hours, to ensure that equilibrium was reached. The samples were then prepared for ICP-MS analysis (described in Sec. II-2.5).

## 2.5 INDUCTIVELY COUPLED PLASMA MASS SPECTROMETRY (ICP-MS) ANALYSES OF THE FLUIDS

Following the ionic strength-dependent adsorption experiments with Cs (Sec. II-2.3) and the equilibrium experiments with the natural river water and sea water samples (Sec. II-2.4), the polypropylene tubes were centrifuged with a Thermo Scientific Sorvall Lynx 4000 centrifuge for 20 minutes at 15,000 x g to separate the solid and liquid phases. After centrifugation, the supernatant was siphoned out of each falcon tube with a ball pipette and injected through a syringe with a 0.22 μm filter to remove the majority of solid particles remaining in suspension and the filtrate passed into an acid-washed polypropylene tube. Then 500 μL of each sample fluid was diluted with 4.5 mL of acid (2% nitric acid, 0.5% hydrochloric acid) to achieve a dilution factor of 10.

The target elements in the analyses of the desorption experiments and the sorption experiments with natural water samples were Na, Ca, Mg, K, S, Sr, Br, Li, Be, B, Al, Si, P, V, Cr, Mn, Fe, Co, Ni, Cu, Zn, As, Se, Cd, Ce, Cs, Pb, and U. The target element in the analyses of the ionic strength-dependent adsorption experiments was Cs. All analyses for cations and Br were performed using an Agilent 8800 Triple Quadrupole ICP-MS (ICP-MS/MS), which has an RF power of 1550 W and a RF reflected power of 18 W. The ICP-MS/MS was operated with a microMist nebulizer and nickel/copper cones. During analysis, MS/MS mode was utilized for greater mass resolution and the collision/reaction cell with He, $O_2$, and $H_2$ gas. To correct for instrumental drift, an inline internal standard system with a solution of 0.5 ppm In was employed. Standards were made in a

matrix of 2% trace metal grade nitric acid and 0.5% trace metal grade hydrochloric acid, and encompassed a range of 0.001 ppm to 125 ppm.

## 2.6 CALCULATIONS AND REPRESENTATIONS OF DATA

### *2.6.1 IONIC STRENGTH-DEPENDENT ADSORPTION EXPERIMENTS WITH $Cs^+$*

If the measured concentration of the cation in solution after equilibration is lower than the original concentration of 0.01 ppm, then we can infer the sorption of that cation onto the clay particles. Therefore, higher concentrations of the cation of interest indicate a relatively low degree of sorption, while low concentrations of the cation of interest suggest a relatively high degree of sorption. Conversely, if the measured values of solution cation concentration after equilibration are in excess of 0.01 ppm, then the logical conclusion is that some quantity of that cation has been transferred to the solution from the clay particles.

The errors on the measured concentrations of $Cs^+$ in solution were calculated as a relative standard deviation (Equation II-1):

$$\mathrm{RSD_X} = \frac{\sigma_X}{\bar{x}_X} \times [X] \qquad \text{(II-1)}$$

$RSD_X = Relative\ standard\ deviation\ for\ measured\ concentration\ of\ element\ X, in\ units\ of\ concentration$

$\sigma_X = standard\ deviation\ of\ instrument\ repetitions\ for\ element\ X$

$\bar{x}_X = mean\ of\ instrument\ repetitions\ for\ element\ X$

$[X] = calculated\ concentration\ of\ element\ X\ in\ sample$

### *2.6.2 EQUILIBRIUM EXPERIMENTS WITH NATURAL RIVER WATER AND SEA WATER SAMPLES*

The calculated percent change values of an element are inherently dependent on the initial concentration of that element in the water sample. If the initial solution concentration of a sorbate element was high, then the sorption of a small amount of this element would yield an almost negligible change in the solution concentration of the element. Conversely, if the initial solution concentration of an element was relatively low, then the sorption of a small amount of this element could result in the solution concentration of this element being changed significantly.

Negative percent change values are presumed to indicate the removal of the element from solution by the clay particles, or adsorption. Positive percent change values are presumed to indicate the addition of the element to the solution by the clay particles, or desorption. Percent change values that are at or near a zero value indicate little to no change in the concentration of the element of interest in solution, and therefore negligible adsorption or desorption.

The percent change in concentration was calculated using Equation II-2:

$$\%\Delta_X = \frac{([X]_f - [X]_o)}{[X]_o} \times 100\% \qquad \text{(II-2)}$$

$$X = element\ of\ interest$$
$$\%\Delta_X = percent\ change\ in\ concentration\ of\ X$$
$$[X]_o = initial\ concentration\ of\ X$$
$$[X]_f = final\ concentration\ of\ X$$

The "initial" concentration of an element was determined by measuring its concentration in the control samples, while the "final" concentration of an

element was determined by measuring its concentration in the experimental suspensions after equilibration. In cases where the initial concentration of the element of interest is below the detection limit of the instrument, then the percent change will be some indeterminate value divided by zero, and therefore cannot be plotted.

The errors on the percent change values mentioned above were calculated using a cumulative error analysis (Equations II-3.1 through II-3.4) of the uncertainties on the individual terms and expressions involved in the calculation of percent change (Equation II-2).

$$u_{xo} = \left(\frac{\sigma_{xo}}{\underline{xo}}\right) \qquad \text{(II-3.1.1)}$$

$$u_{xf} = \left(\frac{\sigma_{xf}}{\underline{xf}}\right) \qquad \text{(II-3.1.2)}$$

$$u_1 = \sqrt{u_{xo}^2 + u_{xf}^2} \qquad \text{(II-3.2)}$$

$$u_2 = \frac{x_f - x_o}{x_o} \times \sqrt{\left(\frac{u_1}{x_f - x_o}\right) + \left(\frac{u_{xo}}{x_o}\right)} \qquad \text{(II-3.3)}$$

$$u_3 = u_2 \times 100\% \qquad \text{(II-3.4)}$$

$$u_{xo} = uncertainty\ in\ measurement\ of\ x_o$$
$$u_{xf} = uncertainty\ in\ measurement\ of\ x_f$$
$$\sigma_{xo} = standard\ deviation\ of\ measurements\ for\ x_o$$
$$\sigma_{xf} = standard\ deviation\ of\ measurements\ for\ x_f$$
$$\underline{x_o} = average\ of\ measurements\ for\ x_o$$
$$\underline{x_f} = average\ of\ measurements\ for\ x_f$$

$$u_1 = uncertainty\ in\ (x_f - x_o)$$

$$u_2 = uncertainty\ in\ \frac{x_f - x_o}{x_o}$$
$$u_3 = cumulative\ error$$

# 3.0 RESULTS

## 3.1 IONIC STRENGTH-DEPENDENT ADSORPTION EXPERIMENTS WITH $Cs^+$

The geochemical data for the ionic strength-dependent adsorption experiments are tabulated in Table II-2 and plotted in Figure II-5. The concentration of Cs in all experimental suspensions is less than the original value of 0.01 ppm after the solutions reach equilibrium (Fig. II-5), suggesting a net removal of Cs from solution by adsorption to the clay particle surfaces. Suspensions containing illite have the lowest Cs concentrations, and therefore the highest degree of sorption. Conversely, the suspensions containing kaolinite have the highest Cs concentrations, and therefore the lowest degree of sorption. The suspensions containing montmorillonite have intermediate Cs concentrations and thus an intermediate degree of sorption, although the values are generally closer to those of kaolinite than to those of illite (Fig. II-5).

For all of the samples, the concentration of Cs in solution increases as solution ionic strength increases, suggesting that less Cs is adsorbed to the clays, regardless of mineralogy, at higher ionic strengths (Fig. II-5). The transition from a steep to shallow data trend (Fig. II-5) may indicate that the influence of ionic strength on Cs sorption is greatest in the 0 M–0.1 M range, and begins to have less of an impact at higher ionic strengths.

## 3.2 EQUILIBRIUM EXPERIMENTS WITH NATURAL RIVER WATER AND SEA WATER SAMPLES

Sorption data for experiments with natural water are tabulated in Table II-3 and Table II-4. Of the 28 elements targeted (see Sec. II-2.5 for complete list), only Ca, Br, K, Mg, Na, S, Si, and Sr were abundant enough to be detected by the instrument. Plots for Ca, Br, K, and Mg are presented in Figure II-6, and plots for Na, S, Si, and Sr are presented in Figure II-7.

When comparing the results of the sorption experiments with natural water samples (Fig. II-6 and Fig. II-7), it is immediately obvious that the signatures for Ca, Mg, and S in river water share many characteristics. These three elements are adsorbed by illite, kaolinite, and montmorillonite at all examined sediment load conditions in river water. Consequently, the degree of element adsorption to the clay particles appears to decrease as the clay concentration increases from 0.5 g/L to 1.0 g/L, and then increases progressively as the clay concentration increases further to 5.0 g/L and 10 g/L.

In the suspensions made in sea water, the percent change values in concentrations of Ca, Mg, and S indicate that a combination of adsorption and desorption processes are occurring in these systems (Table II-4). Of these three elements, the distributions of Ca and S in sea water exhibit the greatest departure from their counterparts in river water. There is little difference in the amount of Ca adsorbed to illite between clay concentrations of 0.5 g/L and 10g /L. At clay concentrations of 1.0 g/L and 5.0 g/L a relatively small proportion of Ca is desorbed from the illite to the sea water.

The sorption signature of S in sea water closely approximates that of Ca. In sea water equilibrated with illite, S exhibits mixed adsorption and desorption behaviours. The magnitude of this variation is slightly greater for S than for Ca. Adsorption of S occurs to the greatest degree in the 0.5 g/L illite suspension, and adsorption of Ca occurs to the greatest degree in the 10 g/L illite suspension. The extent of Ca removal from sea water increases as the concentration of kaolinite increases. By contrast, S is added to sea water at intermediate concentrations (1.0 g/L and 5.0 g/L) of kaolinite, and displays negligible sorption at low (0.5 g/L) and high (10 g/L) concentrations of kaolinite. In suspensions of sea water and montmorillonite, S is increasingly desorbed from montmorillonite as the amount of montmorillonite in suspension increases.

The sorption signatures for Br, K, and Mg in sea water all appear to follow similar patterns with respect to each of the three clay types studied (Fig. II-6). Br, K, and Mg are removed from sea water by adsorption to illite when the clay concentration is 0.5 g/L and 10 g/L. At clay concentrations of 1.0 g/L and 5.0 g/L, the amount of Br, K, and Mg that is adsorbed by illite is negligible. There is little difference in the amount of either Br, K, or Mg adsorbed to illite between low and high sediment load conditions, and at intermediate sediment load conditions a relatively small proportion of these elements are desorbed from the illite to the sea water. The data trends for Br, K, and Mg in sea water samples equilibrated with kaolinite are quite similar to the corresponding trends for Ca. Br, K, and Mg are desorbed from kaolinite to generally similar extents at clay concentrations of 0.5 g/L, 1.0 g/L, and 5.0 g/L. At the relatively high clay concentration of 10 g/L,

these elements are removed from sea water by adsorption to kaolinite. In sea water equilibrated with montmorillonite, there is a transition from desorption to adsorption of Br, K, and Mg as the amount of montmorillonite in suspension increases.

The concentrations of K in both the control solutions and experimental suspensions made with river water were below the detection limit of the instrument. Therefore, the percent change values of K in river water systems could not be calculated.

In river water systems, percent change values of Br could only be calculated for the 0.5 g/L and 5.0 g/L sediment load conditions (Table II-4). These values suggest that, at these intermediate clay concentrations, Br is removed from river water by adsorption to all three clay minerals studied (Fig. II-6). In river water, the extent of Br adsorption is lower at relatively high concentrations of illite compared to relatively low concentrations of illite. Conversely, the extent of Br adsorption to either kaolinite or montmorillonite in river water is higher at relatively high clay concentrations than at relatively low clay concentrations. However, these calculated percent change values fall within each others' ranges of error (Table II-4), and so minimal importance will be assigned to the effect of sediment load conditions on Br adsorption.

Illite and kaolinite appeared to adsorb Na from river water at both measured sediment load conditions, while the montmorillonite suspensions exhibited desorption of Na at both sediment load conditions, with higher percent change values at the lower sediment load condition (Fig. II-7; Table II-4). The

extent of Na adsorption to the clay particles in sea water appears to increase as the concentration of either illite or kaolinite in suspension increases. This implies a correlation between the available surface area of these two clays and the amount of Na that is adsorbed from the sea water. The Na percent change values for illite systems and kaolinite systems are within each others' range of error, and therefore the partitioning behaviour of Na does not differ significantly between these two clays (Table II-4). Compared to the suspensions of river water and montmorillonite, the systems containing montmorillonite and sea water exhibit a notably different sorption signature with respect to Na. While Na was desorbed from montmorillonite in river water, it appears to be adsorbed by montmorillonite in sea water, and to a greater extent at higher sediment load conditions, which correspond with higher sorbent surface areas.

Si is present in the aqueous phase of experimental suspensions made with river water, as well as the river water control solutions (Fig. II-7). In the experimental suspensions made with sea water, as well as the sea water control solutions, Si is below the limit of detection. This precludes the calculation and plotting of percent change values for Si in sea water. The illite and montmorillonite data series show similar trends of increased desorption of Si to the river water with increased clay concentration. This observation suggests that the sorption sites on these clay minerals have a greater affinity for some other species in river water and consequently exchange the Si on their surfaces in favour of these species. By contrast, the kaolinite appears to adsorb Si at all clay concentrations for which a Si percent change value could be calculated.

The relative abundances of Sr in the river water are much lower than in the sea water (Table II-3). However, the proportion of Sr that is desorbed from or adsorbed to the clays is similar for most experimental suspensions (Fig. II-7; Table II-4). Consequently, it can be inferred that in terms of absolute quantities, there is more Sr transferred between the solid and aqueous phases of the sea water systems than in the river water systems. In the river water equilibrated with illite, Sr is adsorbed at all sediment load conditions. In sea water that has been equilibrated with illite, Sr is generally adsorbed to the clay particles, albeit to a lesser extent than in the corresponding sea water suspensions. The Sr percent change values in sea water systems also exhibit less variation than those in river water systems, suggesting that illite concentration has less of a bearing on Sr sorption behaviour in marine conditions than in fresh water conditions (Table II-4). An exception to this trend is in the sea water containing 5.0 g/L of illite, in which Sr appears to be desorbed from the clay. In each of the two types of systems, river water and sea water, the plotted sorption signatures for kaolinite closely resemble those of illite. In suspensions of illite and kaolinite, more Sr is adsorbed as the concentration of clay increases. However, less Sr is adsorbed to kaolinite than illite. In contrast, in river water or sea water that has been equilibrated with montmorillonite, Sr desorption increases as a function of increasing clay concentration. This trend implies the addition of Sr to solution via desorption from the surface complexation sites on montmorillonite.

# 4.0 DISCUSSION

## 4.1 IONIC STRENGTH-DEPENDENT ADSORPTION EXPERIMENTS WITH $Cs^+$

The extent of Cs adsorption to illite, at all ionic strength conditions, was greater than the extent of Cs adsorption to montmorillonite, despite the latter mineral's significantly higher cation exchange capacity (Table II-1). This seeming incongruity has been demonstrated by other researchers to arise from the high selectivity of the frayed edge sites (FES) on illite for Cs (e.g. Brouwer *et al.*, 1983). The FES of illite grains are also highly selective for $Cs^+$ due to this cation's high charge density relative to other monovalent cations, and the compatible size of hydrated $Cs^+$ with the FES (Lee *et al.*, 2017). The sorption of this cation by illite FES is at least partially irreversible. A major reason for this is that the interlayer region can experience a collapse similar to that produced by sorption of $K^+$, resulting in the $Cs^+$ becoming fixed in the illite interlayer (Durrant *et al.*, 2018). Furthermore, the kinetics of $Cs^+$ desorption are demonstrably slow, allowing time for $Cs^+$ cations that are sorbed by FES to diffuse further into the interlayer region and form stronger bonds with the mineral structure (Comans & Hockley, 1992; Comans *et al.*, 1991).

Fuller *et al.* (2014) suggested that the effects of the environmental factors of solution pH and ionic strength on $Cs^+$ sorption to illite are determined by the concentration of $Cs^+$ in solution. Considering that we intend to apply the findings from this research to natural systems in riverine, estuarine, and marine environments, solution pH is not expected to be as influential to $Cs^+$ sorption as

ionic strength. Although the pH of these waters may vary due to factors such as climate, organic matter, and the presence or absence of buffering compounds, river water generally has a pH of approximately 6, while the pH of ocean water tends to be even higher, at approximately 8. As such, we do not anticipate that pH is the controlling factor on $Cs^+$ adsorption at the pH range relevant to the transition from freshwater to marine depositional environments. By contrast, the range of salinity conditions in these environments do correspond to the range of $Na^+$ concentrations over which Fuller *et al.* (2014) determined that $Na^+$ precludes $Cs^+$ sorption. The inverse relationship between ionic strength and $Cs^+$ sorption to sediments has been further supported by the results of this study.

The discrepancy in Cs concentration between the illite suspensions and those of the other two clay minerals studied could be explained by greater affinity of the surface sites on the illite particles for Cs. If there is more $Na^+$ in solution, then there is more competition with $Cs^+$ for sorption sites. These cations have the same charges, and so can substitute easily for each other. However, after a threshold sorbate concentration, the surface sites on the sorbent become saturated, precluding further sorption. The behaviour of $Cs^+$ in the ionic strength-dependent adsorption experiments is somewhat similar to the effect of ionic strength on clay flocculation in estuaries. The most rapid clay flocculation occurs as salinity increases from 0 to 10 psu. As salinity increases above 10 psu, the degree of flocculation does not continue increasing at the same rate, but instead plateaus (Sutherland *et al.*, 2015). This means that the sedimentation rates, and thus the

lithofacies distributions, in high-salinity basins can potentially resemble those of estuaries.

The use of trace elements to predict paleosalinity is an attempt to resolve the ambiguity of sediment distribution patterns in the rock record. Cs sorption follows a similar trend to clay flocculation, and its utility as a paleosalinity indicator corresponds to the transition from freshwater to brackish water. This provides support for the use of Cs distributions in fine-grained siliciclastic sedimentary rocks to infer the spatial location of the freshwater-brackish water transition. Trace element-based proxies for either high- or low-salinity environments may not be imperative, since their deposits tend to have very characteristic trace fossil assemblages (e.g. Ekdale, 1985), among other distinct characteristics.

## 4.2 EQUILIBRIUM EXPERIMENTS WITH NATURAL RIVER WATER AND SEA WATER SAMPLES

### *4.2.1 SORPTION BEHAVIOUR OF Ca AND Mg*

Ca, Mg, and S have similar sorption signatures, and thus analogous responses to given compositions and quantities of clay in river water. These parallels can be attributed to the chemical similarities of these two elements in terms of valence charge and ionic radii (Table II-5). Given that the overall trend of the plots for Ca and Mg is one of increased element adsorption with increased clay concentration, the minima in magnitudes of percent change at the 1.0 g/L sediment load conditions are somewhat puzzling features. We propose an

explanation of these patterns using the flocculation dynamics of the suspended clays: It is possible that the amount of flocculation that occurs at a clay concentration of 1.0 g/L is more significant than at a clay concentration of 0.5 g/L. During flocculation, the relatively small clay particles aggregate into relatively large flocs. This transition is accompanied by a reduction in surface area, and thus a corresponding decrease in the availability of surface sites. Flocculation is likely occurring in the suspensions containing 5.0 g/L and 10 g/L of clay to an extent similar to or greater than in the 1.0 g/L suspensions. However, we do not observe a continued decrease in the degree to which Ca and Mg are adsorbed as clay concentration increases above 1.0 g/L. This observation may be attributed to the relative differences between the quantities of sediment in these suspensions. The difference in the absolute amount of clay between a 1.0 g/L suspension and a 5.0 g/L suspension, or between a 5.0 g/L suspension and a 10 g/L suspension, is extremely large. Conversely, the difference in the absolute amount of clay between a 0.5 g/L suspension and a 1.0 g/L suspension is relatively small. Therefore, although the occurrence of flocculation in the suspensions results in the formation of relatively large aggregates of clay, the volume of these aggregates is relatively high. As a result, the total surface area of the clay is sufficient for appreciable sorption.

#### *4.2.1.1 Sorption Behaviour of Ca*

The activity of Ca cations in sea water is very high relative to the concentration of available complexation sites on the surface of the clay particles.

This discrepancy may explain why, in seawater, similar extents of Ca adsorption to illite are observed for both high and low clay concentrations. The values of percent change in Ca concentrations in sea water equilibrated with low and intermediate concentrations of kaolinite are positive and of comparable magnitudes. In this case, desorption may be instigated by the presence of other abundant cations in solution. If the kaolinite surface sites have a greater affinity for other abundant cations in solution than for Ca, they will exchange their associated Ca cations for these cations. This cation exchange would manifest as apparent Ca desorption from kaolinite. In addition, as solution ionic strength increases, the strength of the electric field around the clay particle surface decreases, reducing the clay's electrostatic attraction for sorbate cations in solution. It is also possible that the elevated activity of $Na^+$ in seawater will result in stronger competition with $Ca^{2+}$ for sorption sites on the clays. Of the three clay minerals examined in this study, kaolinite has the lowest surface area, surface charge, and cation exchange capacity (Table II-1). These factors may explain why, in sea water, the very high clay concentration of 10 g/L is required for kaolinite to adsorb measurable amounts of Ca. The values of percent change in Ca concentration in sea water become increasingly positive as the concentration of montmorillonite in suspension increases. We infer that the amplified levels of Ca desorption from montmorillonite particles at higher sediment load conditions are caused by the exchange of Ca cations for some other cation in solution for which the surface sites on montmorillonite have a greater affinity.

#### *4.2.1.2 Sorption Behaviour of S*

The oxidizing conditions of these experiments signify that S will be present in solution primarily as the species $SO_4^{2-}$ (see Appendix B). As an anionic species, $SO_4^{2-}$ would only adsorb to a negatively-charged surface site on the clay if assisted by cation bridging. The known affinity of $Ca^{2+}$ for $SO_4^{2-}$ , in conjunction with the close correspondence of the sorption signatures for Ca and S (Fig. II-6 and Fig. II-7), lead us to the interpretation that the distribution of S is at least partially controlled by the partitioning of Ca between the solid and aqueous phases in the systems analyzed.

Models of the speciation of major elements in the natural water samples of this study suggest that $SO_4^{2-}$ is the dominant S species in both NSRW and EBSW (Appendix B). The $CaSO_4$ and $MgSO_4$ species are also present at the experimental conditions, although they form a comparatively minor fraction of the S component. The $CaSO_4$ fraction is much lower in the EBSW model than in the NSRW model, indicating that $Ca^{2+}$ does not form complexes with $SO_4^{2-}$ at marine conditions as readily as at riverine conditions.

### *4.2.2 SORPTION BEHAVIOUR OF Br, K, and Mg*

Br, K, and Mg cations all have high concentrations in sea water relative to the concentration of available complexation sites on the clay particles. This may explain why there is comparable adsorption of these elements at both high and low concentrations of illite. The surface area, surface charge, and cation exchange capacity of kaolinite are all relatively low (Table II-1). Therefore, a relatively

high kaolinite concentration (10 g/L) is required for the adsorption of measurable amounts of Br, K, or Mg.

#### *4.2.2.1 Sorption Behaviour of Br*

The behaviour of Br in the experimental suspensions containing either kaolinite or montmorillonite could be explained by the simple relationship between adsorption and surface area. The more sorbent there is in suspension, the more surface sites are available to complex with the sorbate species, in this case Br. There is clearly some limitation on the capacity of illite to adsorb Br. This limitation could arise from illite flocculating to a greater extent at higher clay concentrations, thus reducing the sorbent surface area.

Br exhibits relatively conservative behaviour in environmental waters, and as such is commonly used as a tracer in hydrogeological studies (e.g. Levy & Chambers, 1987). Given that Br anions and the surface complexation sites of clays are both negatively charged, it is likely that the apparent adsorption of Br to the clay particles is facilitated by cation bridging. Consequently, the sorption of Br to clays is dependent on the reactivity of the clays with other ionic species in solution, and the affinity of these cations for both the available clay surface sites and Br anions. The specific cations involved in this bridging mechanism are presumed to be $H^+$, due to the demonstrated dependence of Br partitioning on pH (Goldberg & Kabengi, 2010). The adsorption of Br to clay particles is observed to be inversely proportional to the pH of the background solution in the system, in the range of pH 4 to pH 8. At more acidic pH conditions, the sorption sites on

clay mineral surfaces become protonated. Protonated sorption sites have positive charges, and therefore an increased theoretical ability to adsorb $Br^-$ anions from solution (Goldberg & Kabengi, 2010). It should be noted that $Br^-$ is very rarely adsorbed directly to surface complexation sites. A more apt characterization of $Br^-$ behaviour with respect to clays may be that these anions accumulated in the diffuse layer near the clay mineral surface. The apparent adsorption of Br to montmorillonite changes more slowly than that of either K or Mg, as a function of montmorillonite concentration. This could indicate a slight dependence of the sorption behaviour of Br on the sorption behaviour of other species in the system. Interestingly, the percent change values for Br in river water are orders of magnitude lower than the percent change values for Br in sea water. This discrepancy is attributed to the lower initial solution concentrations of Br in river water, and the lower ionic strength of river water compared to sea water. In the river water suspensions, the average ratio of solution Br to clay is $3.80 \times 10^{-5}$. The average solution Br to clay ratio in the sea water suspensions is $2.73 \times 10^{-4}$, an order of magnitude higher. The initial concentration of Br measured in river water is much lower than that measured in sea water (Table II-3). Therefore, a lesser absolute quantity of Br needs to be adsorbed by clay in river water than by clay in sea water to yield high percent change values. The river water has a far lower ionic strength than sea water, and so the activities of anionic species that compete with Br for clay-associated cations are correspondingly lower in river water relative to sea water. In addition, surface waters in fluvial environments generally have lower pH values than marine waters, and so the sorption sites of

clay particles suspended in river systems would be more protonated. Therefore, river water is presumed to provide a more favourable environment for Br complexation to the clay particles than sea water.

#### *4.2.2.2 Sorption Behaviour of K*

The weathering of oceanic basalt results in the accumulation of relatively high concentrations of K in sea water (e.g. Mottl & Holland, 1978). In fluvial systems, K is primarily introduced to the aqueous phase by the weathering of potassium feldspars and biotite from continental crust (Bowser & Jones, 2002). Therefore, dissolved K is inherently more abundant in sea water than in river water. The implication of this is that there are more $K^+$ cations available in ocean water to be incorporated into the interlayer space of illite particles, a process that has been studied extensively (Weaver, 1967). The filling of the interlayer space by $K^+$ would decrease the amount of surface complexation sites available to other elements. The logical conclusion from this is that trace element concentrations in illite deposited under freshwater conditions would be lower than those of illite deposited under marine conditions. The complexation of $K^+$ with the frayed edge sites (FES) results in the collapse of the interlayer space (Sawhney, 1972). As a result, the exchange of $K^+$ for other elements at this site would be significantly inhibited. However, it is also possible that the high ionic strength of sea water would correspond to the collapse of the electric field around the clay particles, in addition to increased competition between cations for sorption sites (e.g. Liu *et al.*, 2019; Li *et al.*, 2017). This scenario would, in theory, reduce the amount of

$K^+$ associated with illite. Whether by inner-sphere $K^+$ sorption and interlayer collapse, or by increased ionic competition and reduced electric field strength, it is probable that clays deposited in marine settings will contain less adsorbed trace elements than clays deposited in riverine settings.

### *4.2.3 SORPTION BEHAVIOUR OF Na*

The increased magnitude of percent change in solution Na concentration at the 10 g/L sediment load condition is presumed to be a consequence of the higher sorbent surface area. The apparent increased Na concentration in river water after equilibration with montmorillonite could be the result of simple addition. The clay particles could have had associated Na cations prior to equilibration with the water samples. At the 10 g/L concentration of montmorillonite, the clay flocculates significantly. The resulting aggregates are of larger size and lower surface area than the particles at the 1.0 g/L concentration of montmorillonite. The exposed Na cations that can be desorbed or exchanged for other cations in solution is thereby reduced. Illite has a higher surface area, surface charge, and cation exchange capacity than kaolinite (Table II-1), and so it follows that illite has a greater capacity than kaolinite to adsorb Na. The values of percent change in Na concentration in sea water equilibrated with either illite or kaolinite at a clay concentration of 5.0 g/L are positive. This apparent desorption may be the result of amplified flocculation of these clays at 5.0 g/L, as described previously in Sec. II-4.2.1. The apparent difference in the partitioning of Na between river water systems and sea water systems could stem from the difference in solution Na

concentration between these two water samples. Obviously, the concentration of Na in sea water is significantly higher than that in river water (Table II-3), hence the concentration of Na in riverine systems appears more responsive to changes in the amount of clay in suspension.

### *4.2.4 SORPTION BEHAVIOUR OF Si*

The distribution of Si in the systems studied here allows us to interpret this element as a pre-existing component of the river water, rather than being sourced from the clay samples. This interpretation supports our assumption that the clay samples were not damaged during the clay washing process. Previous researchers (Burton *et al.*, 1970) have characterized ocean water as containing a greater proportion of "reactive" silicon than river water. Reactive silicon, as its name implies, is more susceptible to complex with the reactive sites on sorbents such as clay or hydrous metal oxides, and is thus prone to settling out of suspension. The removal of Si from solution at estuarine mouths where the environment transitions from an estuary to a marine basin has been observed in the River Alde (Liss & Pointon, 1973), among others. It has been demonstrated that the mineralogy of the fine suspended sediment fraction determines whether Si is removed from solution at the transition from estuarine to marine waters (Liss & Pointon, 1973). As compelling as the relationship between environmental salinity and Si content is, this element is also a major structural component of the majority of detrital minerals at Earth surface conditions. Therefore, the Si content of

sedimentary rocks is not likely to be useful for the application of determining paleosalinity, as investigated in this research.

### *4.2.5 SORPTION BEHAVIOUR OF Sr*

The greater extent of Sr adsorption at the low and high extremes of illite concentration in river water is attributed to the higher available surface area of the sorbent at these concentrations. At 0.5 g/L, the clay does not tend to aggregate as readily as in higher clay concentrations. At 10 g/L, there is such a large quantity of clay present in suspension that even if the clay particles aggregate, there is still a significant sorbent surface area. The more positive Sr percent change values in kaolinite systems compared to those calculated for illite systems suggests a greater tendency of illite to adsorb Sr. This interpretation is congruent with this mineral's higher surface area, surface charge, and cation exchange capacity (Table II-1). Curiously, in the pH-dependent desorption experiments with the clay samples used in this study (Appendix A), no detectable quantities of Sr were desorbed from any of the clay samples at any pH condition within the range of 3 through 8. As such, it seems unlikely that the clay washing process used was insufficient to remove the trace metals associated with the clay particles. Rather than a simple additive process being responsible for the apparent increase in solution Sr concentration (as suggested for Na in Sec. II-4.2.3), it is more probable that this clay sample exchanges divalent $Sr^{2+}$ for $Na^{+}$, or even $K^{+}$. This is because the montmorillonite used in this study is a Na-montmorillonite, meaning

that it was originally homoionised in Na, and consequently has an affinity for monovalent cations.

## 4.3 LIMITATIONS AND FUTURE WORK

The results of the equilibrium experiments with natural river water and sea water suggest that, for most elements analyzed, there is a positive correlation between the suspended sediment concentration and the proportion of the element that is adsorbed. Element partitioning between the solid and aqueous phases of each system also varied significantly with water chemistry and clay mineralogy: a higher fraction of each element was adsorbed by the clays in river water than in sea water. It is important to put the parameters of these experiments into the context of natural systems. The clay concentrations of the experiments presented here range from 0.5 g/L to 10 g/L, and generally coincide with typical total suspended solids (TSS) concentrations of most modern rivers, which differ greatly between different locations and seasons. Milliman (2001) compiled data from 14 different rivers, whose TSS values range from 0.19 g/L in the case of the Amazon and Orinoco Rivers, to 23 g/L in the case of the Santa Ynez River, for an average of 4.2 g/L (Milliman, 2001). During periods of high river discharge, the increased carrying capacity of the river results in the transport of an increased volume of coarse-grained sediment, which contains comparatively low amounts of trace metals. This influx of coarse material decreases the proportion of sediment in the river that is fine-grained – and thus trace metal-rich – effectively diluting the concentration of trace metals in the water column. There is empirical

evidence to this effect: Cr concentrations in the Rhine River decrease from 1200 mg/kg to 400 mg/kg as river discharge increases from 1000 $m^3/s$ to 4000 $m^3/s$ (Förstner & Wittmann, 1979). Thus, whether the proportionality between sediment concentration and trace metal adsorption observed in this study applies to modern environments and the rock record depends on the grain size of the sediment.

The equilibration times of the experiments presented here are relatively short, on the order of hours to days. As such, the scope of this particular study is limited to relatively instantaneous surface complexation reactions, and neglects to include the effects of longer-term equilibration and diagenesis. Each of these two factors are expected to have significant effects on the trace element signatures of sedimentary rocks deposited in any environmental salinity conditions. Valence charge can partially determine whether a sorbate species becomes associated with a sorbent through weak, transient outer-sphere complexation or comparably stronger inner-sphere complexation. In this way, the charge of the cation being sorbed is a likely determinant of the longevity of its association with the clay particles.

It is well known that, after deposition of sediment, the chemistry of the pore waters changes in response to decreased oxygenation, decreased connectivity with the water column above, and changes in biota, among other factors. Therefore, the conditions of the pore waters will inevitably differ quite significantly from those of the surface waters in which the sediments were initially deposited. This poses a significant challenge to the establishment of a

framework for estimating paleosalinity in the rock record. To reduce this uncertainty, further investigation of the potential relationship between trace element partitioning in modern, natural environments and the salinity of the ambient waters is necessary before this technique is applied to ancient sedimentary successions.

The concentrations of most trace elements analyzed in the water samples were below the detection limit of the instrument. This implies that the feasibility of using trace element concentrations in mudstones to estimate syn-depositional salinity will likely be constrained by the detection limits and errors associated with the instrumental measurement of trace element assemblages. However, there are techniques available with even lower detection limits than the instrument used in this study. Future studies involving similar experiments would do well to use higher resolution techniques, such as an ElementXR HR-ICP-MS.

For the purposes of simplicity and direct correlation of trace element sorption patterns to salinity – as opposed to other environmental factors – the biotic component of sedimentary environments has not been considered here. However, organisms and organic matter have significant and pervasive effects on the chemistry of their environments. Biogenic trace element distributions in sediments may differ significantly relative to those resulting from water salinity. Therefore, it is possible that the trends described in this study may not be directly transferable to natural settings. One possible way in which this issue could be resolved is the use of elemental ratios to refine the paleoenvironmental interpretations. Normalizing the concentration of Cs in a sediment or rock sample

to its total organic carbon (TOC) content and comparing these values to others from different depths and spatial locations would help to determine whether there is a biological control on the distribution of Cs in the sediment.

As mentioned previously (Sec. II-1.1.4), caesium occurs naturally in the Earth's crust and is not redox-sensitive. Furthermore, this element has a relatively long residence time and exhibits conservative behaviour in sea water. Therefore, calculating the enrichment factor of Cs in a sediment or rock sample, relative to upper continental crust (*sensu* Taylor and McLennan, 1985), may elucidate the utility of Cs as a paleosalinity indicator. If calculated Cs enrichment factors of an interval or area of interest are relatively constant in vertical or horizontal space, then it could be inferred that the Cs content of the samples is attributable entirely to the sediment source. However, if the Cs enrichment factors vary spatially or with depth, then it is possible that these fluctuations reflect different ambient water chemistries at their respective times of deposition, and consequently different sorption of Cs by clays in the sediment.

## 5.0 CONCLUSION

In this study, we performed laboratory experiments with illite, kaolinite, and montmorillonite clays to refine our understanding of trace element-clay interactions under various salinity conditions. The effect of solution ionic strength on the adsorption of Cs to each of the three clay minerals of interest was observed to infer whether this element has the potential to act as a proxy for syn-depositional salinity conditions in fine-grained siliciclastic sedimentary rocks.

The amount of $Cs^+$ that was adsorbed to all three clay minerals was inversely proportional to the ionic strength of the solution. This suggests that the Cs content in mudstones may vary predictably according to the salinity of their depositional environment. It was also found that the extent of $Cs^+$ adsorption is considerably influenced by the mineralogy of the clay sorbent: $Cs^+$ is adsorbed to the greatest extent by illite, and to the least extent by kaolinite, and is adsorbed to an intermediate extent by montmorillonite. Each of the three clay minerals investigated was also equilibrated with natural river water and sea water samples to characterize and distinguish between the sorption behaviour of specific elements in river water and sea water with respect to different clay minerals. The proportion of trace elements adsorbed by clays is greater at higher sediment load conditions. Many elements display markedly different sorption patterns between river water and seawater systems, as well as between different clay minerals. Generally, the proportion of each element removed from solution via adsorption to clays is greater in river water than in sea water.

The results of this study support the development of geochemical techniques for estimating paleosalinity in the rock record. Preliminary interpretations of the relationship between Cs adsorption and solution ionic strength suggest that the abundance of Cs in mudstones could be used to approximate the freshwater to brackish water transition zone in the rock record. Element partitioning was also observed to differ significantly between river water and sea water systems, indicating that it may be possible to apply this technique to modern fluvial and marine settings. In addition, these findings allow the

identification of some limitations that should be considered before the technique is brought into widespread use. Instrument detection limits can significantly determine how feasible it is to use trace element enrichments in fine-grained sedimentary rocks as proxies for paleosalinity. The factors of clay concentration, sediment heterogeneity, diagenesis, and organic matter are all expected to significantly affect the sorption of trace elements to clays, and should be considered when attempting to apply these results in the future.

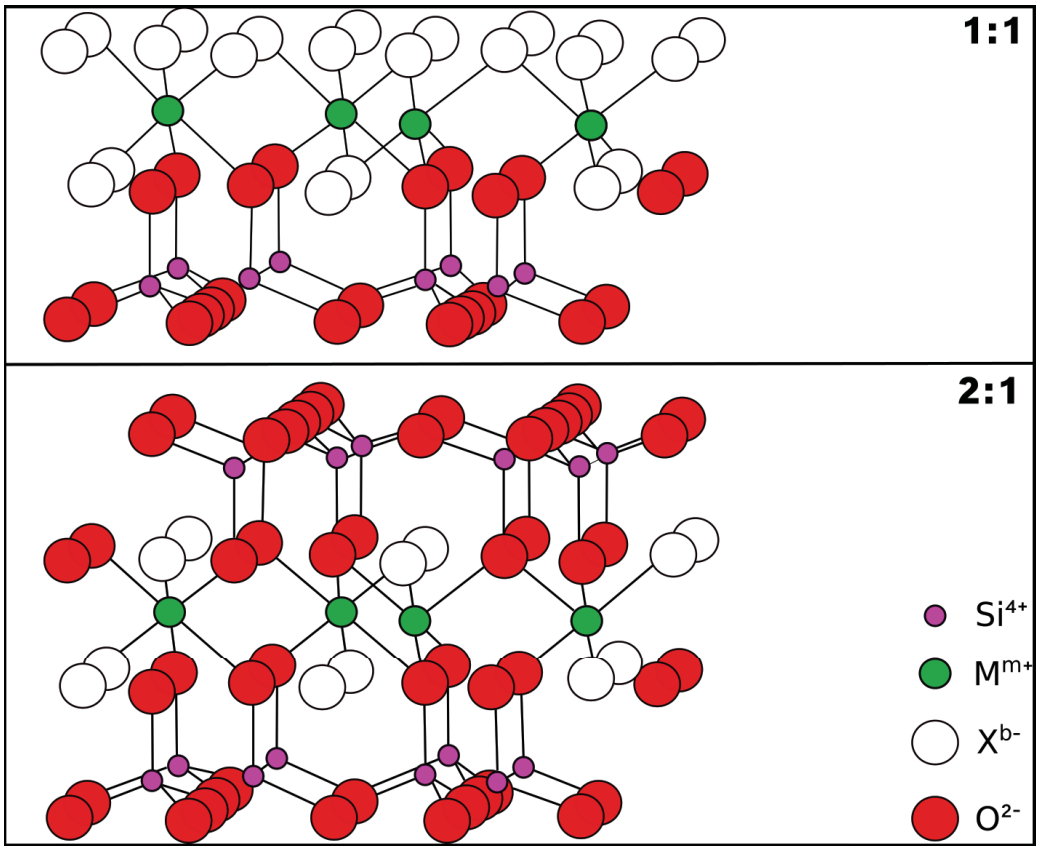
1:1
2:1
Si4+
Mm+
Xb-
O2-

Figure II-1: General crystal structure of single-layer (1:1) and double-layer (2:1) clay minerals. Modified from Sposito *et al.*, 1999.

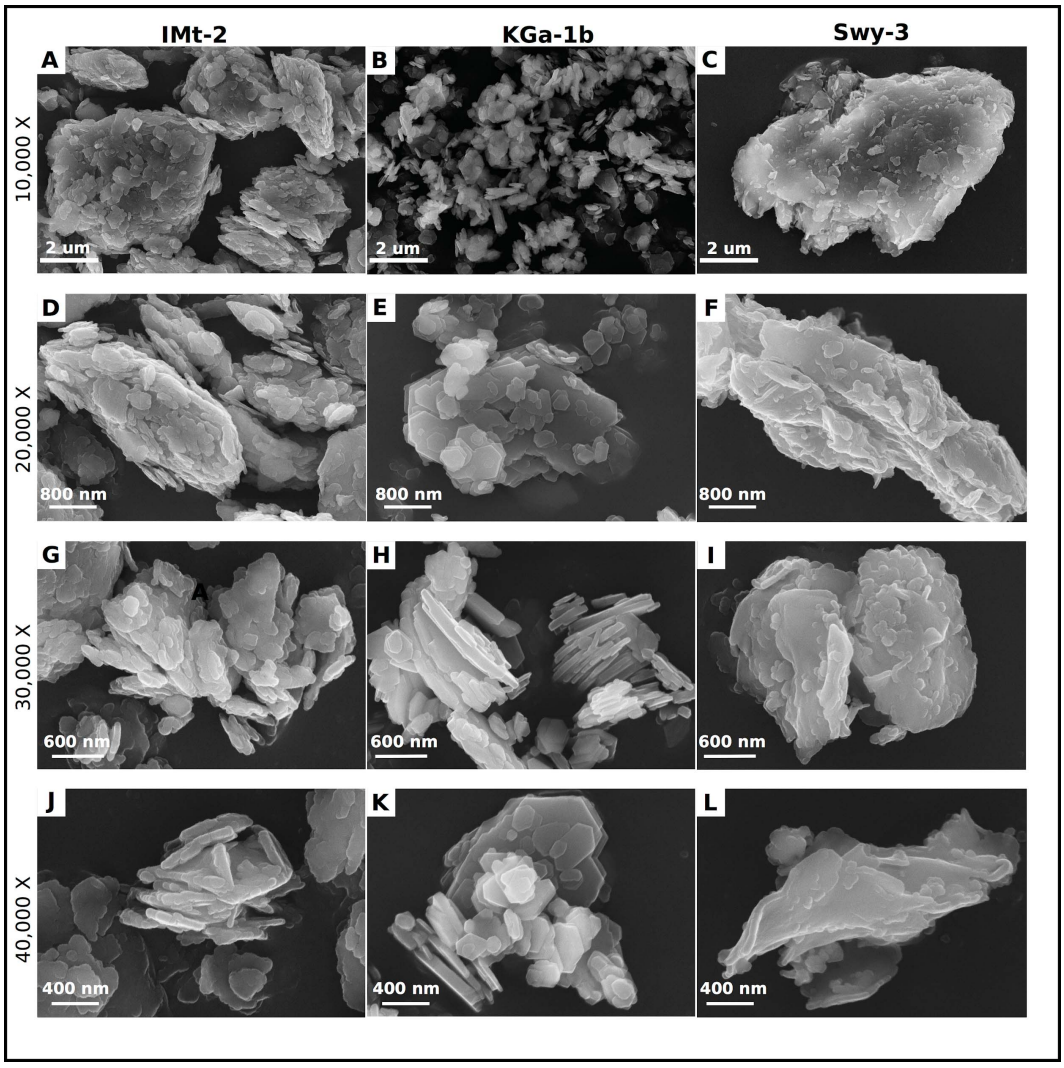
IMt-2
KGa-1b
Swy-3
10,000 X
20,000 X
30,000 X
40,000 X
A
B
C
D
E
F
G
H
I
J
K
L
2 um
2 um
2 um
800 nm
800 nm
800 nm
600 nm
600 nm
600 nm
400 nm
400 nm
400 nm

Figure II-2: Scanning electron microscope images of, from left to right: illite (IMt-2), kaolinite (KGa-1b), montmorillonite (Swy-3). The magnifications of the images are, from top to bottom: 10,000X, 20,000X, 30,000X, and 40,000X.


113°27′00″W
113°24′54″W
N
53°33′39″N
53°33′00″N
North Saskatchewan River
Edmonton
1 km
Google Earth

Figure II-3: Satellite image of a portion of the Edmonton region in central Alberta. The locality of water sample NSRW (North Saskatchewan River Water) is denoted by a red dot. Modified from Google Earth satellite image, retrieved on August 1, 2018.

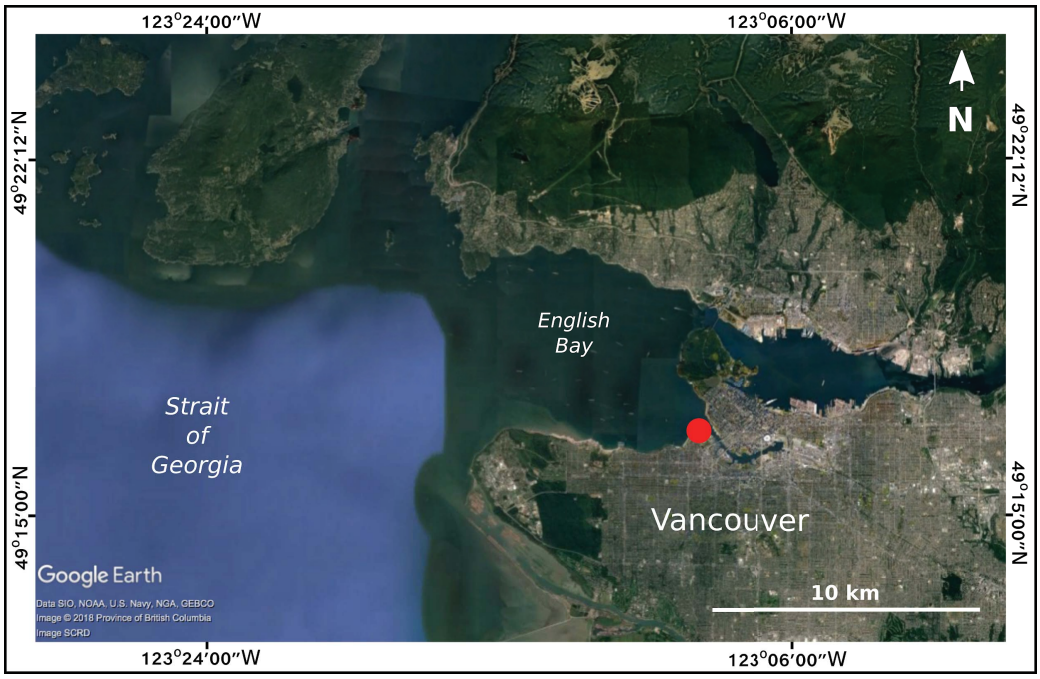
123°24′00″W
123°06′00″W
49°22′12″N
49°15′00″N
N
English
Bay
Strait
of
Georgia
Vancouver
10 km
Google Earth
Data SIO, NOAA, U.S. Navy, NGA, GEBCO
Image © 2018 Province of British Columbia
Image SCRD

Figure II-4: Satellite image of a portion of the southwestern coast of British Columbia. The locality of water sample EBSW (English Bay Sea Water) is denoted by a red dot. Modified from Google Earth satellite image, retrieved on August 1, 2018.

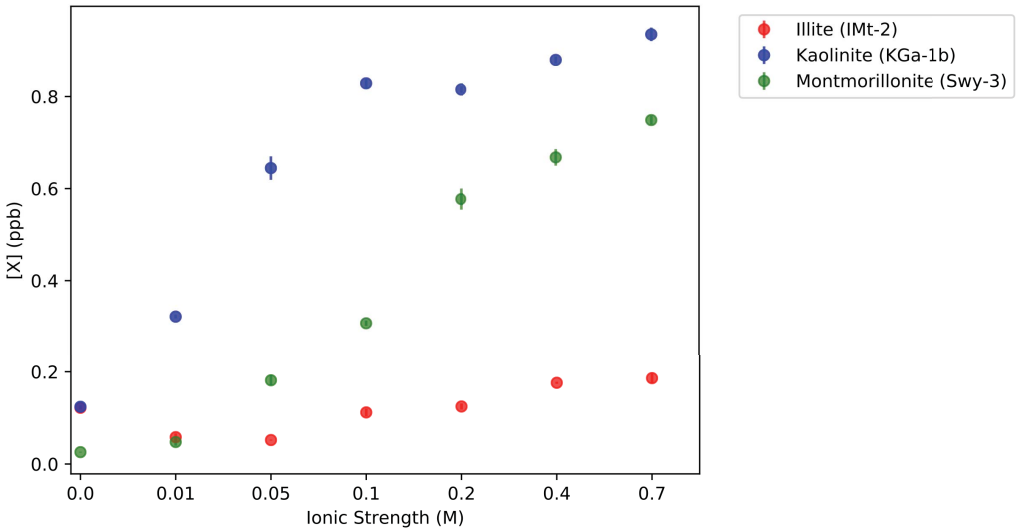
Illite (IMt-2)
Kaolinite (KGa-1b)
Montmorillonite (Swy-3)
[X] (ppb)
0.0
0.2
0.4
0.6
0.8
0.0
0.01
0.05
0.1
0.2
0.4
0.7
Ionic Strength (M)

Figure II-5: Scatter plot of the concentration, in ppb, of Cs remaining in solution after equilibration with each of the three clay samples, as a function of solution ionic strength, in mol/L. The y-axis represents the concentration of the cation of interest, $Cs^+$, that remains in solution after equilibration with the clays, while the x-axis represents the solution ionic strength. Concentration values are based upon ICP-MS measurements of the experimental fluids. Error bars are in units of ppb and represent relative standard deviations of instrument measurements (Equation II-1). The data series for the fluids equilibrated with each of the three clays are distinguished by the colour scheme depicted in the legend.

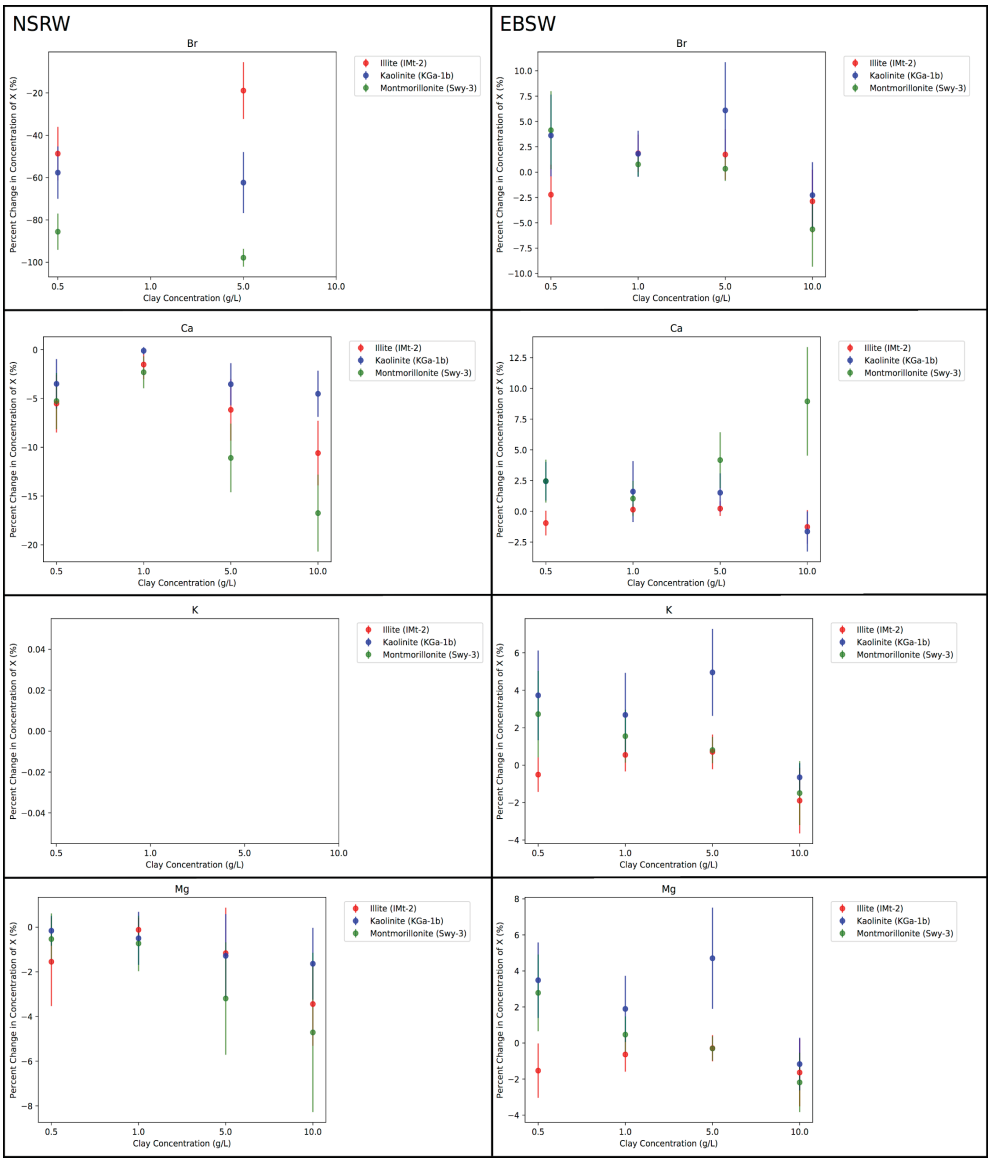
NSRW
EBSW
Br
Ca
K
Mg
Illite (IMt-2)
Kaolinite (KGa-1b)
Montmorillonite (Swy-3)
Percent Change in Concentration of X (%)
Clay Concentration (g/L)
0.5
1.0
5.0
10.0

Figure II-6: Compiled plots of percent change in the concentration of element X in natural water samples after equilibration with each of the three clay minerals. Each of the elements measured were plotted individually as a percent change in concentration as a function of clay concentration in the suspension. The data series for the fluids equilibrated with each of the three clays are distinguished by the colour scheme depicted in the legend. The cumulative errors on each percent change value are represented on the scatter plots as error bars in units of percent. Listed from top to bottom, the elements referred to as X are: Br, Ca, K, and Mg. Plots based on measured concentrations of X in suspensions made from North Saskatchewan River Water are located in the left column and labeled "NSRW". Plots based on measured concentrations of X in suspensions made from English Bay Sea Water are located in the right column and labeled "EBSW".

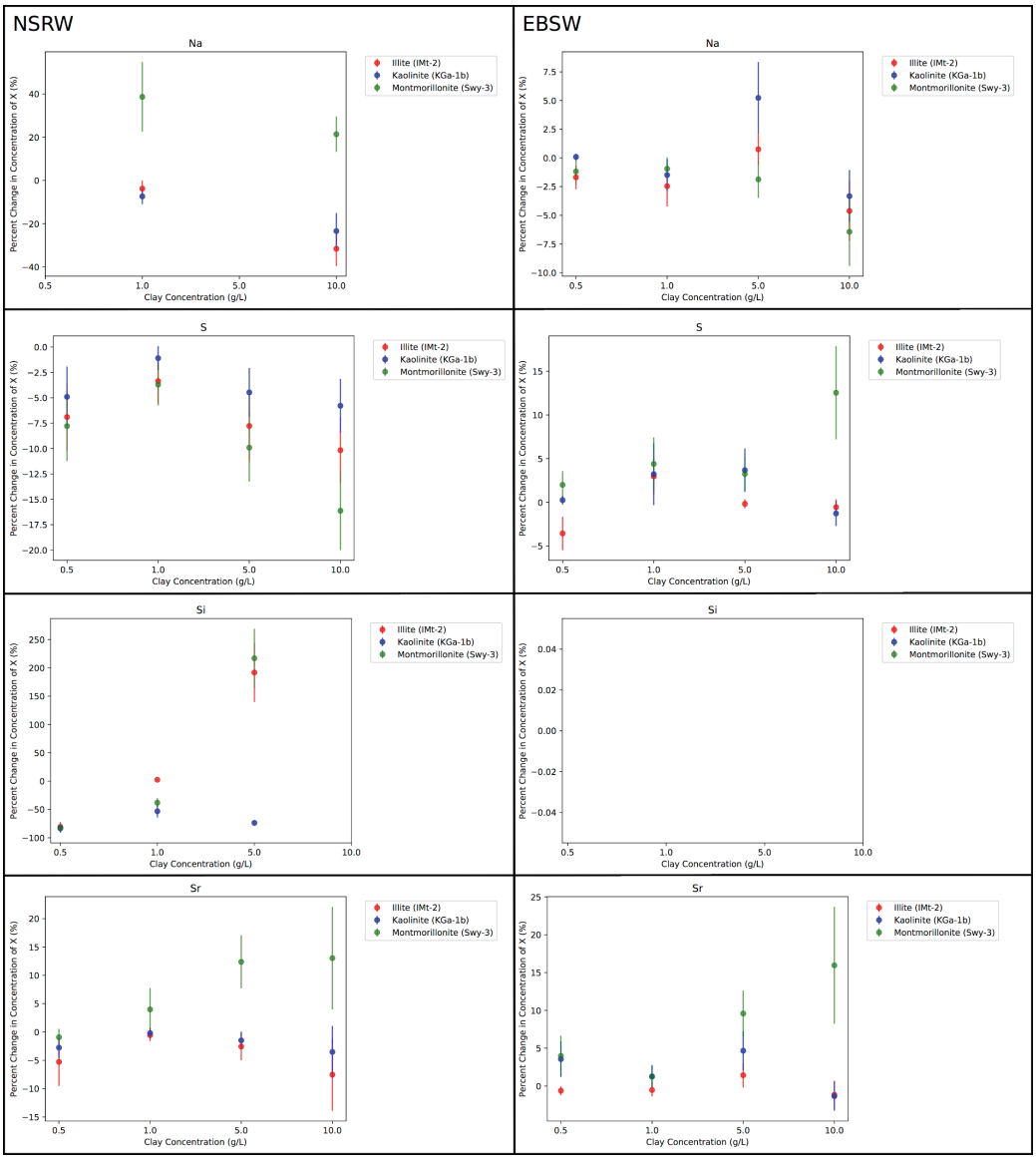
NSRW
EBSW
Na
S
Si
Sr
Illite (IMt-2)
Kaolinite (KGa-1b)
Montmorillonite (Swy-3)
Percent Change in Concentration of X (%)
Clay Concentration (g/L)
0.5
1.0
5.0
10.0

Figure II-7: Compiled plots of percent change in the concentration of element X in natural water samples after equilibration with each of the three clay minerals. Each of the elements measured were plotted individually as a percent change in concentration as a function of clay concentration in the suspension. The data series for the fluids equilibrated with each of the three clays are distinguished by the colour scheme depicted in the legend. The cumulative errors on each percent change value are represented on the scatter plots as error bars in units of percent. Listed from top to bottom, the elements referred to as X are: Na, S, Si, and Sr. Plots based on measured concentrations of X in suspensions made from North Saskatchewan River Water are located in the left column and labeled "NSRW". Plots based on measured concentrations of X in suspensions made from English Bay Sea Water are located in the right column and labeled "EBSW".

| | Illite | Kaolinite | Montmorillonite |
|---|---|---|---|
| **Code** | IMt-2 | Kga-1b | Swy-3 |
| **Notes** | Replacement for IMt-1 | Low-defect; replacement for Kga-1 | Data based upon Swy-1 and Swy-2 |
| **Formation** | – | Tuscaloosa | Newcastle |
| **Age** | – | Cretaceous | Cretaceous |
| **Provenance** | Silver Hill, Montana, USA | Washington County, Georgia, USA | Crook County, Wyoming, USA |
| **Specific Surface Area ($m^2/g$)** | 51 | 10.05 +/– 0.02 | 31.82 +/– 0.22 |
| **Cation Exchange Capacity (meq/100 g)** | 14 | 2 | 76.4 |
| **SiO2** | 49.3 | 44.2 | 62.9 |
| **Al2O3** | 24.25 | 39.7 | 19.6 |
| **TiO2** | 0.55 | 1.39 | 0.09 |
| **Fe2O3** | 7.32 | 0.13 | 3.35 |
| **FeO** | 0.55 | 0.08 | 0.32 |
| **MnO** | 0.03 | 0.002 | 0.006 |
| **MgO** | 2.56 | 0.03 | 3.05 |
| **CaO** | 0.43 | – | 1.68 |
| **Na2O** | 0 | 0.013 | 1.53 |
| **K2O** | 7.83 | 0.05 | 0.53 |
| **F** | – | 0.013 | 0.111 |
| **P2O5** | 0.08 | 0.034 | 0.049 |
| **S** | – | – | 0.05 |
| **LOI (550° C)** | 8.02 | 12.6 | 1.59 |
| **LOI (550-1000° C)** | | 1.18 | 4.47 |
| **CO2** | – | – | 1.33 |

Table II-1: Quantitative structural properties, electrical properties, and provenance information for the three clay minerals used in this study, as well as chemical analyses. All data from the Source Clays Repository.

| Clay | Ionic Strength (M) | Cs [X] (ppb) | σ (ppb) |
|---|---|---|---|
| I | 0 | 0.1218 | 0.0037 |
| I | 0.01 | 0.0582 | 0.0081 |
| I | 0.05 | 0.0519 | 0.0010 |
| I | 0.1 | 0.1118 | 0.0084 |
| I | 0.2 | 0.1246 | 0.0065 |
| I | 0.4 | 0.1760 | 0.0022 |
| I | 0.7 | 0.1860 | 0.0104 |
| K | 0 | 0.1240 | 0.0035 |
| K | 0.01 | 0.3218 | 0.0040 |
| K | 0.05 | 0.6445 | 0.0255 |
| K | 0.1 | 0.8286 | 0.0105 |
| K | 0.2 | 0.8153 | 0.0068 |
| K | 0.4 | 0.8794 | 0.0078 |
| K | 0.7 | 0.9349 | 0.0147 |
| M | 0 | 0.0257 | 0.0009 |
| M | 0.01 | 0.0476 | 0.0079 |
| M | 0.05 | 0.1814 | 0.0112 |
| M | 0.1 | 0.3073 | 0.0059 |
| M | 0.2 | 0.5772 | 0.0230 |
| M | 0.4 | 0.6678 | 0.0180 |
| M | 0.7 | 0.7488 | 0.0093 |

Table II-2: Tabulated results of the ionic strength-dependent adsorption experiments with Cs, as described in Sec. II-2.3. Data include: [X], the concentrations of each of the two sorbate cations of interest remaining in solution after equilibration with the clays at a range of ionic strengths, as well as ˜, the error on each concentration, as a concentration standard deviation. The concentration values are in units of ppb. The two elements analyzed are listed in the column headers. The mineralogy of the clay used in each experiment is listed in the leftmost column and identified as I, K, or M, denoting either illite, kaolinite, or montmorillonite, respectively. The ionic strength of the solution in each experiment is listed in the second column, in units of M. Measurements were obtained via ICP-MS analysis, as described in Sec. II-2.5.

| Water Type | Clay | Clay Concentration (g/L) | Br | | Ca | | K | | Mg | | Na | | S | | Si | | Sr | |
|---|---|---|---|---|---|---|---|---|---|---|---|---|---|---|---|---|---|---|
| | | | [X] (ppm) | σ (ppm) | [X] (ppm) | σ (ppm) | [X] (ppm) | σ (ppm) | [X] (ppm) | σ (ppm) | [X] (ppm) | σ (ppm) | [X] (ppm) | σ (ppm) | [X] (ppm) | σ (ppm) | [X] (ppm) | σ (ppm) |
| NSRW | 0 | 0.5 | 11.5776 | 0.6640 | 56.7483 | 0.8718 | 0.0000 | 0.0000 | 40.3796 | 0.8509 | 0.0000 | 0.1008 | 56.7275 | 0.8714 | 2.7084 | 0.1132 | 0.9274 | 0.0114 |
| NSRW | 0 | 1.0 | 0.0000 | 0.0000 | 51.9605 | 0.2258 | 0.0000 | 0.0000 | 40.4751 | 0.8318 | 0.2137 | 0.0028 | 51.3909 | 0.2233 | 0.4923 | 0.0056 | 0.9004 | 0.0124 |
| NSRW | 0 | 5.0 | 0.9285 | 0.0785 | 52.2401 | 0.6364 | 0.0000 | 0.0000 | 39.8888 | 0.7385 | 0.0000 | 0.0273 | 51.1066 | 0.6226 | 0.3844 | 0.0052 | 0.8794 | 0.0107 |
| NSRW | 0 | 10.0 | 0.0000 | 0.0000 | 48.4368 | 0.4467 | 0.0000 | 0.0000 | 39.3233 | 0.2429 | 0.7366 | 0.0188 | 47.2056 | 0.4353 | 0.0000 | 0.0000 | 0.8713 | 0.0445 |
| NSRW | I | 0.5 | 5.9418 | 0.2320 | 53.6151 | 0.3772 | 0.0000 | 0.0000 | 39.7540 | 0.5953 | 0.0000 | 0.0660 | 52.8165 | 0.3715 | 0.5207 | 0.0258 | 0.8784 | 0.0303 |
| NSRW | I | 1.0 | 0.0000 | 0.0000 | 51.1687 | 0.7365 | 0.0000 | 0.0000 | 40.4268 | 0.5863 | 0.2056 | 0.0076 | 49.6644 | 0.7148 | 0.5039 | 0.0047 | 0.8953 | 0.0116 |
| NSRW | I | 5.0 | 0.7531 | 0.0671 | 49.0212 | 0.6160 | 0.0000 | 0.0000 | 39.4235 | 1.2241 | 0.0000 | 0.0541 | 47.1335 | 0.5923 | 1.1215 | 0.0441 | 0.8568 | 0.0178 |
| NSRW | I | 10.0 | 0.0000 | 0.0000 | 43.3050 | 0.3192 | 0.0000 | 0.0000 | 37.9697 | 0.3264 | 0.5039 | 0.0088 | 42.4065 | 0.3126 | 1.2264 | 0.0063 | 0.8057 | 0.0238 |
| NSRW | K | 0.5 | 4.9025 | 0.1864 | 54.7623 | 0.6262 | 0.0000 | 0.0000 | 40.3143 | 0.7451 | 0.0000 | 0.0473 | 53.9461 | 0.6169 | 0.4496 | 0.0126 | 0.9018 | 0.0026 |
| NSRW | K | 1.0 | 0.0000 | 0.0000 | 51.9035 | 0.6300 | 0.0000 | 0.0000 | 40.2728 | 0.7814 | 0.1979 | 0.0027 | 50.8287 | 0.6170 | 0.2303 | 0.0129 | 0.8986 | 0.0364 |
| NSRW | K | 5.0 | 0.3495 | 0.0151 | 50.3912 | 0.3163 | 0.0000 | 0.0000 | 39.3769 | 0.8039 | 0.0000 | 0.1446 | 48.8222 | 0.3065 | 0.1009 | 0.0008 | 0.8663 | 0.0095 |
| NSRW | K | 10.0 | 0.0000 | 0.0000 | 46.2472 | 0.4294 | 0.0000 | 0.0000 | 38.6793 | 0.5737 | 0.5642 | 0.0183 | 44.4743 | 0.4129 | 0.0839 | 0.0049 | 0.8406 | 0.0304 |
| NSRW | M | 0.5 | 1.6707 | 0.0685 | 53.7630 | 0.3585 | 0.0000 | 0.0000 | 40.1639 | 0.5281 | 0.0000 | 0.0336 | 52.3098 | 0.3488 | 0.4875 | 0.0152 | 0.9189 | 0.0194 |
| NSRW | M | 1.0 | 0.0000 | 0.0000 | 50.7580 | 0.5652 | 0.0000 | 0.0000 | 40.1801 | 0.2416 | 0.2963 | 0.0129 | 49.4917 | 0.5511 | 0.3045 | 0.0098 | 0.9363 | 0.0293 |
| NSRW | M | 5.0 | 0.0198 | 0.0022 | 46.4462 | 0.1467 | 0.0000 | 0.0000 | 38.6146 | 0.3459 | 0.0000 | 0.1121 | 46.0426 | 0.1454 | 1.2178 | 0.0364 | 0.9882 | 0.0097 |
| NSRW | M | 10.0 | 0.0000 | 0.0000 | 40.3270 | 0.2740 | 0.0000 | 0.0000 | 37.4701 | 1.0463 | 0.8940 | 0.0023 | 39.5952 | 0.2690 | 0.6786 | 0.0078 | 0.9848 | 0.0205 |
| EBSW | 0 | 0.5 | 26.2770 | 0.9043 | 160.6608 | 1.3326 | 158.5041 | 2.1252 | 513.0879 | 4.2495 | 457.0467 | 2.6297 | 160.0668 | 1.3277 | 0.0000 | 0.0000 | 3.4212 | 0.0098 |
| EBSW | 0 | 1.0 | 26.0731 | 0.2533 | 158.6131 | 1.9520 | 160.5267 | 1.4193 | 524.3766 | 4.2413 | 469.5849 | 4.3675 | 153.6216 | 1.8906 | 0.0000 | 0.0000 | 3.4829 | 0.0164 |
| EBSW | 0 | 5.0 | 25.3665 | 0.6881 | 156.4213 | 0.8815 | 155.6476 | 0.3346 | 505.7956 | 6.1748 | 437.0563 | 5.4525 | 155.8135 | 0.8781 | 0.0000 | 0.0000 | 3.3502 | 0.0279 |
| EBSW | 0 | 10.0 | 25.0280 | 0.3218 | 149.7133 | 1.8295 | 152.4477 | 1.0618 | 491.8939 | 5.9241 | 434.4411 | 6.4026 | 144.8712 | 1.7703 | 0.0000 | 0.0000 | 3.2701 | 0.0721 |
| EBSW | I | 0.5 | 25.6922 | 0.5427 | 159.1306 | 1.0875 | 157.7015 | 1.6289 | 505.2285 | 6.3942 | 449.3225 | 1.4066 | 154.3673 | 1.0549 | 0.0000 | 0.0000 | 3.4002 | 0.0169 |
| EBSW | I | 1.0 | 26.5569 | 0.4022 | 158.8331 | 1.2626 | 161.4045 | 1.7768 | 521.0466 | 6.2515 | 458.0214 | 4.1493 | 158.1750 | 1.2573 | 0.0000 | 0.0000 | 3.4645 | 0.0407 |
| EBSW | I | 5.0 | 25.8071 | 0.5751 | 156.7705 | 2.3443 | 156.7508 | 1.8520 | 504.3401 | 6.9672 | 440.3389 | 9.2775 | 155.5358 | 2.3259 | 0.0000 | 0.0072 | 3.3982 | 0.0543 |
| EBSW | I | 10.0 | 24.3069 | 0.7840 | 147.8172 | 1.3136 | 149.5573 | 2.2426 | 483.8451 | 8.8688 | 414.3619 | 1.5533 | 144.0661 | 1.2803 | 0.9581 | 0.0365 | 3.2322 | 0.0676 |
| EBSW | K | 0.5 | 27.2278 | 0.7085 | 164.5973 | 0.8725 | 164.4137 | 1.0325 | 530.9692 | 4.6754 | 457.4392 | 3.5437 | 160.4711 | 0.8507 | 0.0000 | 0.0000 | 3.5430 | 0.0528 |
| EBSW | K | 1.0 | 26.5458 | 0.6944 | 161.1646 | 5.7099 | 164.8364 | 2.6167 | 534.3085 | 8.2056 | 462.5882 | 4.3231 | 158.5736 | 5.6181 | 0.2876 | 0.0030 | 3.5272 | 0.0592 |
| EBSW | K | 5.0 | 26.9121 | 0.5790 | 158.7945 | 2.3939 | 163.3615 | 1.6470 | 529.5882 | 5.3702 | 459.9094 | 5.6643 | 161.5432 | 2.4354 | 0.0000 | 0.0000 | 3.5065 | 0.0374 |
| EBSW | K | 10.0 | 24.4591 | 1.1295 | 147.2587 | 1.6487 | 151.4557 | 0.8289 | 486.1495 | 6.8722 | 419.9895 | 2.8528 | 143.0269 | 1.6013 | 0.0000 | 0.0000 | 3.2263 | 0.0571 |
| EBSW | M | 0.5 | 27.3641 | 0.0737 | 164.6120 | 1.4421 | 162.8254 | 2.1925 | 527.3770 | 7.0591 | 451.6460 | 4.3701 | 163.2691 | 1.4303 | 0.0000 | 0.0000 | 3.5575 | 0.0605 |
| EBSW | M | 1.0 | 26.2727 | 0.4140 | 160.2609 | 2.5206 | 163.0125 | 1.4810 | 526.8310 | 10.6563 | 465.1389 | 2.2500 | 160.3708 | 2.5224 | 0.0067 | 0.0003 | 3.5261 | 0.0512 |
| EBSW | M | 5.0 | 25.4510 | 0.8430 | 162.9465 | 1.6712 | 156.8997 | 0.8905 | 504.2728 | 4.7664 | 428.8992 | 2.8914 | 160.8765 | 1.6500 | 0.0321 | 0.0130 | 3.6712 | 0.0089 |
| EBSW | M | 10.0 | 23.6148 | 0.5306 | 163.1103 | 2.5013 | 150.1696 | 2.8067 | 481.1514 | 2.0294 | 406.4848 | 0.3258 | 163.0355 | 2.5002 | 0.5186 | 0.0184 | 3.7919 | 0.0843 |

Table II-3: Tabulated results of the sorption experiments with natural river water and sea water, as described in Sec. II-2.4. Data include: [X], the concentrations of each of the elements measured in solution after equilibration with the clays at a range of sediment load conditions, as well as ˜, the error on each concentration. The errors are calculated as concentration standard deviations All concentrations and errors are in units of ppm. The elements analyzed are listed in the column headers. The water type, either North Saskatchewan River Water (NSRW) or English Bay Sea Water (EBSW), in each sample is listed in the first column. The mineralogy of the clay used in each experiment is listed in the second column and identified as I, K, or M, denoting either illite, kaolinite, or montmorillonite, respectively. The control solutions, which do not contain clay, are identified by 0. The concentration of clay in each experimental suspension is listed in the third column, in units of g/L. Measurements were obtained via ICP-MS analysis, as described in Sec. II-2.5.

| Water Type | Clay | Clay Concentration (g/L) | Br | | Ca | | K | | Mg | | Na | | S | | Si | | Sr | |
|---|---|---|---|---|---|---|---|---|---|---|---|---|---|---|---|---|---|---|
| | | | %Δ (%) | $u_3$ (%) | %Δ (%) | $u_3$ (%) | %Δ (%) | $u_3$ (%) | %Δ (%) | $u_3$ (%) | %Δ (%) | $u_3$ (%) | %Δ (%) | $u_3$ (%) | %Δ (%) | $u_3$ (%) | %Δ (%) | $u_3$ (%) |
| NSRW | I | 0.5 | -48.6783 | -12.6422 | -5.5212 | -2.9619 | - | - | -1.5493 | -1.9834 | - | - | -6.8943 | -3.2838 | -80.7757 | -8.5760 | -5.2789 | -4.2527 |
| NSRW | I | 1 | - | - | -1.5239 | -1.4997 | - | - | -0.1194 | -0.5475 | -3.7784 | -3.7692 | -3.3595 | -2.2015 | 2.3658 | 1.9001 | -0.5729 | -1.0393 |
| NSRW | I | 5 | -18.8932 | -13.4144 | -6.1618 | -3.1597 | - | - | -1.1664 | -2.0384 | - | - | -7.7742 | -3.5121 | 191.7263 | 52.0968 | -2.5642 | -2.4459 |
| NSRW | I | 10 | - | - | -10.5947 | -3.3127 | - | - | -3.4422 | -1.8677 | -31.5950 | -7.9708 | -10.1664 | -3.2541 | - | - | -7.5277 | -6.3780 |
| NSRW | K | 0.5 | -57.6552 | -12.3615 | -3.4997 | -2.5360 | - | - | -0.1617 | -0.6725 | - | - | -4.9031 | -2.9764 | -83.4015 | -7.7464 | -2.7559 | -1.8423 |
| NSRW | K | 1 | - | - | -0.1098 | -0.3760 | - | - | -0.4998 | -1.1850 | -7.3797 | -3.5551 | -1.0939 | -1.1796 | -53.2205 | -10.9543 | -0.1998 | -0.9240 |
| NSRW | K | 5 | -62.3643 | -14.4244 | -3.5393 | -2.1592 | - | - | -1.2833 | -1.8659 | - | - | -4.4698 | -2.4137 | -73.7492 | -5.2525 | -1.4886 | -1.5466 |
| NSRW | K | 10 | - | - | -4.5205 | -2.3651 | - | - | -1.6379 | -1.6058 | -23.4026 | -8.3224 | -5.7858 | -2.6543 | - | - | -3.5210 | -4.5975 |
| NSRW | M | 0.5 | -85.5692 | -8.5687 | -5.2606 | -2.8832 | - | - | -0.5342 | -1.1484 | - | - | -7.7876 | -3.4575 | -81.9992 | -8.0486 | -0.9175 | -1.4902 |
| NSRW | M | 1 | - | - | -2.3143 | -1.6394 | - | - | -0.7287 | -1.2445 | 38.6362 | 16.0962 | -3.6957 | -2.0535 | -38.1499 | -8.4068 | 3.9775 | 3.7764 |
| NSRW | M | 5 | -97.8729 | -4.2345 | -11.0910 | -3.5166 | - | - | -3.1945 | -2.5183 | - | - | -9.9086 | -3.3466 | 216.7818 | 52.1039 | 12.3748 | 4.7071 |
| NSRW | M | 10 | - | - | -16.7431 | -3.9406 | - | - | -4.7127 | -3.5688 | 21.3693 | 8.1601 | -16.1217 | -3.8833 | - | - | 13.0343 | 9.0499 |
| EBSW | I | 0.5 | -2.2253 | -2.9599 | -0.9524 | -1.0061 | -0.5064 | -0.9230 | -1.5318 | -1.5075 | -1.6900 | -1.0423 | -3.5607 | -1.9150 | - | - | -0.6145 | -0.5919 |
| EBSW | I | 1 | 1.8555 | 1.8483 | 0.1387 | 0.4511 | 0.5468 | 0.8816 | -0.6350 | -0.9548 | -2.4625 | -1.7615 | 2.9640 | 2.1187 | - | - | -0.5288 | -0.8156 |
| EBSW | I | 5 | 1.7372 | 2.4947 | 0.2232 | 0.5981 | 0.7088 | 0.9263 | -0.2878 | -0.7271 | 0.7511 | 1.3625 | -0.1782 | -0.5330 | - | - | 1.4330 | 1.6215 |
| EBSW | I | 10 | -2.8810 | -3.1062 | -1.2665 | -1.3732 | -1.8960 | -1.7496 | -1.6363 | -1.8750 | -4.6218 | -2.5873 | -0.5557 | -0.9134 | - | - | -1.1582 | -1.8628 |
| EBSW | K | 0.5 | 3.6185 | 4.0336 | 2.4502 | 1.5745 | 3.7283 | 2.3967 | 3.4850 | 2.0957 | 0.0859 | 0.2880 | 0.2526 | 0.4994 | - | - | 3.5603 | 2.3712 |
| EBSW | K | 1 | 1.8129 | 2.2740 | 1.6086 | 2.4803 | 2.6847 | 2.2455 | 1.8940 | 1.8345 | -1.4900 | -1.3890 | 3.2235 | 3.5449 | - | - | 1.2717 | 1.4995 |
| EBSW | K | 5 | 6.0933 | 4.7548 | 1.5172 | 1.5771 | 4.9560 | 2.3247 | 4.7040 | 2.8073 | 5.2289 | 3.1221 | 3.6773 | 2.4872 | - | - | 4.6667 | 2.5846 |
| EBSW | K | 10 | -2.2731 | -3.2558 | -1.6395 | -1.6322 | -0.6507 | -0.7563 | -1.1678 | -1.4621 | -3.3265 | -2.2812 | -1.2730 | -1.4415 | - | - | -1.3401 | -1.9310 |
| EBSW | M | 0.5 | 4.1371 | 3.8566 | 2.4593 | 1.7481 | 2.7263 | 2.3133 | 2.7849 | 2.1299 | -1.1816 | -1.1448 | 2.0007 | 1.5724 | - | - | 3.9827 | 2.6793 |
| EBSW | M | 1 | 0.7655 | 1.1960 | 1.0388 | 1.4496 | 1.5485 | 1.4142 | 0.4681 | 1.0127 | -0.9468 | -0.9911 | 4.3934 | 3.0418 | - | - | 1.2409 | 1.3861 |
| EBSW | M | 5 | 0.3332 | 1.1968 | 4.1715 | 2.2665 | 0.8044 | 0.7022 | -0.3011 | -0.6806 | -1.8664 | -1.6100 | 3.2494 | 1.9893 | - | - | 9.5834 | 3.0207 |
| EBSW | M | 10 | -5.6463 | -3.6865 | 8.9485 | 4.4160 | -1.4944 | -1.7106 | -2.1839 | -1.6501 | -6.4350 | -2.9809 | 12.5383 | 5.3324 | - | - | 15.9580 | 7.7303 |

Table II-4: Tabulated percent change values calculated for the sorption experiments with natural river water and sea water, as described in Sec. II-2.4. Data include: %˜, the percent change in concentrations of each of the elements measured in solution after equilibration with the clays at a range of ionic strength conditions, as well as $u_3$, the cumulative error on each percent change value, as calculated in Sec. II-2.6.2. All percent change values and cumulative errors are in units of percent. Calculations are based upon the values in Table II-3. The elements analyzed are listed in the column headers. The water type, either North Saskatchewan River Water (NSRW) or English Bay Sea Water (EBSW), in each sample is listed in the first column. The mineralogy of the clay used in each experiment is listed in the second column and identified as I, K, or M, denoting either illite, kaolinite, or montmorillonite, respectively. The concentration of clay in each experimental suspension is listed in the third column, in units of g/L.

| Ion | Radius (Å) |
|---|---|
| $Br^-$ | 1.98 |
| $Ca^{2+}$ | 1.03 |
| $Cl^-$ | 1.80 |
| $Cs^+$ | 1.73 |
| $K^+$ | 1.41 |
| $Mg^{2+}$ | 0.70 |
| $Na^+$ | 0.97 |
| $SO_4^{2-}$ | 2.42 |
| $Sr^{2+}$ | 1.25 |

Table II-5: Ionic radii for cations and anions of interest to this study, in units of Angstroms. Values are calculated for ionic radii in solution, in octahedral coordination. From Marcus, 1983.

# CHAPTER III

# TRACE ELEMENT DISTRIBUTIONS IN SEDIMENT AND SURFACE WATERS FROM ARCACHON BAY AND THE GIRONDE ESTUARY, SW FRANCE

## 1.0 INTRODUCTION

Estuaries are complex environments characterized by multiple hydrodynamic influences and sediment sources. These qualities, in conjunction with the gradational nature of the transitions between continental to marine environments, pose considerable challenges to the interpretation and mapping of estuarine lithofacies in the rock record. The accurate attribution of these subsurface deposits to particular depositional environments is essential for reconstructing palaeoenvironmental and palaeoclimatic conditions and deciphering geologic histories. One of the most commonly used methods for establishing paleoenvironmental conditions from the rock record is trace fossil analysis (e.g. Gingras *et al.*, 2016). However, ichnological assemblages are not always reliable indicators of ambient salinity, and may vary in location, density, and diversity according to other parameters (e.g. Blanchet *et al.*, 2005). As such, this research explores geochemical techniques aimed at quantifying interpretations of depositional conditions in estuarine settings.

Modern estuarine environments are ideal settings for the study of the relationship between clay flocculation dynamics, salinity, and trace element distributions. Water salinity within an estuarine system varies spatially along its length and this variability results in different depositional patterns within sub-

environments of the system. The samples for this research were collected from the Arcachon Bay and Gironde estuary, both located in the Nouvelle-Aquitaine region of southwest France (Fig. III-1). These two environments differ in terms of their hydrodynamic regimes, and thus have contrasting spatial distributions and relative proportions of marine waters and river waters. Arcachon Bay is a wave-dominated system, while the Gironde Estuary is dominated by tidal-fluvial processes.The significant variation in aqueous geochemical conditions between these two systems may influence the evolution of their respective sediments. The objective of this study is to investigate sediment evolution in estuaries from a geochemical perspective for application to the rock record. To that end, we characterized the major and trace element distributions in sediment and surface water samples from two modern estuaries to assess the effects of contrasting hydrodynamic regimes on sediment geochemistry.

## 1.1 BACKGROUND

Lab experiments (Liu *et al.*, 2018; Tachi & Yotsuji, 2014; Turner *et al.*, 2006) and field studies (Lanceleur *et al.*, 2011; Elbaz-Poulichet *et al.*, 1996; Balistrieri *et al.*, 1981) have demonstrated the importance of fine sediments as sinks for trace elements in the environment. Adsorption, the electrostatic adhesion of an ion or molecule to a solid surface as a solvated complex, is the primary means by which clay particles scavenge trace elements from solution (Smith, 1999; Adamczyk & Warszynski, 1996; Calvert, 1990; Forstner & Wittman, 1979). This process is generally reversible: if the pH, ionic strength, or other

chemical conditions of the ambient solution change, then either desorption or ion exchange may occur (Tertre *et al.*, 2013; Comans *et al.*, 1991; Egozy, 1980). In this way, the distribution of specific trace elements between the solid and liquid phases of a system are dependent on the environmental solution chemistry. The logical extension of this relationship is that trace elements associated with clays have the potential to act as proxies for the geochemical conditions in which these sediments were deposited.

Sedimentary rocks tend to have similar chemical compositions with respect to rare earth elements (REEs); indeed, the measured abundances of REEs are relatively consistent across a wide variety of shales (Taylor & McLennan, 1985; Nance & Taylor, 1976). This congruence arises because the REEs in sedimentary rocks are typically sourced from the upper continental crust and concentrated by means of ubiquitous sedimentary processes (Haskin *et al.*, 1966; Goldschmidt, 1938).

However, if there are components in the sediment, such as organic matter, capable of sorbing or forming complexes with REEs, then the REE signature of the sediment may vary significantly from that one may expect from purely detrital accumulations. There is a large body of experimental evidence demonstrating the inverse relationship between high solution ionic strength and the proportion of specific cations that are adsorbed to clay mineral surfaces (e.g. Liu *et al.*, 2018; Fuller *et al.*, 2014; Missana *et al.*, 2014a, 2014b; Manning *et al.*, 1996; Comans *et al.*, 1991; Garcia-Miragaya & Page, 1976, among others). The continental to marine transition is marked by an overall increase in solution ionic strength due to

elevated concentrations of major element cations in marine waters. Assuming that these cations are competitors with trace elements for surface sites on fine particulate sediments, it may be possible to infer the depositional conditions of the sediments from their trace element assemblages.

It is essential to consider the effects of earlier processes in sediments' history to be able to recognize and define trace element signatures produced by environmental salinity. Ratios of trace elements in siliciclastic sediments are commonly employed to discriminate between different tectonic settings – e.g. oceanic island arc, continental island arc, active continental margin, or passive margin – and to aid in the interpretation of sediment provenance (e.g. Bhatia & Crook, 1986).

Felsic rocks are typically enriched in incompatible Th and La and depleted in compatible Sc and Co (Rudnick & Gao, 2014; Salters & Stracke, 2004). The opposite is true of mafic rocks, which tend to be depleted in Th and La, and enriched in Sc and Co (Rudnick & Gao, 2014; Salters & Stracke, 2004). Consequently, ratios of these elements can serve as indices of chemical differentiation, and allow the determination of the relative importance of mafic and felsic sediment sources.

Rocks of felsic composition typically have high $La_N/Yb_N$ ratios relative to rocks of mafic composition (Taylor & McLennan, 1985). Categorization of light rare earth elements (LREEs), medium rare earth elements (MREEs), and heavy rare earth elements (HREEs) in the literature has been somewhat variable. For the purposes of this research, LREEs will be defined as those with atomic numbers

57-61 (La, Ce, Pr, Nd), MREEs will be defined as those with atomic numbers 62-65 (Sm, Eu, Gd, Tb), and HREEs will be defined as those with atomic numbers 66-71 (Dy, Ho, Er, Tm, Yb, Lu).

The majority of REEs are trivalent. However, Eu can also assume a stable divalent state in reducing conditions, with the consequence that Eu tends to exhibit partitioning behaviour that differs slightly from that of the other REEs. While Eu (III) is incompatible with respect to magma, Eu (II) is compatible and may substitute for divalent $Ca^{2+}$ cations, a phenomenon most commonly seen in plagioclase (Sinha, 2012). The preferential incorporation of Eu into plagioclase, and chemical fractionation during magmatic differentiation, leads to anomalous Eu concentrations in most rocks.

### *1.1.1 CHEMICAL INDICES OF ALTERATION (CIA)*

The chemical index of alteration (CIA), first introduced by Nesbitt & Young (1982), is a quantitative estimate of the extent of chemical weathering undergone by siliciclastic sediments and sedimentary rocks. Feldspars comprise approximately 62% of the upper crust (Wedepohl, 1971), and hence constitute the dominant reactive minerals in upper crustal rocks. By this logic, the extent to which feldspar minerals have been converted to clay minerals via hydrolysis or similar processes is an appropriate measure of the degree of chemical weathering undergone by the sample as a whole (Nesbitt & Young, 1982). The equation used to calculate the CIA of siliciclastic sediments is premised on the differential stabilities of the major element cations during weathering processes: $Al^{3+}$ and $Ti^{4+}$

are generally immobile, while the cations $Ca^{2+}$, $Na^{+}$, and $K^{+}$ are more reactive and consequently, more subject to removal (Nesbitt & Young, 1982).

High CIA values can be correlated with low molecular proportions of $CaO^{*}$, $Na_2O$, and $K_2O$, and thus high degrees of chemical alteration, while low CIA values are indicative of high molecular proportions of these cations and thus represent low degrees of chemical alteration. To the best of the authors' knowledge at the time of this writing, the results presented in this paper are the first published CIA values for sediments in either Arcachon Bay or the Gironde Estuary.

### *1.1.2 DISTRIBUTION COEFFICIENTS (Kd)*

The widespread and continuous reactions between the solid and liquid phases of environmental systems require that field studies examine both water and sediment samples in order to constrain the effects of depositional setting on trace element behaviour, and vice versa. Defining the distribution of trace elements between solid and liquid phases of a system can give insight into the syn-depositional geochemical conditions and enhance our ability to characterize the system in detail. Distribution coefficients are specific to the environmental conditions for which they are calculated (e.g. Reardon, 1981), and therefore the ones presented here are only intended to inform our understanding of the specific areas of study, and not necessarily to be applied to other settings.

Within each of the the two marginal marine environments discussed in this paper, the sediments and surface waters are assumed to be derived from the same

source areas. Consequently, one would expect that the total REE content would be fairly consistent across the sampling locations within either the Gironde Estuary or Arcachon Bay, unless the REE distributions were affected by current depositional conditions.

## 1.2 STUDY AREA

### *1.2.1 GEOLOGICAL SETTING*

The Gironde is fed by the Dordogne and Garonne Rivers. The headwaters of the Dordogne River are located in the Massif Central region of southern France. The Massif Central contains Les Monts Dore, an eroded stratovolcano comprised of basalt, rhyolite, phonolite, and ignimbrite deposits overlying a crust of granitic and gneissic composition, and La Chaine des Puys, a series of trachytic cinder cones, lava domes and basaltic maars. Mont-Dore was active between 3.1 Ma and 1.1 Ma (Nomade *et al.*, 2014), and la Chaine des Puys began forming 100 ka and last erupted 4040 years before present (Condomines *et al.*, 1982). In addition to large volcanic deposits, this region also contains a multitude of thermal hot springs, such as Les Chaides Aigues, Vals-les Bains, and La Bourboule, among others. The Garonne River has its headwaters in the Aran Valley of the Spanish central Pyrenees, which are an intracontinental mountain chain formed during multiple orogenic cycles during the Cretaceous and early Eocene (Boillot & Capdevila, 1977).

Downstream, the Dordogne and the Garonne flow through the Aquitaine Basin, a foreland basin associated with the Northern Pyrenean thrust (Boillot &

Capdevila, 1977), before entering the Gironde Estuary. The two major freshwater sources to Arcachon Bay each have their source within the Aquitaine Basin: the headwaters of l'Eyre River are in the southern portion of the basin, while the Porges Canal has its headwaters in the northern tip of the basin. The stratigraphy of this foreland encompasses a wide variety of lithologies ranging in age from the Triassic to the Quaternary, and the rivers that feed the coastal environments of interest in this study may erode multiple intervals.

### *1.2.2 GIRONDE ESTUARY*

The Gironde is formed at the confluence of the Dordogne and Garonne rivers (Fig. III-3), which debouche into the Bay of Biscay and drain a watershed of 80,000 $km^2$ in area (Dabrin *et al.*, 2009). This estuary, the largest in Western Europe, measures 170 km in length and 635 $km^2$ in area (Dabrin *et al.*, 2009), and varies in width from 2 km to 12 km (Mikhailova & Isupova, 2006). Classified as a macrotidal estuary, the Gironde has tidal ranges that vary from 4 m up to 7 m, and has a tidal reach of 150 m upstream (Allen *et al.*, 1980). The Gironde, like many other macrotidal estuaries (e.g. Shchepetkina *et al.*, 2016; Ayles & LaPointe, 1996), displays a characteristic longitudinal zonation of facies (Dalrymple *et al.*, 2010). Allen (1991) described the Gironde as exhibiting a tripartite zonation, the characteristics of which are summarized in Table III-1. The mean annual freshwater discharge to this estuary is approximately $3.15 \times 10^{10}$ $m^3$ $s^{-1}$, and water has a residence time in the estuary of 0.5 to 3.0 months (Jouanneau & Latouche, 1981). Due to the high-frequency fluctuations as a function of seasonal and

temporal variations in tides, freshwater input, and wind regime, the salinity of the surface waters in the Gironde Estuary is difficult to quantify consistently. Measured salinity values in the distal portion of the Gironde are typically less than the average of 35.6 psu reported for the central Bay of Biscay, reaching average minimum values of ~31.2 psu during the winter and spring, and average maximum values of ~34.8 psu during the summer and early autumn (Lazure *et al.*, 2006). In the upper estuary, where fluvial influence is greater, the surface water salinity may be less than 1.0 psu (Kraepiel *et al.*, 1997). Although the maximum turbidity zone is quite pronounced in the upper estuary, its exact location varies significantly with seasonal freshwater input and tidal cycles (Doxaran *et al.*, 2009; Sottolichio & Castaing, 1999). The concentration of suspended particulate matter (SPM) in the maximum turbidity zone generally increases downward through the water column, amounting to 1 g/L in surface waters and $n \times 100$ g/L near the sediment-water interface (Doxaran *et al.*, 2009; Sottolichio & Castaing, 1999).

### *1.2.3 ARCACHON BAY*

Arcachon Bay is located just 100 km south of the Gironde Estuary on the southwestern coast of France (Fig. III-2). However, this bay differs significantly from the Gironde Estuary in terms of dimensions and hydrodynamic regime. The morphology of Arcachon Bay, covering 174 $km^2$, is often compared to that of an equilateral triangle with 20 km-long sides and a 3.8 km-wide inlet connecting it with the larger Bay of Biscay (Plus *et al.*, 2009). Formerly a wave-dominated estuary, Arcachon Bay has gradually become enclosed by the evolution of the

Cap-Ferret spit over the last 2800 years and now manifests as an ebb-dominated lagoon (Allard *et al.*, 2009), with a tidal range of 0.8 m to 4.6 m (Plus *et al.*, 2009). In terms of volume, the flux of seawater into Arcachon Bay from the external Bay of Biscay ranges between to 384 ~ $10^6$ $m^3$ during spring tide periods and 264 ~ $10^6$ $m^3$ during neap tide periods (Glé *et al.*, 2008). The Leyre River, at the southeastern margin of the lagoon, and the Porges Canal, at the northern margin, are the only freshwater inputs to the Bay. Fluvial influence on Arcachon Bay is moderate: the Leyre River and other secondary channels which debouche into the bay contribute a combined mean annual freshwater discharge of $1.25 \times 10^6$ $m^3$ (Glé *et al.*, 2008). In contrast to the Gironde Estuary, the Arcachon Bay exhibits a binary zonation, which many authors (e.g. Deborde *et al.*, 2008; Glé *et al.*, 2008) subdivide into an external, marine-dominated hydrological zone and an internal, continental-dominated zone, each of which are described further in Table III-2. The salinity of the surface waters is generally between 22 psu and 32 psu in the inner lagoon, and between 34 psu and 35 psu in the outer lagoon (Deborde *et al.*, 2008; Bouchet, 1968).

# 2.0 MATERIALS AND METHODS

## 2.1 SAMPLING SITES AND COLLECTION STRATEGY

During low tide periods in late June of 2017, sediment and water samples were collected from each of four locations in Arcachon Bay (Fig. III-2) and five locations in the Gironde Estuary (Fig. III-3). The sample locations in the Gironde Estuary formed a transect along the salinity gradient, and the Arcachon Bay

sample locations were distributed around the margins of the lagoon, so as to encompass a range of salinity and hydrodynamic energy conditions within both coastal sub-environments: inner and outer lagoon. Water samples were collected from the surface of the water column, in sterile polypropylene sample bottles that were subsequently sealed with laboratory film. Sediment samples were collected from the upper 15 cm of fine-grained deposits and sealed in two layers of plastic bags. All samples were kept refrigerated prior to analyses.

## 2.2 ANALYSIS OF WATER SAMPLES

In a class 1000 clean lab, water samples were filtered, acidified with trace metal grade nitric acid, and diluted by a factor of 25 in 2% trace metal grade nitric acid containing 2 ppb of indium for monitoring instrumental drift. Major elements were measured using a Jobin Yvon Ultima 2 ICP-AES, and trace elements using a Thermo ElementXR HR-ICP-MS, at the Pôle Spectrométrie Océan at the European Institute for Marine Studies in Brest. Both instruments were calibrated using commercial multi-element standards adjusted to seawater salinity with reagent-grade NaCl and accuracy was controlled by the repeated analysis of certified seawater reference materials CASS-4 and NASS-6. The ElementXR HR-ICP-MS was tuned to minimize the production of oxides and operated in low, medium, and high resolution modes as a function of the element analyzed. Precision of the method ranged from <2% (1 relative standard deviation) for elements measured in low resolution mode to circa 10-15% for insoluble elements analyzed in medium and high resolution mode.

## 2.3 ANALYSIS OF SEDIMENT SAMPLES

In the class 1000 clean lab, sediment samples were weighed before and after being heated to a temperature of 550˚ to quantify the loss on ignition (LOI). Samples were prepared for analysis by HF digestion. The major elements were measured using a Jobin Yvon Ultima 2 ICP-AES, and the trace elements were measured using a ElementXR HR-ICP-MS.

## 2.4 CALCULATIONS AND REPRESENTATIONS OF DATA

### *2.4.1 CRITICAL ELEMENT RATIOS (Eu/Eu*, Th/Co, La/Sc, $La_N/Yb_N$, Th/Sc, Zr/Sc)*

In this study, we plot the compositions of the sediment samples collected from Arcachon Bay and the Gironde Estuary on a cross plot of Th/Sc–Zr/Sc (*sensu* McLennan *et al.*, 1993), as well as ternary diagrams in Th–Co–Zr/10 space and Th–Sc–Zr/10 space (*sensu* Bhatia & Crook, 1986). The results of the samples from this study will be used to infer the tectonic setting and sediment provenance of the sediments collected from Arcachon Bay and the Gironde Estuary.

Ratios of light rare earth elements (LREEs) to heavy rare earth elements (HREEs) are used to infer source rock composition, in which La is used as a proxy for LREEs and Yb is used as a proxy for HREEs (Equation III-1).

$$\frac{La_N}{Yb_N} = \frac{[La]_{Sample}/[La]_{PAAS}}{[Yb]_{Sample}/[Yb]_{PAAS}} \qquad \text{(III-1)}$$

$$La_N = PAAS\text{–}normalized\ concentration\ of\ La$$

$$Yb_N = PAAS\text{–}normalized\ concentration\ of\ Yb$$

$$[La]_{Sample} = concentration\ of\ La\ measured\ in\ sample$$

$$[La]_{PAAS} = concentration\ of\ La\ in\ PAAS$$

$$[La]_{Sample} = concentration\ of\ La\ measured\ in\ sample$$

$$[Yb]_{PAAS} = concentration\ of\ Yb\ in\ PAAS$$

$$[Yb]_{PAAS} = concentration\ of\ Yb\ measured\ in\ samples$$

The enrichment or depletion of Eu relative to its neighbouring REEs, Sm and Gd, is quantitatively defined by calculating the ratio of the measured Eu concentration with the theoretical Eu concentration for a particular sample (Equation III-2, *sensu* Taylor & McLennan, 1985):

$$\frac{Eu}{Eu^*} = \frac{[Eu]_N}{\sqrt{[Sm]_N \times [Gd]_N}} \qquad \text{(III-2)}$$

$Eu = actual\ concentration\ of\ Eu\ measured\ in\ sample\ of\ interest$

$Eu^* = theoretical\ concentration\ of\ Eu, based\ upon\ relative$
$concentrations\ of\ Sm\ and\ Gd$

$[Eu]_N = concentration\ of\ Eu\ measured\ in\ sample\ of\ interest,$
$normalized\ to\ corresponding\ concentration\ in\ PAAS$

$[Sm]_N = concentration\ of\ Sm\ measured\ in\ sample\ of\ interest,$
$normalized\ to\ corresponding\ concentration\ in\ PAAS$

$[Gd]_N = concentration\ of\ Gd\ measured\ in\ sample\ of\ interest,$
$normalized\ to\ corresponding\ concentration\ in\ PAAS$

Interpretations of the Eu anomaly can vary. However, for this study, values of 0.95 or less are generally taken to indicate Eu depletion, while Eu enrichment is inferred from values of 1.05 or greater.

### *2.4.2 CHEMICAL INDEX OF ALTERATION (CIA)*

The CIA is expressed as a percent ratio between the molecular proportion of aluminium oxide to the sum of aluminium oxide, calcium oxide, sodium oxide, and potassium oxide (Equation III-3).

$$CIA = \left(\frac{Al_2O_3}{Al_2O_3 + CaO^* + Na_2O + K_2O}\right) \times 100\% \qquad \text{(III-3)}$$

$CIA$ = chemical index of alteration

$Al_2O_3$= molecular proportion of $Al_2O_3$in sample

$CaO^*$ = molecular proportion of $CaO^*$ in sample

$K_2O$ = molecular proportion of $K_2O$ in sample

$Na_2O$ = molecular proportion of $Na_2O$ in sample

$CaO^*$ is defined as the amount of calcium oxide that is contained exclusively in the siliciclastic fraction of the sample, corrected for the sample's carbonate and apatite content (Equation III-4):

$$CaO^* = CaO - \text{calcite} - \text{dolomite} - \text{apatite} \qquad \text{(III-4.0)}$$

$$\text{Calcite} = [CO_2]_{\text{moles}} = \frac{[CO_2]_{wt.\%}}{44.01} \qquad \text{(III-4.1)}$$

$$\text{Dolomite} = \frac{[CO_2]_{moles}}{2} \qquad \text{(III-4.2)}$$

$$\text{Apatite} = \frac{10}{3} \times [P_2O_5]_{moles} \qquad \text{(III-4.3)}$$

$$[P_2O_5]_{moles} = \frac{[P_2O_5]_{wt.\%}}{141.95} \qquad \text{(III-4.4)}$$

However, in cases where $CO_2$ data are not available, such as in this study, then an approximation of $CaO^*$ based upon the ratio of CaO to $Na_2O$ may be used (McLennan *et al.*, 1993). First, the molecular proportion of total CaO is corrected for apatite using the method above. The resultant apatite-corrected CaO value is

then compared with the molecular proportion of $Na_2O$: if the molecular proportion of CaO (excluding apatite) is less than the molecular proportion of $Na_2O$, then the apatite-corrected CaO value is taken to be $CaO^*$; however, if the molecular proportion of CaO, excluding apatite, is greater than the molecular proportion of $Na_2O$, then the value of the molecular proportion of $Na_2O$ is taken to be $CaO^*$ (e.g. Huang *et al.*, 2014; Singh, 2005). It should be noted that the CIA value calculated using this approximation of $CaO^*$ represents the minimum CIA for the sample analyzed, as Ca tends to be more labile than Na (McLennan *et al.*, 1993). CIA is graphically depicted in $Al_2O_3$-($Ca_2O^*$ + $Na_2O$)-$K_2O$ space on an A-CN-K ternary diagram.

### *2.4.3 DISTRIBUTION COEFFICIENTS (Kd)*

Distribution coefficients are calculated here as simple ratios between the concentration of the element of interest in the solid phase and the concentration of the element of interest in the liquid phase (Equation III-5).

$$K_d = \frac{[X]_{Dry\ solid}(mg\ kg^{-1})}{[X]_{Water}(mg\ L^{-1})} \qquad \text{(III-5)}$$

*X = element of interest*

*$K_d$ = distribution coefficient, or distribution coefficient, of X*

The resulting value is a dimensionless, linear distribution coefficient, typically expressed as Log(Kd) (e.g. Lanceleur *et al.*, 2011; Turner, 1996; Balls, 1989;). If the distribution coefficient of some element of interest, X, is less than 1, then element X is primarily concentrated in the aqueous phase of the system. If the enrichment factor of an element of interest is greater than 1, then element X is

primarily concentrated in the sediment fraction. Therefore, elements with smaller $K_d$ values have a greater proportion of their concentration in the aqueous phase of the system than do elements with larger $K_d$ values.

### *2.4.4 SUMS OF RARE EARTH ELEMENTS (∑REEs)*

The ∑REEs in a sample is calculated as the sum total of the parts per million abundance of all of the rare earth elements detected in a sample of interest (Equation III-6):

$$\Sigma(REEs) = \sum_{i=1}^{n}[X]_i \qquad \text{(III-6)}$$

In Equation III-6, $[X]_i$ may be equal to the ppm concentration of either La, Ce, Pr, Nd, Sm, Eu, Gd, Tb, Dy, Ho, Er, Tm, Yb, or Lu. There is no data available for Pr, Tb, Ho, Tm, or Lu in the sediment samples of this study, and so the ∑REEs values in the solids only include the concentrations of La, Ce, Nd, Sm, Eu, Gd, Dy, Er, and Yb. To determine spatial variations in REE content within each environment studied, the ∑REEs of each sediment and surface water sample are plotted in order of increasing marine influence, approximated by their proximity to the Bay of Biscay.

### *2.4.5 POST-ARCHEAN AUSTRALIAN SHALE-NORMALIZED RARE EARTH ELEMENT DIAGRAM (REEs-PAAS DIAGRAM)*

The concentration of REEs in the sediment sample of interest are normalized to the corresponding REEs concentrations in post-Archean Australian shale (PAAS: Taylor & McLennan, 1985) to minimize the effect caused by the

phenomenon in which elements with even atomic numbers are more abundant than elements with odd atomic numbers (Harkins, 1917; Oddo, 1914), and to determine specific compositional differences between the sample and PAAS, and thus infer specific conditions or processes at play in the deposition of that sediment. The values on each plot are concentration ratios, rather than measured values. A ratio greater than 1.05 is taken to indicate the enrichment of an element in the sediment sample of interest relative to the PAAS standard, while a ratio less than 0.95 is taken to indicate the depletion of an element in the sediment sample relative to the PAAS standard. A ratio between 0.95 and 1.05 indicates no change in the concentration of an element in the sediment sample of interest relative to the PAAS reference standard.

## 3.0 RESULTS

The weight percent oxide abundances of the major elements in each sediment sample are presented in Table III-3. Converted major element cation concentrations in ppm are presented in Table III-4. The major element content of each surface water sample is presented in Table III-5. The trace element content of the sediment samples and surface water samples are tabulated in Table III-6 and Table III-7, respectively.

### 3.1 CRITICAL ELEMENT RATIOS (Eu/Eu*, Th/Co, La/Sc, $La_N/Yb_N$, Th/Sc, Zr/Sc)

The Th/Sc and Zr/Sc ratios of sediments from Arcachon Bay and the Gironde Estuary are listed in Table III-8 and plotted against each other in Figure III-4. The majority of sediment samples from both Arcachon Bay and the Gironde Estuary plot within a narrow range, in between the values of 0.8 and 1.0. Essentially all of the sediment samples from Arcachon Bay and the Gironde Estuary in this study have Zr/Sc values less than 10.0. The compositions of the sediment samples from Arcachon Bay and the Gironde Estuary on the Th–Co–Zr/10 ternary diagram (Fig. III-5, top) exhibit narrow clustering near the centre of the diagram. In general, the Arcachon Bay samples appear to be slightly more enriched in Th those from the Gironde Estuary. This difference is much more apparent in Th–Co–Zr/10 space than in Th–Sc–Zr/10 space, indicating discrepancies between the Th/Co and Th/Sc ratios of the sediment samples. Sediment samples from the two coastal environments studied have similar proportions of Co, but differ slightly with respect to Sc, with the proportion of Sc in the Arcachon Bay sediments being elevated slightly above that in the Gironde Estuary sediments (Fig. III-5, bottom). Collectively, the Gironde Estuary sediments contain a greater proportion of Zr/10 than do the Arcachon Bay sediments. In Th–Co–Zr/10 space (Fig. III-5, top), all of the data points for the sediment samples plot within the field corresponding to sediments formed in an active continental margin setting (Bhatia & Crook, 1986), as do the Gironde Estuary sediment samples in Th–Sc–Zr/10 space (Fig. III-5, bottom). However,

the Arcachon Bay sediment samples plot outside of the active continental margin area by virtue of their relatively high proportion of Sc and relatively low proportion of Zr/10 (Fig. III-5, bottom).

The $La_N/Yb_N$ of the sediment sub-samples from Arcachon Bay have an average value of 1.30 at both Locations A3 and A4 (Table III-8). The $La_N/Yb_N$ ratios calculated for sediment sub-samples from the Gironde Estuary are comparable, and have average values of 1.27 at Location G1/5/6 (lower estuary), 1.24 at Location G2 (middle estuary), 1.28 at Location G3 (upper estuary), and 1.32 at Location G4 (fluvial: Garonne River) (Table III-8). However, the range of values is in fact quite narrow and indicates overall minor enrichment in LREEs compared to HREEs.

In the Gironde Estuary sediment samples, the average Eu/Eu* value is 1.00; the minimum and maximum are 0.86 (Sample G5-MDX) and 1.17 (Sample G1-MD-GS), respectively (Table III-8). In the sediment samples from Arcachon Bay, the average Eu/Eu* value is slightly higher, at 1.03; the minimum value is 0.97 (A3-MDX) and the maximum value is 1.12 (A3-MD-2) (Table III-8). Overall, the Eu/Eu* values in these two environments indicate a combination of non-existent to slightly positive Eu anomalies.

In the Gironde Estuary surface waters, the average Eu/Eu* value is 2.09; the minimum and maximum are 1.95 (Sample G1-SW-C) and 2.48 (Sample G5-SW-C), respectively (Table III-9). In the surface waters from Arcachon Bay, the average Eu/Eu* value is higher, at 2.91; the minimum value is 2.08 (A1-SW-C) and the maximum value is 3.33 (A3-SW-C) (Table III-9). All of the calculated

values of Eu/Eu* exceed 1.05, and therefore suggest Eu enrichment in the surface waters of both environments. This contrasts strongly with the Eu depletion normally observed for typical river water and seawater (e.g. Table III-9, this chapter; Taylor & McLennan, 1985).

### 3.2 CHEMICAL INDICES OF ALTERATION (CIA)

All of the Arcachon Bay and Gironde Estuary sediment compositions plot along the UCC-PAAS trend, which can be extrapolated to the illite composition (Fig. III-6). The chemical indices of alteration (CIA) for the Arcachon Bay sediment samples (Locations A3 and A4) range from 52.74 to 65.74, with a mean of 60.10, and those for the Gironde Estuary sediment samples (Locations G1, G2, G3, G4, G5, and G6) range from 45.48 to 70.76 with a mean of 64.02 (Fig. III-6, Table III-10). The CIA of both of the sediment samples from Location A4 in Arcachon Bay correspond to early stage weathering. At Location A3, the apparent weathering stages of the sediments are more variable: A3-MD-1 and A3-MD-2 have CIA values that correspond to an intermediate stage of weathering, while that of A3-MD-X corresponds to an early weathering stage (Fig. III-6, Table III-10). The majority of Gironde Estuary sediment samples have CIA values suggestive of an intermediate stage of weathering, with the exception of those from Location G1, which indicate an early weathering stage (Fig. III-6, Table III-10). The minimum CIA value for the Gironde Estuary samples corresponds to one (Sample G1-MD-GS) of the two samples from Location G1 and is less than the lower limit of early stage weathering (Fig. III-6, Table III-10).

## 3.3 DISTRIBUTION COEFFICIENTS (Kd)

The distribution coefficients ($K_d$) of the distribution of selected trace elements between the sediment and surface waters at each sample site are tabulated as log($K_d$) values in Table III-11. All of the calculated distribution coefficients presented here are greater than 1, and thus suggest an overall tendency of the analyzed trace elements to be concentrated into the solid phase of the system, in this case the fine sediment. Enrichment factors were also calculated for the major and trace elements in the sediment and surface water samples at each sample site; they are tabulated and described in greater detail in Appendix C.

The distribution coefficients of the transition metals and lanthanide/actinide elements measured in the Gironde Estuary are plotted as log($K_d$) values in Figure III-7 and Figure III-8, respectively, as a function of their proximity to the Bay of Biscay. Distribution coefficients could only be calculated for two out of the four sampling locations in Arcachon Bay, and therefore corresponding data for this study area were not plotted.

At all locations in the Gironde Estuary (Fig. III-7), the distribution coefficient of Zr is significantly greater than that of any of the other elements. This indication that Zr is highly concentrated in the sediment phase is congruent with a terrigenous clastic detrital source for this element. Conversely, the distribution coefficient of Sr is significantly lower than that of any of the other elements at all locations in the Gironde Estuary (Fig. III-7). This indicates that Sr is weakly concentrated in the sediment phase, an observation congruent with its relatively greater solubility and longer residence time in sea water compared to

the other elements plotted (Taylor and McLennan, 1985). The signatures of Sr and Zr appear to mirror each other: their distribution coefficients are relatively consistent between Locations G1/5/6 (lower estuary), G3 (upper estuary), and G4 (fluvial: Garonne River), with anomalies at Location G2 (middle estuary), where the distribution coefficient for Zr has a minimum and the distribution coefficient for Sr has a maximum. The distribution coefficients of the other transition metals plotted are intermediate between the values for Zr and Sr, and decrease slightly from Location G4 to G3 (Fig. III-7). Overall, Ba and Y become more highly concentrated in the sediment phase with increasing marine influence and display their lowest distribution coefficient values at Location G3 (Fig. III-7). Sc, Cr, V, Co, and Ni also become more concentrated in the sediment phase with greater proximity to the estuarine mouth, although their lowest distribution coefficient values occur at Location G2 (Fig. III-7). The chemical similarity between $Ba^{2+}$ and $Sr^{2+}$ is displayed in the fact that the $K_d$ values of both divalent cations abruptly increase at Location G2. By contrast, Rb is less concentrated into the sediment phase at locations closer to the mouth of the estuary (Fig. III-7).

The relationship between the distribution coefficients of the lanthanide/actinide elements and the location within the Gironde Estuary closely resemble those of Sc, Cr, V, Co, and Ni. An overall increase in the extent to which the lanthanide/actinide elements are sequestered in the sediment phase is observed in the transition from fluvial to coastal environments, and the lowest distribution coefficient values occur at Location G3 (Fig. III-8).

### 3.4 SUMS OF REEs (∑REEs)

The ∑REEs values of the sediment samples are several orders of magnitude greater than those of the surface water samples at all locations in either Arcachon Bay or the Gironde Estuary (Fig. III-9, Fig. III-10; Table III-8, Table III-9). This observation is congruent with the positive distribution coefficients of the REEs with respect to the sediment and surface waters in this study (Table III-11). In Arcachon Bay, the highest surface water ∑REEs values occur at Location A1 (inner bay), followed by, in decreasing order, A4 (inner bay), A2 (outer bay), and A3 (outer bay). A similar trend is seen in the Gironde Estuary: the highest abundances of ∑REEs in surface waters are measured at Location G3 (upper estuary), followed by, in decreasing order, G4 (fluvial: Garonne River), G2 (middle estuary), G1 (lower estuary), G6 (lower estuary), and G5(lower estuary).

### 3.5 POST-ARCHEAN AUSTRALIAN SHALE-NORMALIZED RARE EARTH ELEMENT DIAGRAMS (REEs-PAAS DIAGRAMS)

The sediment samples from Arcachon Bay and the Gironde Estuary exhibit generally similar patterns (Fig. III-11; Fig. III-12). On both plots, the PAAS-normalized REE signatures display a convex-upward morphology. In addition, there appears to be a binary grouping of samples in which the PAAS-normalized REE signature for each sediment sample falls into an upper category of relatively high $[X]_{sample}/[X]_{PAAS}$ values, or a lower category of relatively low $[X]_{sample}/[X]_{PAAS}$ values (Fig. III-11; Fig. III-12).

The plot of PAAS-normalized REE signatures of the the analyzed Arcachon Bay samples (Fig. III-11) shows that, in terms of REE concentrations relative to PAAS, the variability between sediment samples from the same location (e.g. Samples A4 and A4-MD) is similar in magnitude to the variability between sediment samples from different locations (e.g. A3-MD-X and A4). All of the signatures for the Arcachon Bay sediment samples display depletion in all REEs relative to PAAS, with the greatest degree of depletion in HREEs and moderate depletion in LREEs. The MREEs are the least depleted in all samples; there are some instances of an element's abundance in a sample being nearly equivalent to that in PAAS (e.g. Eu in A3-MD-1; Gd in A3-MDX). Measured REEs are consistently more depleted in Samples A3-MD-2 and A4-MD than in Samples A3-MDX, A3-MD-1, and A4. The abundance of Er relative to PAAS is highly variable between samples: in both of the sediment samples from Location A4, Er is strongly depleted relative to its neighbouring elements; in the three sediment samples from Location A3, the abundance of Er is relatively consistent with that of its neighbouring elements.

The plot of PAAS-normalized REE signatures of the the analyzed Gironde Estuary samples (Fig. III-12) looks quite similar to that for the Arcachon Bay samples (Fig. III-11). Most of the signatures for the Gironde Estuary sediment samples display depletion in all REEs relative to PAAS, with the greatest degree of depletion in HREEs and moderate depletion in LREEs. Similar to the Arcachon Bay samples, the MREEs in the Gironde Estuary samples are the least depleted. The abundances of Gd in Sample G2-MD-GS, Nd, Sm, and Eu in Sample G2-

MD-MT, and Eu in Sample G5-MDX are nearly equivalent to those in PAAS. In contrast to the Arcachon Bay samples, the abundances of Gd in Sample G2-MD-MT, Nd, Sm, Eu, and Gd in Samples G3-1 and G3-2, Sm and Gd in Sample G5-MDX, and Sm, Eu, and Gd in Sample G6 are enriched relative to their respective abundances in PAAS. Measured REEs are consistently more depleted in Samples G1-MD-GS, G1-MD-MT, G2-MD-GS, and G4 than in Samples G2-MD-MT, G3-1, G3-2, G5-MDX, and G6. Among the Gironde Estuary sediment samples, there is significant variation in their abundances of Er relative to PAAS. Er is strongly depleted relative to its neighbouring elements in Samples G2-MD-GS, G2-MD-MT, G3-1, G3-2, and G5-MDX, while in Samples G1-MD-GS, G1-MD-MT, and G6, the abundance of Er is relatively consistent with that of its neighbouring elements. Interestingly, the magnitude of a sample's negative Er anomaly appears to be inversely proportional to the magnitude of its positive Gd anomaly: samples for which Er is strongly depleted relative to neighbouring elements Dy and Yb also display strong enrichment of Gd relative to neighbouring elements Eu and Dy.

# 4.0 DISCUSSION

## 4.1 SEDIMENT PROVENANCE, COMPOSITION, AND ALTERATION

Typical Th/Sc ratios for the upper continental crust are approximately 1.0, and rocks of mafic composition tend to have Th/Sc ratios of less than 0.8 (McLennan *et al.*, 1993; McLennan, 2001; Taylor & McLennan, 1985). Zr/Sc ratios in excess of 10.0 have been interpreted by McLennan *et al.* (1993) to

indicate a significant degree of zircon addition through sediment recycling and re-working, which can be visualized along a trendline extending from the point Th/Sc = 1.0, Zr/Sc = 10.0. The proportion of Th in Arcachon Bay sediments was greater than that in Gironde Estuary sediments, suggesting a higher proportion of incompatible elements, and thus a slightly more felsic composition in Arcachon Bay sediments compared to Gironde Estuary sediments. The proportion of Zr measured in sediment samples from the Gironde Estuary was greater than that measured in Arcachon Bay. This observation implies a slightly larger flux of terrigenous detrital material into the Gironde Estuary than into Arcachon Bay. The zircon grains in the Gironde Estuary may be further concentrated by tidal current reworking. $La_N/Yb_N$ ratios, demonstrating slight enrichment of LREEs compared to HREEs, also may be associated with a felsic sediment source for both the Gironde and the Arcachon. These chemical differentiation indices are spatially variable and indicate mineralogical heterogeneity throughout both coastal environments. Similar to the case of the spatial distributions of ∑REEs, the Eu/Eu* values calculated for the sediment samples analyzed may vary significantly between sub-samples from the same location, suggesting that sedimentological heterogeneity largely determines Eu abundance. Whether the Eu anomaly is positive or negative in sedimentary rock depends upon whether a sample is enriched or depleted, respectively, in plagioclase or clays derived from the weathering of plagioclase (Sinha, 2012; Gao & Wedepohl, 1995), mafic detrital minerals (e.g. Mazzucchelli *et al.*, 1992), or typically Eu-rich mineral phases such as epidote (e.g. Frei *et al.*, 2004). Positive Eu anomalies may arise in

reducing conditions derived from oxygen-poor or anoxic diagenetic conditions and the subsequent reduction of $Eu^{3+}$ to the more mobile species $Eu^{2+}$ (Schieber, 1988), or from the high-temperature alteration of plagioclase in hydrothermal settings (e.g. Campbell *et al.*, 1988). Nakada *et al.* (2017) demonstrated that positive Eu anomalies can also occur in waters at relatively low ($\leq$ 100˚) temperature conditions, and that there is an inverse relationship between the amount of total REEs released during the degradation of plagioclase and the salinity of the ambient waters: as the salinity of the system increases, the amount of REEs that are mobilized into the aqueous phase during the breakdown of plagioclase decreases. The excursion of the Eu anomalies in the Arcachon Bay and Gironde Estuary sediment samples from the typically negative Eu anomalies of most sedimentary rocks (e.g. Table III-8, this chapter; Taylor & McLennan, 1985) implies localized enrichment of either plagioclase or other mafic grains in the sediments of the study area. The positive Eu anomalies in the surface water samples of this study could result from the chemical weathering of plagioclase and/or mafic minerals in the solid phase of the system. Furthermore, hypoxic conditions have been documented in both Arcachon Bay (e.g. Deborde *et al.*, 2008) and the Gironde Estuary (e.g. Lanoux *et al.*, 2013), presumably leading to the reduction of many dissolved species.

The observed low Zr/Sc values in sediments from both Arcachon Bay and the Gironde Estuary indicates a minimal degree of sediment recycling, congruent with the fact that the samples are modern sediments as opposed to ancient sedimentary rocks. The discrepancy in Zr/10 between samples from Arcachon

Bay can be explained by comparing the mean annual discharge of the rivers flowing into each of the two environments. The mean annual freshwater discharge in to the Gironde Estuary is $3.2 \times 10^9$ $m^3$ (Jouanneau & Latouche, 1981), orders of magnitude above the mean annual freshwater discharge of $1.25 \times 10^6$ $m^3$ measured for Arcachon Bay (Glé *et al.*, 2008). Lower-energy hydrodynamic conditions in the more sheltered environment of Arcachon Bay could also result in finer-grained sediment deposits or greater retention of neritic material, diluting the compositional signature of relatively coarse-grained terrigenous detritus. The Gironde Estuary also has a considerable fraction of fine sediments, due to high riverine flux, flocculation, and tidal concentration and reworking of fine sediments. However, the distribution of fine sediments within each of these two coastal environments is very different, due to their different morphologies and hydrodynamic regimes. This interpretation is supported by the greater proportion of Zr/10 in the Gironde Estuary sediments than in the Arcachon Bay sediments, and the presumed slightly larger flux of terrigenous detrital material into the Gironde Estuary than into Arcachon Bay. The relative proportions of Th, Co, and Zr/10 in the Gironde Estuary and, to a lesser degree, the Arcachon Bay sediments suggest a sediment source area influenced by an active continental margin. The compositions of the Arcachon Bay sediments plot as outliers on the Th–Sc–Zr/10 ternary diagram, and the relative proportions of Th, Sc, and Zr in the Arcachon Bay sediments do not coincide with any of the fields defined for a particular tectonic setting (Fig. III-5, bottom). However, we can infer an active continental margin influence on the sediment source area from the locations of the Massif

Central and Spanish Central Pyrenees relative to the Acquitaine Basin, which hosts Arcachon Bay. This discrepancy between the interpretations made from the Th–Sc–Zr/10 ternary diagram and those based on the drainage patterns and geologic history of the region indicate that using relative proportions of trace elements may not always be a reliable method for determining the tectonic setting of a sediment source area. Dubious relationships between tectonic setting and trace element ratios would be even more difficult to resolve in ancient systems, and caution should be exercised when using these tools.

The trajectory of of the chemical indices of alteration (CIA) in the Arcachon Bay and Gironde Estuary sediments suggest a tendency towards illitization, rather than kaolinitization. This trend also corresponds to that predicted for the degradation of upper continental crust (UCC) to post-Archean Australian shale (PAAS), even with the minimum CIA values calculated with the $Na_2O$ method for estimating CaO* proportions. Therefore, the alteration process of K-metasomatism, whether by replacement of kaolinite to illite, or the conversion of plagioclase to K-feldspar, is not considered to apply to the sediments studied here. However, petrographic data would be needed to confirm this interpretation (*sensu* Fedo *et al.*, 1995).

The discrepancies between the CIA of the sediment samples from Locations A3 and A4 in Arcachon Bay are likely the result of the differing hydrodynamic regimes between the outer estuary and inner estuary. The consistent observation of CIA values that correspond to early stage weathering in sediment sub-samples from Location A4 (inner lagoon, near the L'Eyre River

Delta) are representative of the greater degree of fluvial influence and comparatively low sediment residence time in this part of the bay. The mixed early and intermediate weathering stages apparent in sediment samples from Location A3 are likely a function of the greater marine influence in this part of the bay, as sediments would be reworked more extensively in the outer lagoon by wave action. The intermediate stage of weathering inferred for the majority of Gironde Estuary sediment samples is congruent with continental sediments transported a significant distance from their source area and redistributed throughout the estuary by tides. Tidal energy is likely the dominant textural and mineralogical maturing process. The anomalously low CIA values observed in the samples from Location G1 may be due to a localized concentration of mafic minerals.

The tectonic setting and sediment composition of both Arcachon Bay and the Gironde Estuary are complex and multivariate, and so it is difficult to determine the relative significance of various influences such as sediment source formations and chemical weathering processes. Nevertheless, it is clear that these factors exert a strong chemical signature on the sediments in these coastal systems. This relationship poses severe complications to the objective of using trace elements in estuary sediments of the rock record to interpret syn-depositional geochemical conditions: it would be nearly impossible to ascertain whether measured trace element distributions are ascribable to the sediment source or the depositional conditions. This conclusion is similar to that drawn by other authors (Nath *et al.*, 2000), who performed analogous geochemical analyses

of muddy sediments in a lake and continental shelf fed by multiple rivers from different source areas in India. As in this research, Nath *et al.* (2000) observed that the trace element signatures of the sediments differed significantly from the UCC and that there were no appreciable variations between sediments from fluvial, brackish, or marine settings. Our results closely correspond with those for a study area with notably different depositional system and climate (Nath *et al.*, 2000). This provides compelling evidence in support of sediment source composition and weathering exerting primary control on trace element distributions in sediments, perhaps universally.

However, we believe that future work would do well to exclusively analyze clay minerals exclusively, rather than bulk sediment samples. The chemical weathering of silicate minerals to clays has the potential to cause leaching or re-distribution of the associated trace elements, and the high cation-exchange capacity of clays with respect to trace elements in their environment of deposition could allow for the chemical signature of the sediment source to be overprinted with that of the depositional environment.

## 4.2 RARE EARTH ELEMENT (REE) AND TRACE ELEMENT DISTRIBUTIONS AND TRENDS IN SEDIMENTS AND SURFACE WATERS

Values of ∑REEs in surface waters decrease with increasing marine influence (approximated by proximity to the basin). This observation is in agreement, *sensu lato*, with data from many other authors demonstrating that

∑REEs are more abundant in typical river water than in typical sea water (Table III-8; Table III-9). However, it should be noted that the ∑REEs calculated for the surface waters in this study are significantly larger than those published for typical river and sea water (Broecker & Peng, 1982; Li, 1982; Martin *et al.*, 1976, as found in Taylor & McLennan, 1985). There are several possible explanations which may account for this discrepancy. As Li (1982) pointed out, the proportions and flux of elements varies widely between river mouths around the world, due to differences in regional geology and climate, as well as varying types and extents of anthropogenic activities.

Although the area of interest in this study is generally considered to be subject to a lower degree of pollution than many other watersheds by virtue of its relatively low population density, it is apparent that agriculture, industry, and transportation are significant influences in this region. In particular, the Er and Gd anomalies observed in the REEs-PAAS diagrams are inferred to be anthropogenic, based upon similar REEs-PAAS signatures for the Neuse River, North Carolina (Smith & Liu, 2018). The muddy sediments of the Gironde Estuary are frequently dredged to allow the passage of boats, and Arcachon Bay has extensive oyster farms. Each of these activities could disturb the sediment deposits in their respective environments, perhaps displacing and redistributing any REEs originally associated with the particulate phases. However, the sediment REE concentrations are relatively high throughout fluvial-dominated and marine-dominated locations within both Arcachon Bay and the Gironde

Estuary. This consistency suggests the the REEs in these sediments are inherent and resulting from the source rock composition, as opposed to anthropogenic.

The binary distribution of of REEs-PAAS signatures for sediment samples does not appear to be related to sample location within either of the coastal environments studied. Relatively high $[X]_{sample}/[X]_{PAAS}$ values and relatively low $[X]_{sample}/[X]_{PAAS}$ values frequently co-occur in sub-samples of sediment from the same location. These observations contradict the interpretation that REE distributions within estuarine sediments change as a function of location, and consequently syn-depositional salinity. It is similarly unlikely that redox state can be invoked as a determining factor of PAAS-normalized REE variability between samples. Each of the sediment samples were collected from a similar depth interval relative to the sediment-water interface, well within the suboxic zone, and analyzed as bulk sediment samples.. A convex-upward morphology is common to the REEs-PAAS signatures for all of the sediment samples from both coastal environments. It follows that this general chemical signature is imparted by some condition common to all sample locations. Freslon *et al.* (2014) described similar trends of elevated MREE concentrations in PAAS-normalized REE patterns for sedimentary organic matter, and attributed these REE distributions to biogeochemical processes. This provides strong support for a biological control on REE signatures in the sediments of Arcachon Bay and the Gironde Estuary. Previous work by Leybourne & Johannesson (2008) has indicated that sedimentary organic matter, along with Fe- and Mn-hydroxides, is one of the primary sinks for REEs and Y in modern fluvial environments. Following this

reasoning, it is probable that whether a sediment sample is classified as having relatively high $[X]_{sample}/[X]_{PAAS}$ values or relatively low $[X]_{sample}/[X]_{PAAS}$ values is determined by the amount of organic matter present in the sediment. Organic matter may be quite localized within sediments, introducing significant heterogeneity within sub-samples from the same location.

In both Arcachon Bay and the Gironde Estuary, the ∑REEs in the sediment samples vary less between sample locations within each system, and less between the two systems studied, than do the surface water samples (Fig. III-9; Fig. III-10). In fact, some of the more significant discrepancies in ∑REEs values occur between sub-samples from the same location (e.g. A3-B vs. A3-C, Fig. III-9; G2-A vs. G2-B, Fig. III-10). This observation suggests that the abundance and distributions of REEs in these systems is controlled by factors other than aqueous chemistry and hydrodynamic conditions. As a result, we infer that these sediments are heterogeneous in properties and, perhaps, provenance.

Distribution coefficients calculated for REEs and other trace elements in both coastal environments studied suggest that these elements tend to become increasingly concentrated in the sediment as marine influence increases. This interpretation is supported by the ∑REEs values measured in the water samples from Arcachon Bay and the Gironde Estuary, which appear to decrease in a seaward direction. These two observations are congruent with an interpretation of extensive REE and trace element removal from the water column by fine sediments in the upper to middle estuary. Fine siliciclastic sediments may sequester large amounts of REEs, as they contain intrinsic REEs from their source

material, in addition to dissolved REEs that they adsorb from their environment (McLennan *et al.*, 1990; Taylor & McLennan, 1985). However, the mass of inorganic chemical species delivered to oceans in particulate form far exceeds that in dissolved form (Milliman & Meade, 1983; Garrels & Mackenzie, 1971). This implies that the majority of REEs measured in sediments from the Gironde Estuary and Arcachon Bay are inherent in the mineral crystal structure of the sediments, rather than adsorbed from the water column. Indeed, the ∑REEs values measured in the sediment samples from Arcachon Bay and the Gironde Estuary do not exhibit significant differences between different sampling locations in either study area, which could be the result of the small magnitude of the change in ∑REEs relative to the magnitude of absolute ∑REEs measured for each sediment sample.

The scavenging of trace elements from the water column by fine sediments in the upper estuary is a plausible mechanism for the increase in $K_d$ values and decrease in the aqueous ∑REEs values towards the marine basin, as described above. However, many trace elements are in fact structurally bound to the clay mineral lattice through isomorphic substitution, and are thus present in quantities that are unrelated to the ambient water chemistry. HF digestions of bulk sediment samples, as used in the analyses presented here, release all trace elements from the clay lattice. Therefore, it is impossible to discern which elements were sorbed to the clay mineral surface, and which elements were integrated into the structure of the clay, from the dataset of this study. Sequential extractions of the elements desorbed from the clays (*sensu* Keene *et al.*, 2014;

Poulton & Canfield, 2005) would determine the proportion of each element that is reversibly sorbed as opposed to structurally bound. This distinction is significant, as it is probable that the percent changes in ∑REEs between sediment samples, within the reversibly sorbed fraction of the elements analyzed, are much greater in magnitude than those presented here.

It appears that the trace element and REE signatures of the sediment samples are more likely to reflect their source area and composition than their current aqueous geochemical settings. We infer that the inverse relationship between ∑REEs abundance in surface waters and proximity to the marine environment is more likely to be a function of early removal of REEs from solution in the upper estuary, than of the actual geochemical conditions in the water column. Thus, we do not consider either salinity or redox state to be significant influences on the abundance and relative proportions of REEs in the estuarine sediments presented here. The discrepancies in REE and trace element distributions between sediment sub-samples from the same location suggest a certain degree of heterogeneity within the sediment samples. Such heterogeneity could be contributed by either mineralogy and grain size variations in the sediment itself, or variable organic matter contents.

There is an inverse relationship between sediment grain size and trace element content (e.g. Regnier & Wollast, 1993). This is due to the fact that fine sediments have relatively high surface areas, and thus high concentrations of reactive surface sites, resulting in an increased capacity to sorb trace element cations from solution. Within coastal environments, grain size is controlled by

hydrodynamics: deposition of mud occurs primarily in the freshwater-saltwater mixing zone (Dashtgard *et al.*, 2012). Consequently, the locus of fine-grained sedimentation emulates the location of the turbidity maximum. In the Gironde, the turbidity maximum zone migrates considerably according to seasonal changes in tidal flux and and riverine discharge (Doxaran *et al.*, 2009; Jalón-Rojas, 2015). Despite this migration, the sediment deposits of the Gironde Estuary still exhibit relatively consistent longitudinal zonation, whereby sediment grain size generally decreases with increasing distance from the sediment source (Allen, 1991). If grain size were the primary control on REE and trace element distributions in the sediment samples, then the REE and trace element content of the bulk sediments would vary spatially. However, in this study we preferentially sampled from mud deposits, which were found in abundance throughout the Gironde Estuary and Arcachon Bay. This suggests that the relationship between sediment grain size and REE and trace element abundances is not especially relevant for the purposes of this study. Our comparisons of REE abundances between samples from the same sediment size fraction suggest no significant variation between different locations within each depositional system, implying that there is not a strong correlation between the distance the sediments were transported from their source and their REE content.

Some slight mineralogical variability in sediments is indicated by the chemical indices of differentiation discussed in Sec. III-4.1. However, the siliciclastic sediments within each coastal environment investigated here are assumed to be derived from the same continental source area. Therefore, any

appreciable differences in mineralogy would arise from the chemical maturity of sediments increasing along the length of the estuary as they are progressively altered from their original composition.

As mentioned previously, the REE and trace element distributions in the sediment samples analyzed in this study do not follow a spatial trend. This observation precludes the interpretation that either grain size or mineralogy are the primary controls on the variability of REE and trace element content in sediments of Arcachon Bay and the Gironde Estuary. An explanation may be found by considering the organic matter present in the sediments of interest. The distribution of organic matter in sediments may be sufficiently localized to contribute a significant degree of heterogeneity to sediment deposits in similar areas. In Arcachon Bay and the Gironde Estuary, this heterogeneity appears to be spatially unpredictable. This calls into question the clarity and ease with which trace element assemblages may be used in paleoenvironmental reconstructions of marginal marine environments such as estuaries and bays.

## 4.3 IMPLICATIONS

There is a large body of literature on trace elements as indicators of the geochemical conditions of the environments in which they occur. Several different studies have utilized trace elements in mudstones as proxies of paleoclimate (e.g. Johnson *et al.*, 2006; Wei *et al.*, 2004), paleoproductivity (e.g. Large *et al.*, 2015, 2014; Dymond *et al.*, 1992), and paleoredox (Dahl *et al.*, 2013; Algeo & Lyons, 2006; Rimmer, 2004) conditions. However, the findings of this

study emphasize the complexity of interpreting the depositional environmental conditions of fine-grained siliciclastic sedimentary rocks based upon their geochemical signatures.

Distribution coefficients calculated for REEs and other trace elements in both coastal environments studied suggest that these elements tend to become increasingly concentrated in the sediment as marine influence increased. However, absolute abundances of REEs in sediments did not vary significantly throughout the estuary. Scavenging of trace elements from the water column by fine sediments is proposed as the mechanism driving the change in aqueous REEs content along each estuary, although further experiments involving sequential extractions of elements from the sediment samples are needed to confirm this hypothesis. Therefore, we conclude that the preservation potential of REEs in fine siliciclastic sediment deposits may not be universally sufficient for the interpretation of syn-depositional aqueous geochemical conditions from the rock record.

In the case presented here, the *spatial variability* of REE and trace element concentrations in sediments is not predicated on mineralogy, grain size, salinity, or redox, but rather on organic matter identity and abundance. However, the *identity* and *relative proportions* of the REE and trace element assemblages may be dictated by such factors as the composition of the sediment source, the extent of chemical weathering, and hydrodynamic regime. The latter point is in turn influenced by climate, seasonality, and tidal cycles, all of which may vary considerably over geologically short time scales. All of this to say that the factors

controlling trace element distributions in the rock record are multivariate and non-ubiquitous. As such, aqueous geochemical conditions may not have as high a preservation potential as previously supposed. A thorough knowledge of the sedimentary processes and sedimentary environment involved in the deposition of a particular sedimentary succession is thus essential when attempting to infer paleoenvironments from trace elements in the rock record.

## 5.0 CONCLUSION

This chapter presents geochemical data for sediment and surface water samples collected from two modern coastal environments in southwestern France: Arcachon Bay and the Gironde Estuary. The primary aim of this research was to characterize the evolution of sediments between proximal and distal sub-environments of modern estuaries with tidal-fluvial and wave-dominated hydrodynamic regimes. By so doing, we intended to develop an analogue for trace element distributions in sedimentary rocks deposited in sub-environments of varying geochemical conditions.

Trace element ratios of sediment samples from both Arcachon Bay and the Gironde Estuary are indicative of a sediment source with a mixed felsic and mafic composition derived from an active continental margin setting. The chemical indices of alteration calculated for the sediment samples in this chapter represent the first recorded CIA values for either Arcachon Bay or the Gironde Estuary, and indicate that these modern sediments have undergone a combination of early and intermediate weathering. A lack of detailed mineralogical and grain size data

precluded the differentiation of geochemical signatures based upon sediment type, and inhibited corrections for sediment heterogeneity. The REE and trace element distributions measured in the sediment samples of both environments did not show clear, spatially-correlative trends, which causes us to conclude that these parameters are not controlled by variations in salinity, redox state, grain size, or mineralogy. However, future experiments to distinguish between structural and reversibly sorbed trace elements in each sediment sample may allow the amount of trace elements that are adsorbed by sediment to be correlated to that sediment sample's location within an estuary. The diversity and abundance of REEs and trace elements available in the system is a function of the source rock composition and tectonic setting, as well as the weathering and alteration processes of the system. Conversely, the preservation potential of REEs and trace elements in sediments is controlled primarily by their organic matter content. Although sediment is well mixed by tidal processes, mineralogical variability and organic matter distributions are the main agents of geochemical variability.

In summary, trace element assemblages in sedimentary rocks are more likely to be indicative of the sediment source and organic matter content, rather than the geochemical conditions at the time of deposition. The sediment source area for Arcachon Bay and the Gironde Estuary, like most sedimentary environments, has a convolute geologic history and multi-lithic composition. This, in conjunction with the unpredictable distributions and unknown quantities and types of sediment-associated organic matter, renders accurate and precise interpretations of geochemical signatures in sediments exceedingly difficult.

Moreover, the variables of sediment source composition, chemical weathering processes, and organic matter distributions differ significantly between different depositional systems. Individual estuaries located in regions with mutually distinct prevailing climates, ecological communities, and the tectonic settings of their sediment source and sink areas will manifest geochemically variable sediment deposits. In light of these results, the use of trace element geochemistry to infer syn-depositional conditions is somewhat problematic to the complexity of the systems of interest and often insufficient ability of sediments to accurately preserve signatures corresponding to their syn-depositional geochemical conditions. Further research on the interplay between all of these factors, and the ubiquity or otherwise of these relationships between different environments and time periods, is essential.

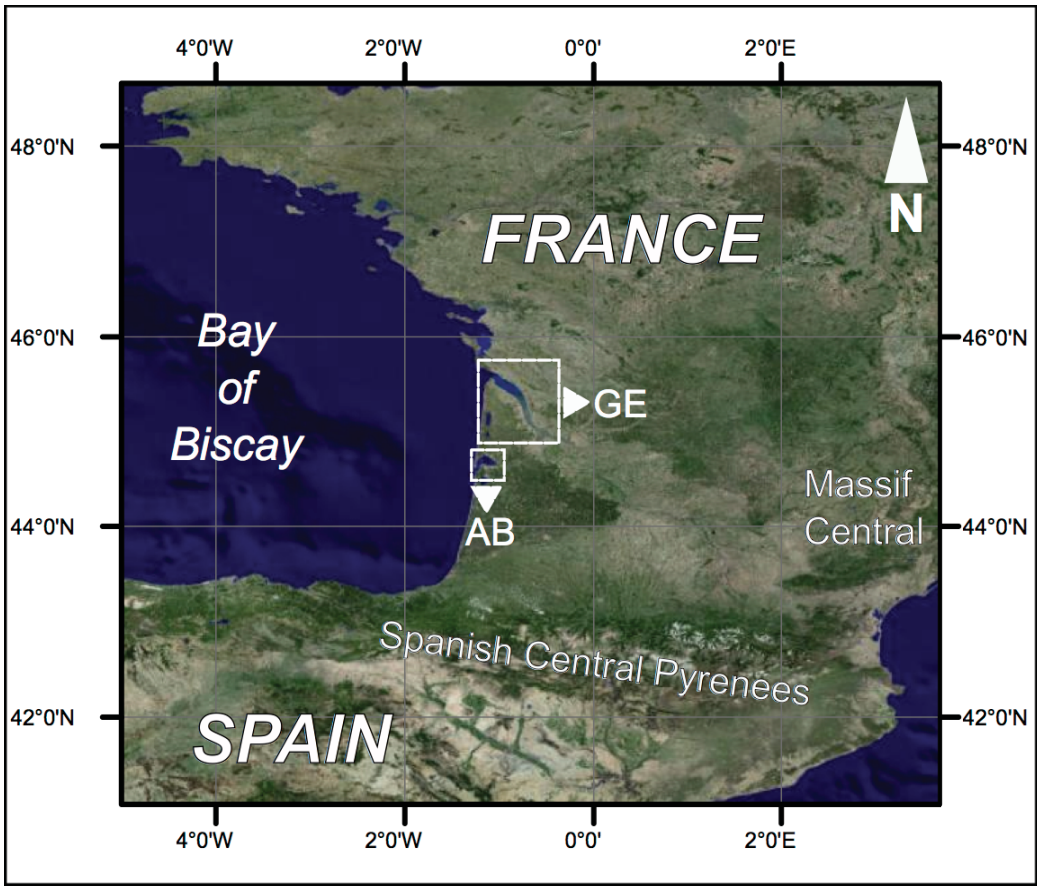
4°0'W
2°0'W
0°0'
2°0'E
48°0'N
46°0'N
44°0'N
42°0'N
FRANCE
N
Bay
of
Biscay
GE
AB
Massif
Central
Spanish Central Pyrenees
SPAIN

Figure III-1: Satellite image of southwestern France, northern Spain, and the Bay of Biscay at a scale of 1:300,000. The locations of Arcachon bay (AB) and the Gironde Estuary (GE) are marked with white boxes.

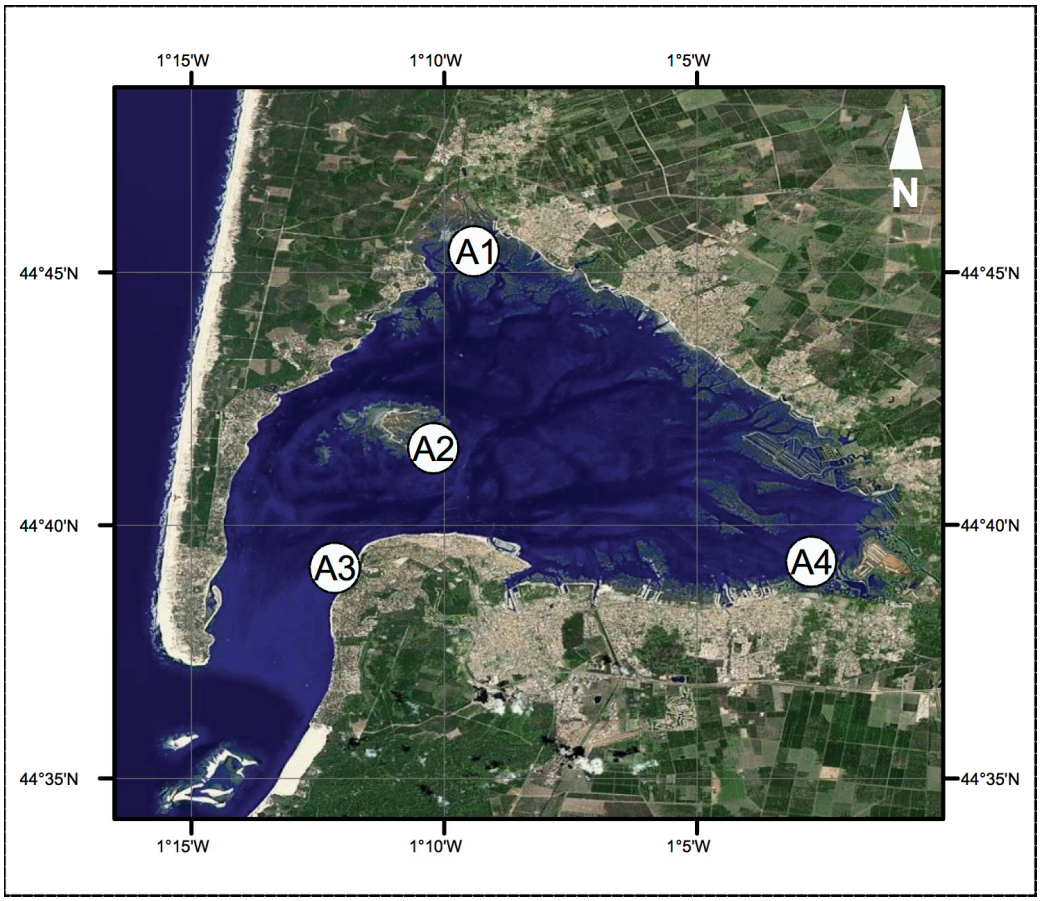
1°15'W
1°10'W
1°5'W
44°45'N
44°40'N
44°35'N
N
A1
A2
A3
A4

Figure III-2: Satellite image of Arcachon Bay, annotated with the names and locations of the four sampling locations: A1, A2, A3 and A4. Scale is 1:300,000.

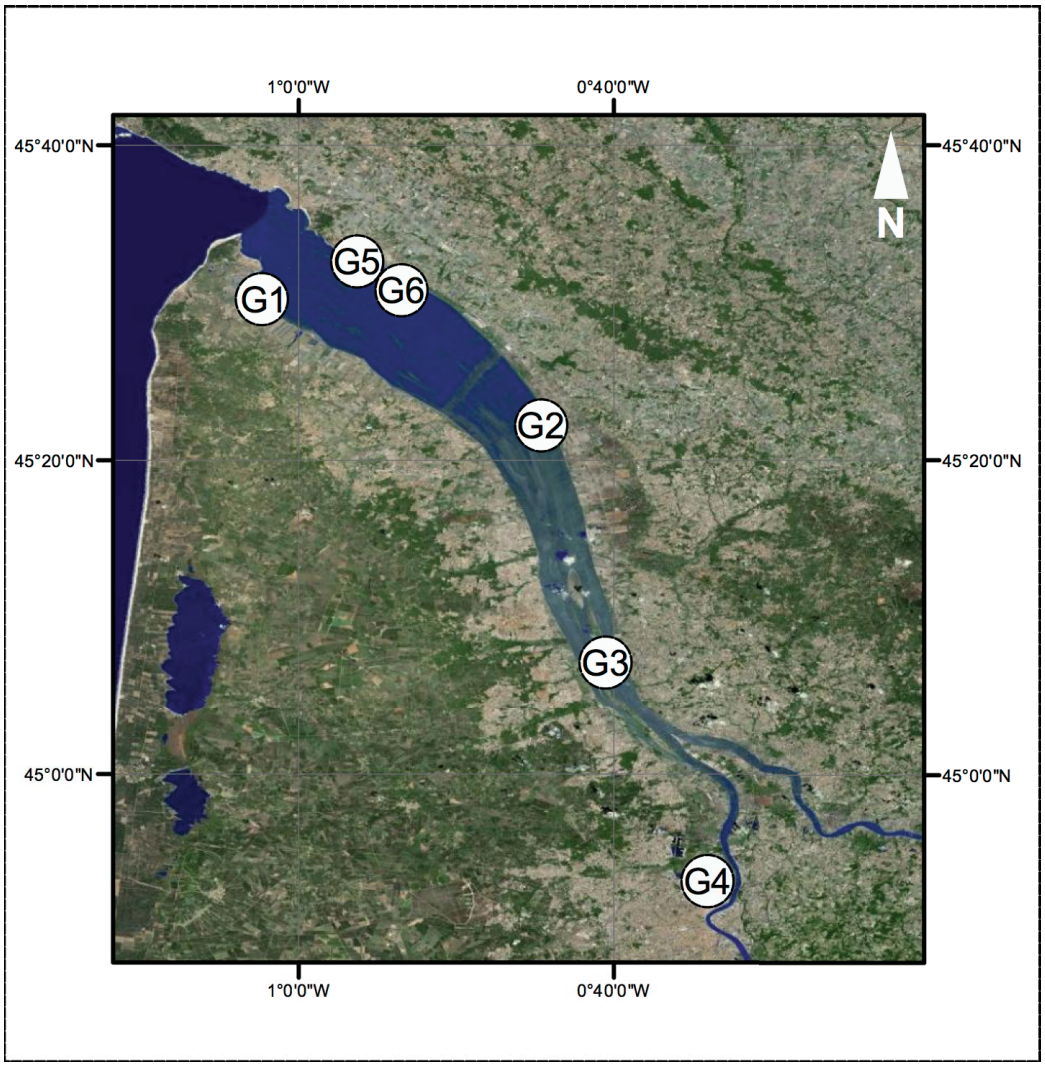
1°0'0"W
0°40'0"W
45°40'0"N
45°20'0"N
45°0'0"N
N
G1
G5
G6
G2
G3
G4

Figure III-3: Satellite image of the Gironde Estuary, annotated with the five sampling locations: G1, G2, G3, G4, and G5/6. Scale is 1:1,000,000.

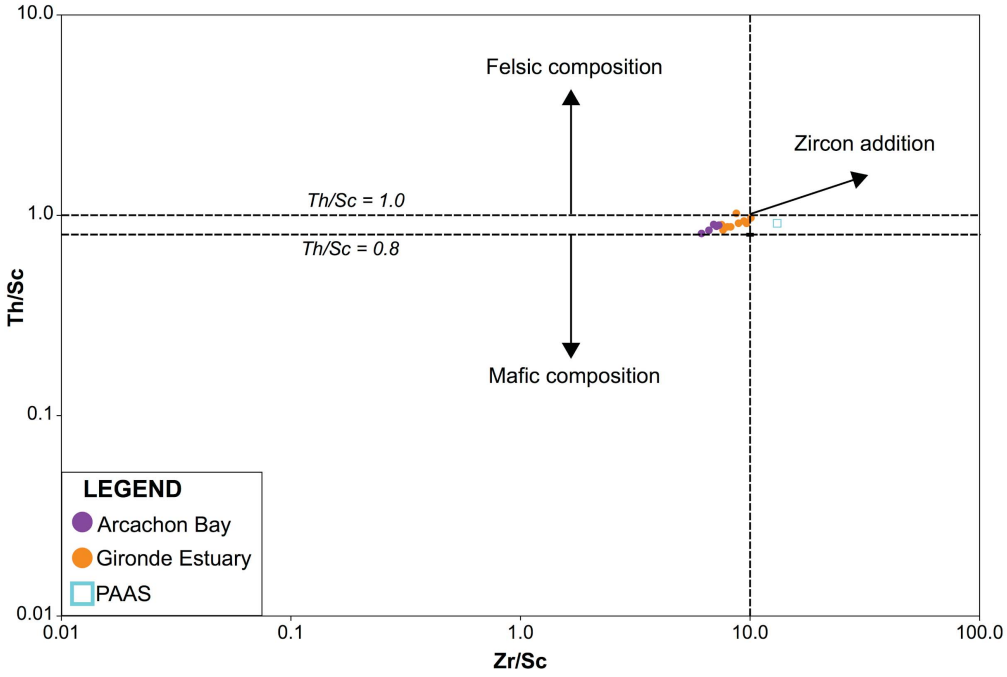
10.0
1.0
0.1
0.01
Th/Sc
Felsic composition
Zircon addition
Th/Sc = 1.0
Th/Sc = 0.8
Mafic composition
LEGEND
Arcachon Bay
Gironde Estuary
PAAS
0.01
0.1
1.0
10.0
100.0
Zr/Sc

Figure III-4: Cross-plot of Th/Sc as a function of Zr/Sc for the Arcachon Bay and Gironde Estuary sediment samples from this study, as well as the post-Archean average shale (PAAS: Taylor & McLennan, 1985) reference composition. Plot divisions are based on those of McLennan *et al.* (1993). The element ratios are dimensionless. See Table III-6 for tabulated trace element data.

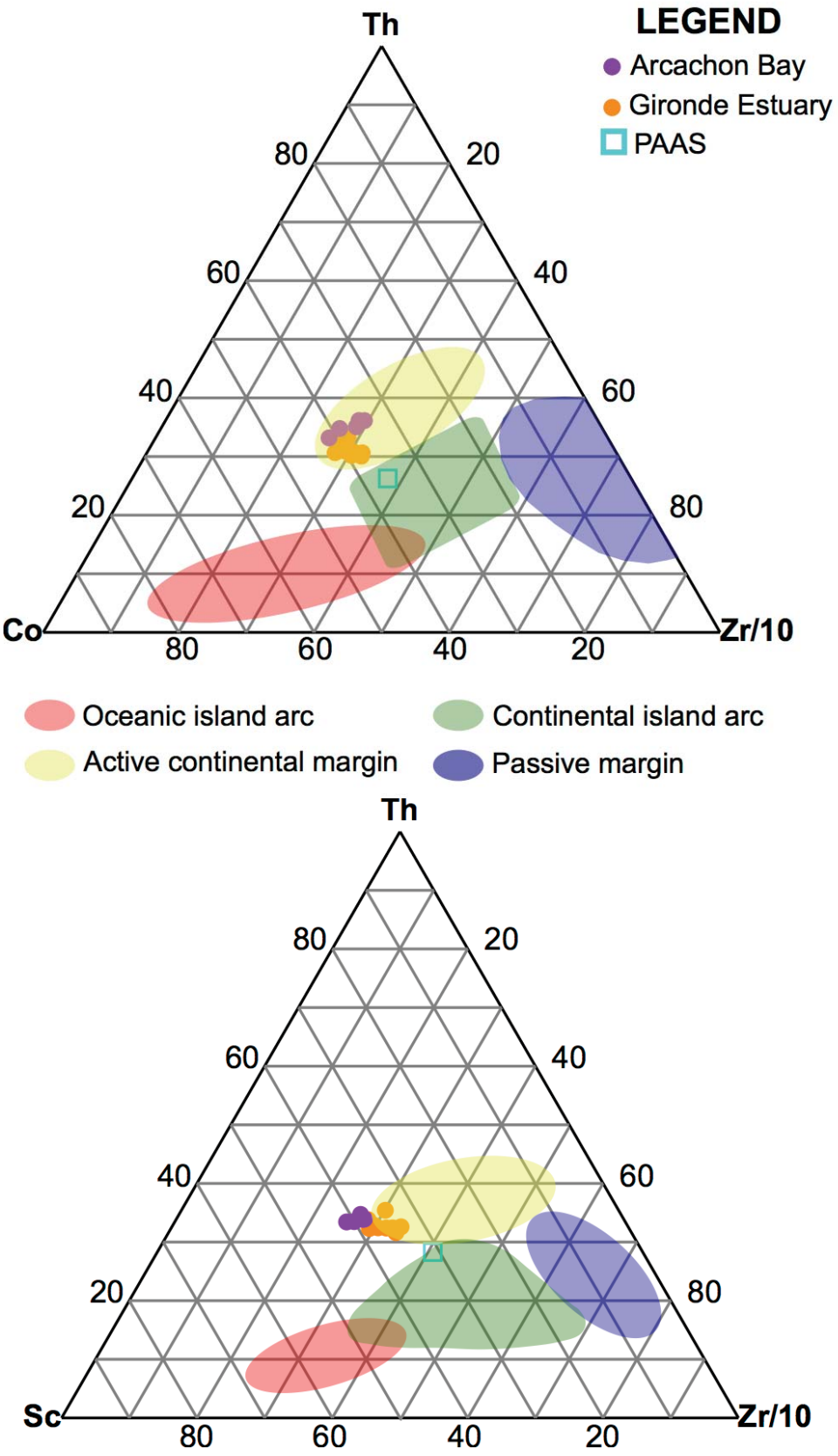
Th
LEGEND
Arcachon Bay
Gironde Estuary
PAAS
80
20
60
40
40
60
20
80
Co
80
60
40
20
Zr/10
Oceanic island arc
Continental island arc
Active continental margin
Passive margin
Th
80
20
60
40
40
60
20
80
Sc
80
60
40
20
Zr/10

Figure III-5: The compositions of the Arcachon Bay and Gironde Estuary sediment samples of this study, along with the composition of post-Archean average shale (PAAS: Taylor & McLennan, 1985) on ternary plots of the relative proportions of (top) Th, Co, and Zr/10, and (bottom) Th, Sc, and Zr/10. See Table III-6 for absolute concentrations of these elements in each sample. Shaded fields correspond to typical compositions of sediments from various tectonic settings and are based on those defined by Bhatia & Crook (1986).

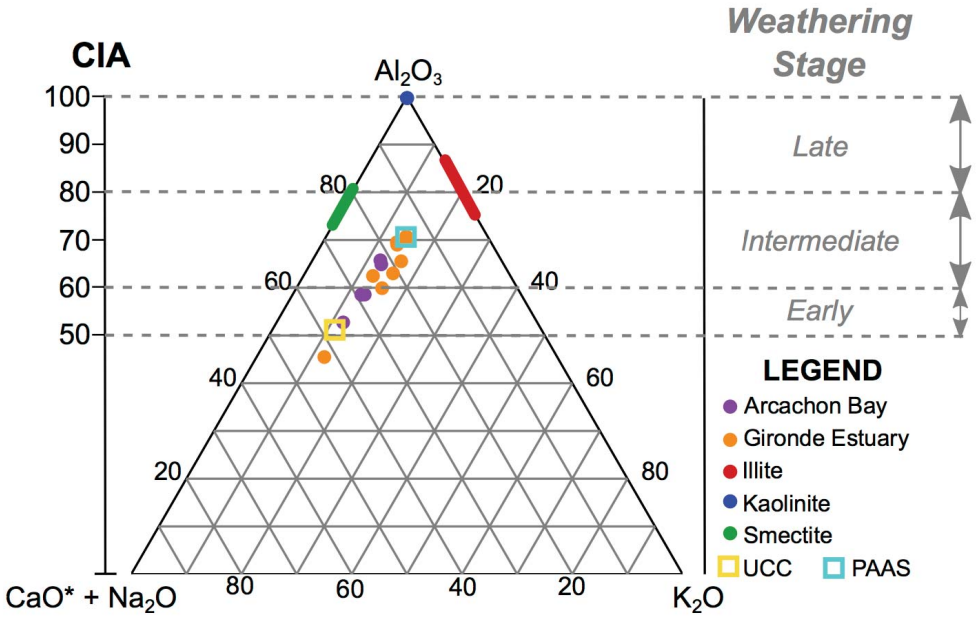
CIA
Weathering Stage
Al2O3
100
90
80
70
60
50
80
20
60
40
40
60
20
80
80
60
40
20
CaO* + Na2O
K2O
Late
Intermediate
Early
LEGEND
Arcachon Bay
Gironde Estuary
Illite
Kaolinite
Smectite
UCC
PAAS

Figure III-6: Ternary plot, in $Al_2O_3$ -(CaO* + $Na_2O$)-$K_2O$ space, of the sediment samples collected from Arcachon Bay and the Gironde Estuary for this study, along with the compositions of the upper continental crust (UCC: Rudnick & Gao, 2014) and post-Archean average shale (PAAS: Taylor & McLennan, 1985). The typical values for the common alteration products smectite, illite, and kaolinite (Fedo *et al.*, 1995) are included for reference. The scale of chemical index of alteration (CIA) is to the left of the ternary diagram, while the corresponding weathering stages are to the right of the ternary diagram and are based upon classifications by Fedo *et al.* (1995).

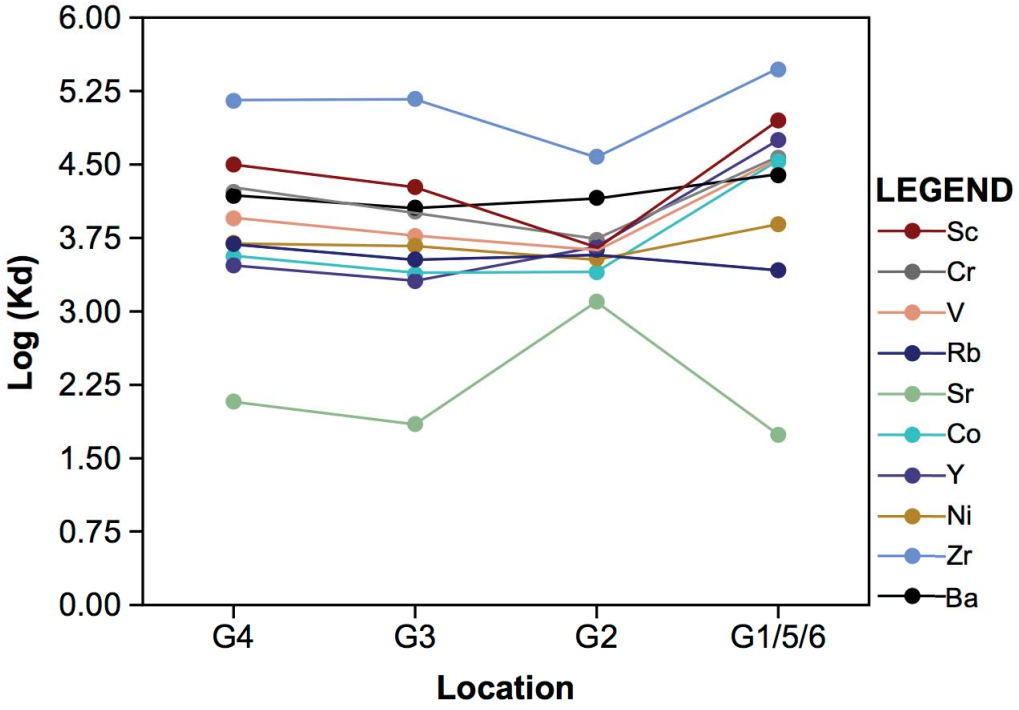
6.00
5.25
4.50
3.75
3.00
2.25
1.50
0.75
0.00
Log (Kd)
G4
G3
G2
G1/5/6
Location
LEGEND
Sc
Cr
V
Rb
Sr
Co
Y
Ni
Zr
Ba

Figure III-7: The logarithm of the distribution coefficient ($Log(K_d)$) for selected transition metals between sediment and surface waters, plotted as a function of sample location in the Gironde Estuary. The distribution coefficients for all elements were calculated using Equation III-5, and are listed in Table III-11. On the x-axis, sample locations are listed left to right in order of increasing proximity to the marine environment (see Fig. III-3). Where multiple sub-samples of sediment from a particular location were analyzed, the average $K_d$ value of all of the pertinent sediment-surface water pairs from that location were plotted.

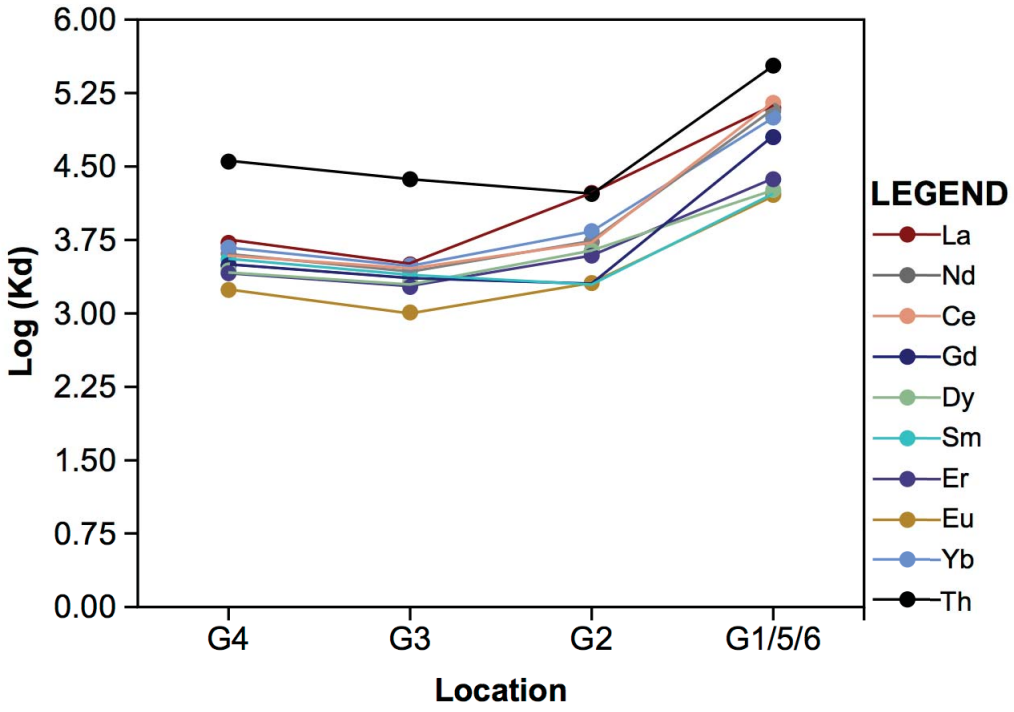
6.00
5.25
4.50
3.75
3.00
2.25
1.50
0.75
0.00
Log (Kd)
G4
G3
G2
G1/5/6
Location
LEGEND
La
Nd
Ce
Gd
Dy
Sm
Er
Eu
Yb
Th

Figure III-8: The logarithm of the distribution coefficient ($Log(K_d)$) for selected REEs and Th between sediment and surface waters, plotted as a function of sample location in the Gironde Estuary. The distribution coefficients for all elements were calculated using Equation III-5, and are listed in Table III-11. On the x-axis, sample locations are listed left to right in order of increasing proximity to the marine environment (see Fig. III-3). Where multiple sub-samples of sediment from a particular location were analyzed, the average $K_d$ value of all of the pertinent sediment-surface water pairs from that location were plotted.

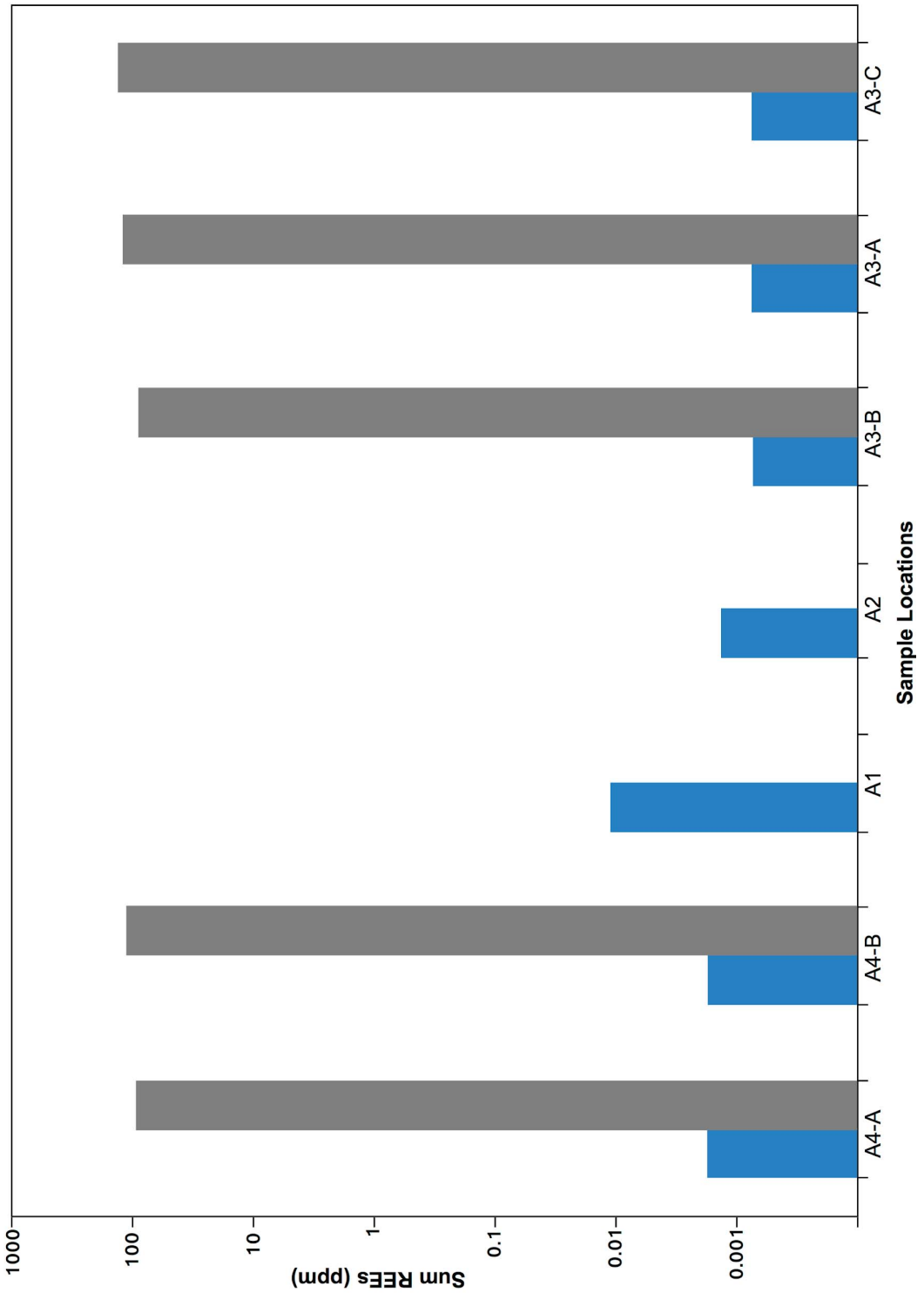
Sum REEs (ppm)
1000
100
10
1
0.1
0.01
0.001
A4-A
A4-B
A1
A2
A3-B
A3-A
A3-C
Sample Locations

Figure III-9 : Sum totals, in ppm, of measured REEs in the solid and liquid phases at each study location in Arcachon Bay. The blue bars represent the sums of the concentrations of La, Ce, Pr, Nd, Sm, Eu, Gd, Tb, Dy, Ho, Er, Tm, Yb in the water samples (see Table III-9). The gray bars represent the sums of the concentrations of La, Ce, Nd, Sm, Eu, Gd, Dy, Er, and Yb in the sediment samples (see Table III-8). ∑REEs values are in ppm and are shown on a logarithmic scale. Samples are arranged left to right in order of increasing proximity to the marine environment (see Fig. III-2). Where multiple sub-samples of sediment from a particular location were analyzed, the corresponding surface water sample was plotted multiple times, with each sediment sub-sample. There was no REE data available for the sediment samples from Locations A1 and A2, and so only the surface water data at these locations were plotted. The names of each surface water-sediment pair correspond to those in Table III-11.

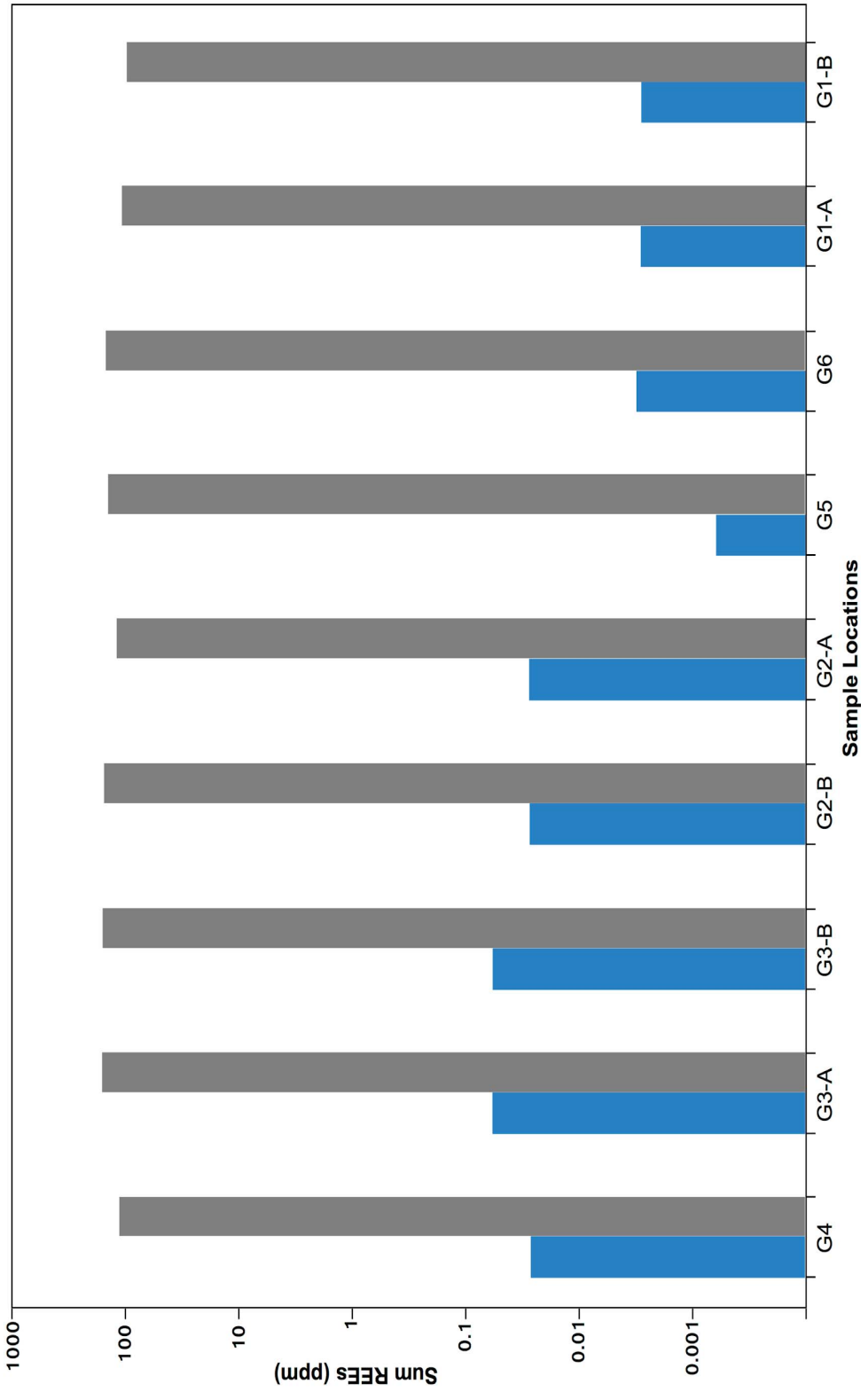
1000
100
10
1
0.1
0.01
0.001
Sum REEs (ppm)
G4
G3-A
G3-B
G2-B
G2-A
G5
G6
G1-A
G1-B
Sample Locations

Figure III-10: Sum totals, in ppm, of measured REEs in the solid and liquid phases at each study location in the Gironde Estuary. The blue bars represent the sums of the concentrations of La, Ce, Pr, Nd, Sm, Eu, Gd, Tb, Dy, Ho, Er, Tm, Yb in the water samples (see Table III-9). The gray bars represent the sums of the concentrations of La, Ce, Nd, Sm, Eu, Gd, Dy, Er, and Yb in the sediment samples (see Table III-8). ∑REEs values are in ppm and are shown on a logarithmic scale. Samples are arranged left to right in order of increasing proximity to the marine environment (see Fig. III-3). Where multiple sub-samples of sediment from a particular location were analyzed, the corresponding surface water sample was plotted multiple times, with each sediment sub-sample. The names of each surface water-sediment pair correspond to those in Table III-11.

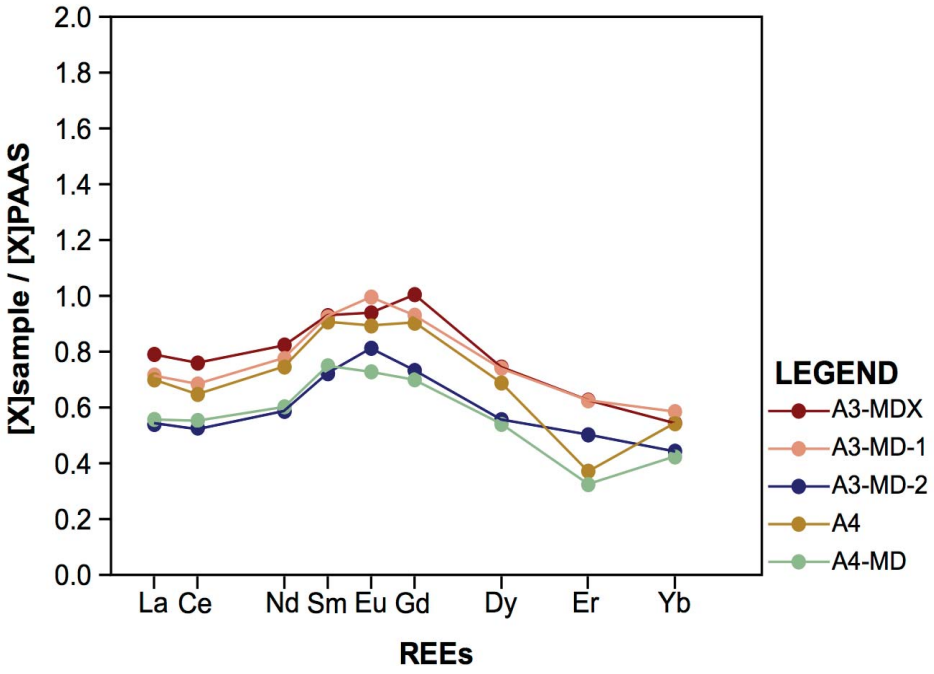
2.0
1.8
1.6
1.4
1.2
1.0
0.8
0.6
0.4
0.2
0.0
[X]sample / [X]PAAS
La Ce Nd Sm Eu Gd Dy Er Yb
REEs
LEGEND
A3-MDX
A3-MD-1
A3-MD-2
A4
A4-MD

Figure III-11: Post-Archean average shale-normalized REE diagram of sediment samples from Arcachon Bay. PAAS-normalized REE concentrations are calculated from the ppm values in Table III-6.

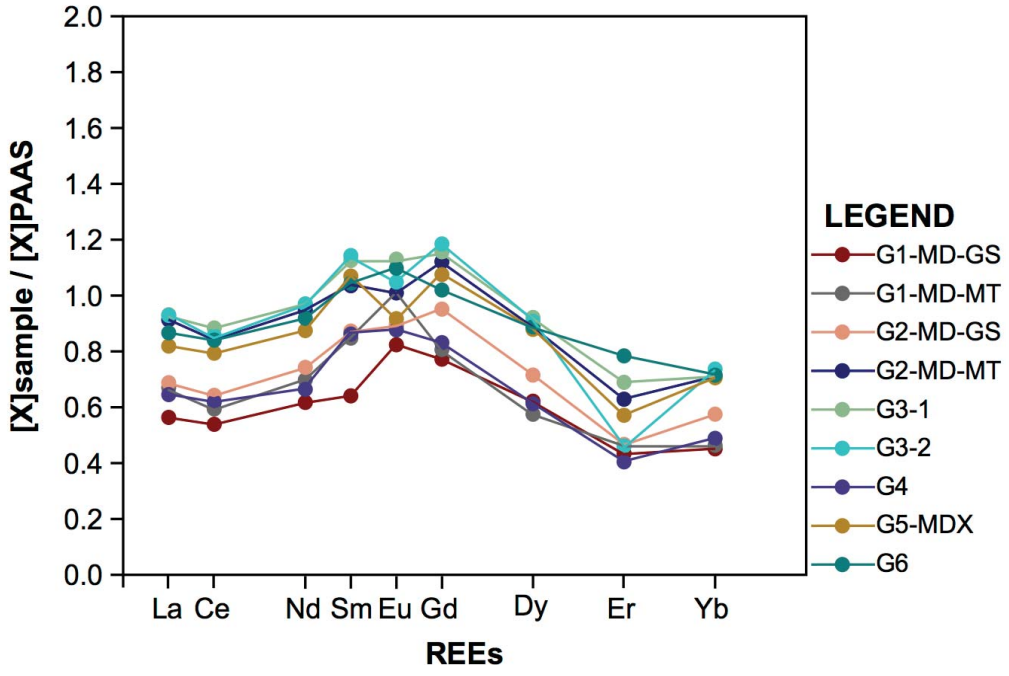
2.0
1.8
1.6
1.4
1.2
1.0
0.8
0.6
0.4
0.2
0.0
[X]sample / [X]PAAS
La Ce Nd Sm Eu Gd Dy Er Yb
REEs
LEGEND
G1-MD-GS
G1-MD-MT
G2-MD-GS
G2-MD-MT
G3-1
G3-2
G4
G5-MDX
G6

Figure III-12: Post-Archean average shale-normalized REE diagram of sediment samples from the Gironde Estuary. PAAS-normalized REE concentrations are calculated from the ppm values in Table III-6.

| Facies | Location | Dominant Hydrodynamic Force(s) | Morphology | Depositional Features | Sedimentological Character |
|---|---|---|---|---|---|
| 1 | Upper estuary. | Fluvial; tidal. | Meandering. | Fluvial and tidal point bars | Coarse sand and gravel (fluvial point bars); sand and mud (tidal point bars). |
| 2 | Lower estuary. | Tidal. | Funnel-shaped. | Non-erosional channels; elongate tidal bars. | Mud (channels); sand (bars). |
| 3 | Inlet. | Wave; tidal. | | Coastal barrier bars; tidal delta shoals. | Sand. |

Table III-1: The morphological and sedimentological characteristics of the three major longitudinally defined facies of the Gironde estuary. Modified from Allen, 1991.

| | Dominant Hydrodynamic Force(s) | Depositional Features | Sedimentological Character |
|---|---|---|---|
| **Outer Lagoon** | Wave; tidal. | Intertidal flats and marshes; seaward-coalescing tidal channels. | Fine-coarse sand (tidal channels); medium silty sand (outer tidal flats). |
| **inner Lagoon** | Fluvial; tidal. | Intertidal flats and marshes; seaward-coalescing tidal channels; transverse channels; Leyre delta. | Fine-coarse sand (seaward-coalescing tidal channels); mixed sand and silt (transverse channels); vegetated muds (inner tidal flat). |

Table III-2: The hydrodynamic and sedimentological characteristics of the two major zones of the Arcachon Bay. Based upon descriptions found in Allard *et al.*, 2009; Blanchet *et al.*, 2005; Bouchet, 1968; Glé *et al.*, 2008.

| | SiO2 | TiO2 | Al2O3 | Fe2O3 | MnO | MgO | CaO | Na2O | K2O | P2O5 | Total |
|---|---|---|---|---|---|---|---|---|---|---|---|
| **UCC** | 66.6 | 0.64 | 15.4 | 5.04 | 0.1 | 2.48 | 3.59 | 3.27 | 2.8 | 0.15 | 100.07 |
| **PAAS** | 62.8 | 1 | 18.9 | 6.5 | 0.11 | 2.2 | 1.3 | 1.2 | 3.7 | 0.16 | 99.9 |
| **G1-MD-GS** | 71.87 | 0.55 | 10.98 | 3.67 | 0.07 | 1.53 | 5.38 | 3.10 | 2.74 | 0.13 | 100 |
| **G1-MD-MT** | 73.16 | 0.55 | 11.36 | 3.80 | 0.07 | 1.35 | 5.44 | 1.42 | 2.72 | 0.13 | 100 |
| **G2-MD-GS** | 72.79 | 0.64 | 12.01 | 3.98 | 0.09 | 1.43 | 5.16 | 1.02 | 2.74 | 0.15 | 100 |
| **G2-MD-MT** | 69.23 | 0.80 | 13.89 | 5.14 | 0.11 | 1.66 | 5.36 | 0.87 | 2.73 | 0.20 | 100 |
| **G3-1** | 63.97 | 0.88 | 16.58 | 6.46 | 0.10 | 2.19 | 5.34 | 1.26 | 3.05 | 0.17 | 100 |
| **G3-2** | 63.11 | 0.86 | 17.11 | 6.51 | 0.11 | 2.27 | 5.53 | 1.28 | 3.05 | 0.18 | 100 |
| **G4** | 74.51 | 0.61 | 11.72 | 4.00 | 0.08 | 1.37 | 3.65 | 1.19 | 2.74 | 0.14 | 100 |
| **G5-MDX** | 68.47 | 0.80 | 13.85 | 5.15 | 0.11 | 1.72 | 6.22 | 0.88 | 2.62 | 0.18 | 100 |
| **G6** | 63.49 | 0.83 | 16.37 | 6.19 | 0.09 | 2.20 | 5.63 | 1.98 | 3.05 | 0.18 | 100 |
| **A3-MD-X** | 67.59 | 0.73 | 15.63 | 6.23 | 0.04 | 1.90 | 1.93 | 2.75 | 3.07 | 0.12 | 100 |
| **A3-MD-1** | 76.09 | 0.56 | 11.47 | 5.94 | 0.03 | 1.31 | 0.45 | 2.03 | 1.99 | 0.14 | 100 |
| **A3-MD-2** | 82.54 | 0.41 | 8.29 | 4.23 | 0.02 | 1.01 | 0.36 | 1.51 | 1.52 | 0.13 | 100 |
| **A4** | 72.55 | 0.62 | 13.00 | 5.40 | 0.03 | 1.65 | 0.99 | 2.94 | 2.68 | 0.14 | 100 |
| **A4-MD** | 76.39 | 0.49 | 9.79 | 3.97 | 0.05 | 1.27 | 3.88 | 1.99 | 2.07 | 0.12 | 100 |

Table III-3: Measured proportions of major element oxides for typical upper continental crust (Rudnick & Gao, 2014), post-Archean average shale (Taylor & McLennan, 1985), and sediment samples from Arcachon Bay and the Gironde Estuary (this study). All values are in units of weight percent oxide, normalized to exclude LOI weight (volatiles and organic matter).

| | Si | Ti | Al | Fe | Mn | Mg | Ca* | Na | K | P |
|---|---|---|---|---|---|---|---|---|---|---|
| **UCC** | 253239.37 | 3906.65 | 33149.54 | 17955.68 | 629.96 | 30182.48 | 20870.13 | 31837.69 | 9453.10 | 93.79 |
| **PAAS** | 344300.16 | 5287.80 | 69130.43 | 20060.20 | 846.21 | 23194.04 | 9750.31 | 10121.05 | 22974.57 | 346.63 |
| **G1-MD-GS** | 372153.41 | 2737.33 | 37932.87 | 10689.60 | 493.53 | 15188.02 | 23781.15 | 24685.38 | 16064.52 | 260.43 |
| **G1-MD-MT** | 387231.66 | 2818.43 | 40131.80 | 11314.96 | 527.22 | 13775.39 | 11102.78 | 11524.94 | 16328.31 | 268.75 |
| **G2-MD-GS** | 387401.57 | 3285.54 | 42642.60 | 11915.17 | 677.79 | 14593.93 | 8020.25 | 8325.20 | 16526.35 | 308.40 |
| **G2-MD-MT** | 376134.42 | 4187.13 | 50359.54 | 15712.32 | 803.20 | 17340.77 | 7032.17 | 7299.55 | 16822.26 | 431.49 |
| **G3-1** | 353296.06 | 4686.86 | 61099.44 | 20080.67 | 812.54 | 23209.91 | 10319.07 | 10711.43 | 19053.77 | 368.79 |
| **G3-2** | 350111.13 | 4575.21 | 63347.93 | 20343.67 | 847.40 | 24186.81 | 10502.07 | 10901.39 | 19165.33 | 396.74 |
| **G4** | 388766.67 | 3045.86 | 40780.62 | 11744.62 | 574.06 | 13720.54 | 9182.32 | 9531.46 | 16212.96 | 286.24 |
| **G5-MDX** | 375317.10 | 4231.83 | 50633.52 | 15891.85 | 870.83 | 18139.22 | 7122.47 | 7393.29 | 16267.08 | 389.71 |
| **G6** | 347900.64 | 4371.55 | 59843.87 | 19105.62 | 669.13 | 23150.04 | 16116.52 | 16729.31 | 18936.74 | 384.87 |
| **A3-MD-X** | 354451.03 | 3679.87 | 54700.53 | 18402.30 | 315.96 | 19163.24 | 15231.14 | 22159.14 | 18231.14 | 254.35 |
| **A3-MD-1** | 390583.78 | 2773.11 | 39273.25 | 17172.71 | 200.59 | 12946.58 | 2234.38 | 16048.93 | 11544.63 | 277.71 |
| **A3-MD-2** | 412518.62 | 1970.23 | 27631.74 | 11889.21 | 120.13 | 9662.93 | 1562.12 | 11624.76 | 8618.44 | 252.26 |
| **A4** | 374036.07 | 3105.37 | 44712.75 | 15680.87 | 231.68 | 16313.09 | 6798.30 | 23287.78 | 15632.44 | 282.79 |
| **A4-MD** | 391677.76 | 2400.00 | 33493.79 | 11451.33 | 325.04 | 12505.41 | 15090.11 | 15663.88 | 12025.78 | 236.10 |

Table III-4: Measured concentrations of major elements in typical upper continental crust (Rudnick & Gao, 2014), post-Archean average shale (Taylor & McLennan, 1985), and sediment samples from Arcachon Bay and the Gironde Estuary (this study). All values are in units of parts per million.

| | Si | Ti | Al | Fe | Mn | Mg | Ca | Na | K | P |
|---|---|---|---|---|---|---|---|---|---|---|
| **River Water** | 6.50E+00 | 3.00E-03 | 5.00E-02 | 4.00E-02 | 7.00E-03 | 4.10E+00 | 1.50E+01 | 6.30E+00 | 2.30E+00 | 2.00E-02 |
| **Sea Water** | 2.80E+00 | 9.60E-04 | 8.00E-04 | 6.00E-05 | 3.00E-04 | 1.29E+03 | 4.13E+02 | 1.08E+04 | 3.99E+02 | 7.10E-02 |
| **G1-SW-C** | - | 2.39E-02 | 6.58E-01 | 9.55E-01 | 9.44E-02 | 7.55E+02 | 2.82E+02 | 8.31E+03 | 2.78E+02 | 1.32E-01 |
| **G2-SW-C** | - | 6.62E-01 | 6.08E+00 | 7.61E+00 | 3.58E-01 | 4.50E+00 | 7.02E+01 | 6.42E+02 | 1.22E+01 | 2.27E-01 |
| **G3-SW-C** | - | 5.55E-02 | 2.36E+00 | 6.44E+00 | 7.17E-01 | 2.90E+02 | 1.57E+02 | 3.19E+03 | 1.03E+02 | 5.19E-01 |
| **G4-SW-C** | - | 1.50E-02 | 8.51E-01 | 2.88E+00 | 4.98E-01 | 1.41E+02 | 1.04E+02 | 9.96E+02 | 5.55E+01 | 3.04E-01 |
| **G6-SW-C** | - | 7.94E-03 | 2.59E-01 | 4.70E-01 | 3.55E-02 | 6.92E+02 | 2.65E+02 | 7.12E+03 | 2.49E+02 | 1.53E-01 |
| **A1-SW-C** | - | 6.97E-02 | 1.27E+00 | 4.83E+00 | 7.17E-02 | 9.74E+02 | 3.43E+02 | 9.46E+03 | 3.48E+02 | 1.84E-01 |
| **A2-SW-C** | - | 1.11E-03 | 3.53E-02 | 3.90E-02 | 4.97E-03 | 1.07E+03 | 3.74E+02 | 1.11E+04 | 3.73E+02 | 1.44E-01 |
| **A3-SW-C** | - | 2.15E-04 | 1.12E-02 | 5.43E-02 | 2.29E-03 | 2.60E+01 | 2.68E+00 | - | - | 3.08E-02 |
| **A4-SW-C** | - | 1.10E-03 | 2.40E-02 | 7.79E-02 | 1.64E-03 | 1.04E+03 | 3.65E+02 | 1.00E+04 | 3.73E+02 | 1.09E-01 |

Table III-5: Measured concentrations of major elements in typical river water (Li, 1982; Martin *et al.*, 1976, as found in Taylor & McLennan, 1985), sea water (Broecker & Peng, 1982; Li, 1982, as found in Taylor & McLennan, 1985), and surface water samples from Arcachon Bay and the Gironde Estuary (this study). All values are in units of parts per million.

| | Sc | V | Cr | Co | Ni | Rb | Sr | Y | Zr | Nb | Ba | La | Ce | Nd | Sm | Eu | Gd | Dy | Er | Yb | Th |
|---|---|---|---|---|---|---|---|---|---|---|---|---|---|---|---|---|---|---|---|---|---|
| **UCC** | 14 | 97 | 92 | 17.3 | 47 | 84 | 320 | 21 | 193 | 12 | 628 | 31 | 63 | 27 | 4.7 | 1 | 4 | 3.9 | 2.3 | 1.96 | 10.5 |
| **PAAS** | 16 | 150 | 110 | 23 | 55 | 160 | 200 | 27 | 210 | 19 | 650 | 38 | 80 | 32 | 5.6 | 1.1 | 4.7 | 4.4 | 2.9 | 2.8 | 14.6 |
| **G1-MD-GS** | 7.3 | 68 | 51 | 8.3 | 21 | 94 | 165 | 14.5 | 65 | 11.1 | 364 | 21.4 | 43.1 | 19.8 | 3.6 | 0.91 | 3.6 | 2.7 | 1.3 | 1.26 | 6.6 |
| **G1-MD-MT** | 7.2 | 72 | 53 | 8.5 | 22 | 90 | 164 | 15.2 | 63 | 12.0 | 390 | 25.5 | 47.5 | 22.3 | 4.7 | 0.98 | 3.8 | 2.5 | 1.3 | 1.30 | 7.4 |
| **G2-MD-GS** | 8.5 | 72 | 58 | 10.3 | 25 | 91 | 123 | 17.8 | 80 | 12.9 | 416 | 26.1 | 51.4 | 23.8 | 4.9 | 0.99 | 4.5 | 3.1 | 1.4 | 1.61 | 7.9 |
| **G2-MD-MT** | 10.5 | 92 | 80 | 12.5 | 31 | 96 | 127 | 22.6 | 106 | 16.2 | 420 | 34.7 | 68.3 | 30.3 | 5.8 | 1.11 | 5.3 | 3.9 | 1.8 | 1.99 | 10.2 |
| **G3-1** | 12.9 | 112 | 90 | 14.6 | 37 | 119 | 139 | 23.0 | 106 | 17.7 | 390 | 35.4 | 70.7 | 31.0 | 6.3 | 1.24 | 5.4 | 4.1 | 2.0 | 2.00 | 11.3 |
| **G3-2** | 13.2 | 112 | 90 | 14.2 | 39 | 110 | 142 | 22.9 | 99 | 17.1 | 394 | 35.3 | 68.5 | 31.0 | 6.4 | 1.15 | 5.6 | 4.0 | 1.3 | 2.06 | 11.8 |
| **G4** | 8.2 | 72 | 54 | 9.3 | 23 | 93 | 130 | 15.5 | 65 | 13.4 | 410 | 24.5 | 49.5 | 21.3 | 4.8 | 0.96 | 3.9 | 2.7 | 1.2 | 1.37 | 7.2 |
| **G5-MDX** | 10.9 | 88 | 74 | 12.5 | 29 | 91 | 131 | 21.3 | 105 | 16.2 | 394 | 31.1 | 63.5 | 28.0 | 6.0 | 1.01 | 5.1 | 3.9 | 1.7 | 1.98 | 9.9 |
| **G6** | 12.7 | 113 | 88 | 14.5 | 37 | 121 | 146 | 22.1 | 97 | 16.8 | 398 | 32.9 | 67.2 | 29.4 | 5.8 | 1.21 | 4.8 | 3.9 | 2.3 | 2.00 | 10.7 |
| **A3-MDX** | 11.7 | 123 | 81 | 10.6 | 33 | 119 | 133 | 17.4 | 72 | 15.6 | 353 | 30.0 | 60.7 | 26.4 | 5.2 | 1.03 | 4.7 | 3.3 | 1.8 | 1.52 | 9.5 |
| **A3-MD-1** | 9.2 | 106 | 67 | 10.3 | 24 | 73 | 87 | 19.4 | 64 | 11.3 | 232 | 27.2 | 54.7 | 24.8 | 5.2 | 1.10 | 4.4 | 3.3 | 1.8 | 1.64 | 8.3 |
| **A3-MD-2** | 7.0 | 82 | 51 | 6.4 | 17 | 50 | 72 | 13.8 | 51 | 8.6 | 188 | 20.5 | 42.1 | 18.8 | 4.0 | 0.89 | 3.4 | 2.4 | 1.5 | 1.24 | 6.2 |
| **A4** | 9.8 | 108 | 70 | 8.0 | 25 | 99 | 115 | 16.8 | 65 | 13.6 | 329 | 26.6 | 51.7 | 23.8 | 5.1 | 0.98 | 4.2 | 3.0 | 1.1 | 1.52 | 8.2 |
| **A4-MD** | 7.4 | 82 | 55 | 6.2 | 19 | 69 | 154 | 12.9 | 53 | 11.3 | 280 | 21.2 | 44.3 | 19.3 | 4.2 | 0.80 | 3.3 | 2.4 | 0.9 | 1.18 | 6.5 |

Table III-6: Measured concentrations of trace elements in typical upper continental crust (Rudnick & Gao, 2014), post-Archean average shale (Taylor & McLennan, 1985), and sediment samples from Arcachon Bay and the Gironde Estuary (this study). All values are in units of parts per million.

| | River Water | Sea Water | G1-SW-C | G2-SW-C | G3-SW-C | G4-SW-C | G5-SW-C | G6-SW-C | A1-SW-C | A2-SW-C | A3-SW-C | A4-SW-C |
|---|---|---|---|---|---|---|---|---|---|---|---|---|
| **Li** | 3.00E-03 | 1.70E-01 | 2.22E-01 | 1.27E-02 | 5.65E-02 | 3.16E-02 | 3.66E-03 | 2.06E-01 | 4.05E-01 | 3.43E-01 | 5.26E-03 | 5.00E-01 |
| **Sc** | 4.00E-06 | 6.70E-07 | 2.82E-04 | 1.81E-03 | 6.99E-04 | 2.56E-04 | 1.12E-05 | 1.35E-04 | 2.76E-04 | 1.58E-04 | 3.81E-05 | 2.26E-04 |
| **V** | 9.00E-04 | 1.20E-03 | 5.48E-03 | 1.70E-02 | 1.90E-02 | 8.09E-03 | 1.75E-03 | 2.37E-03 | 2.34E-02 | 4.64E-03 | 1.52E-04 | 2.09E-03 |
| **Cr** | 1.00E-03 | 2.00E-04 | 2.42E-03 | 1.27E-02 | 8.64E-03 | 3.25E-03 | 7.96E-04 | 2.01E-03 | 6.35E-03 | 1.05E-03 | 5.88E-04 | 1.26E-03 |
| **Co** | 1.00E-04 | 2.00E-06 | 6.04E-04 | 4.51E-03 | 5.99E-03 | 2.56E-03 | 7.27E-05 | 3.62E-04 | 1.34E-03 | 3.72E-04 | 3.43E-05 | 8.04E-05 |
| **Ni** | 3.00E-04 | 5.00E-04 | 4.23E-03 | 7.96E-03 | 8.14E-03 | 4.55E-03 | 2.27E-03 | 3.45E-03 | 6.49E-03 | 3.61E-03 | 2.18E-03 | 4.53E-03 |
| **Cu** | 7.00E-03 | 3.00E-04 | 8.56E-03 | 6.99E-03 | 1.61E-02 | 1.01E-02 | 1.69E-03 | 2.80E-03 | 5.97E-03 | 2.85E-03 | 7.19E-04 | 1.74E-03 |
| **Zn** | 2.00E-02 | 4.00E-04 | 1.31E-02 | 4.87E-02 | 1.49E-01 | 6.58E-02 | 1.24E-02 | 6.67E-03 | 2.65E-02 | 3.78E-01 | 2.50E-03 | 5.25E-03 |
| **As** | 2.00E-03 | 1.70E-03 | 3.69E-03 | 1.27E-02 | 1.29E-02 | 9.91E-03 | 2.57E-03 | 2.71E-03 | 9.28E-03 | 2.55E-03 | 2.05E-04 | 2.08E-03 |
| **Se** | 6.00E-05 | 1.30E-04 | 1.96E-02 | 1.40E-02 | 2.35E-02 | 1.39E-02 | 1.57E-02 | 1.29E-02 | 1.87E-02 | 2.19E-02 | 1.64E-02 | 2.15E-02 |
| **Rb** | 1.00E-03 | 1.20E-01 | 1.11E-01 | 2.19E-02 | 3.37E-02 | 1.92E-02 | 1.67E-03 | 9.03E-02 | 1.81E-01 | 1.54E-01 | 5.10E-03 | 1.82E-01 |
| **Sr** | 7.00E-02 | 7.60E+00 | 7.98E+00 | 9.81E-02 | 1.98E+00 | 1.09E+00 | 1.30E-01 | 6.66E+00 | 1.20E+01 | 1.10E+01 | 1.59E-01 | 1.35E+01 |
| **Y** | 4.00E-05 | 7.00E-06 | 5.48E-04 | 4.36E-03 | 1.11E-02 | 5.28E-03 | 6.16E-05 | 5.37E-04 | 2.30E-03 | 2.30E-04 | 9.49E-05 | 2.44E-04 |
| **Zr** | - | 3.00E-05 | 4.15E-04 | 2.40E-03 | 6.94E-04 | 4.63E-04 | 1.12E-04 | 2.82E-04 | 2.04E-04 | 1.47E-04 | 1.01E-04 | 1.42E-04 |
| **Mo** | 6.00E-04 | 1.10E-02 | 5.70E-02 | 7.89E-04 | 1.36E-02 | 6.40E-03 | 3.66E-03 | 5.16E-02 | 1.26E-01 | 9.74E-02 | 9.58E-04 | 1.43E-01 |
| **Cd** | 1.00E-05 | 8.00E-05 | 2.05E-04 | 8.14E-05 | 2.93E-04 | 2.65E-04 | 2.13E-05 | 1.42E-04 | 1.48E-04 | 6.32E-05 | 3.11E-05 | 9.08E-05 |
| **Ba** | 2.00E-02 | 1.40E-02 | 2.15E-02 | 2.89E-02 | 3.41E-02 | 2.73E-02 | 4.87E-03 | 2.69E-02 | 1.21E-02 | 1.15E-02 | 1.22E-02 | 1.16E-02 |
| **La** | 4.80E-05 | 4.50E-06 | 4.06E-04 | 4.91E-03 | 1.04E-02 | 4.69E-03 | 3.05E-05 | 4.54E-04 | 1.86E-03 | 9.35E-05 | 4.64E-05 | 8.62E-05 |
| **Ce** | 7.90E-05 | 3.50E-06 | 7.88E-04 | 1.11E-02 | 2.36E-02 | 1.05E-02 | 3.80E-05 | 9.58E-04 | 4.36E-03 | 1.02E-04 | 6.23E-05 | 6.67E-05 |
| **Pr** | 7.30E-06 | 1.00E-06 | 1.31E-04 | 1.29E-03 | 2.67E-03 | 1.30E-03 | 2.60E-05 | 1.43E-04 | 5.48E-04 | 6.26E-05 | 3.07E-05 | 6.95E-05 |
| **Nd** | 3.80E-05 | 4.20E-06 | 3.85E-04 | 4.94E-03 | 1.13E-02 | 5.22E-03 | 3.11E-05 | 4.20E-04 | 1.99E-03 | 4.47E-05 | 5.08E-05 | 6.25E-05 |
| **Sm** | 7.80E-06 | 8.00E-07 | 3.37E-04 | 1.26E-03 | 2.70E-03 | 1.36E-03 | 1.62E-04 | 3.72E-04 | 7.38E-04 | 3.04E-04 | 1.81E-04 | 4.72E-04 |
| **Eu** | 1.50E-06 | 1.50E-07 | 7.52E-05 | 5.19E-04 | 1.17E-03 | 5.52E-04 | 3.17E-05 | 9.14E-05 | 2.52E-04 | 5.57E-05 | 3.82E-05 | 7.14E-05 |
| **Gd** | 8.50E-06 | 1.00E-06 | 9.56E-05 | 1.13E-03 | 2.75E-03 | 1.25E-03 | 2.18E-05 | 1.10E-04 | 4.30E-04 | 2.00E-05 | 1.62E-05 | 2.75E-05 |
| **Tb** | 1.20E-06 | 1.70E-07 | 1.36E-04 | 2.26E-04 | 4.59E-04 | 2.62E-04 | 6.73E-05 | 1.43E-04 | 2.67E-04 | 1.90E-04 | 8.65E-05 | 2.55E-04 |
| **Dy** | 7.20E-06 | 1.10E-06 | 2.26E-04 | 8.12E-04 | 1.99E-03 | 9.77E-04 | 7.97E-05 | 2.28E-04 | 5.37E-04 | 2.45E-04 | 9.15E-05 | 2.87E-04 |
| **Ho** | 1.40E-06 | 2.80E-07 | 1.60E-04 | 2.29E-04 | 4.49E-04 | 2.83E-04 | 9.73E-05 | 1.69E-04 | 2.41E-04 | 1.82E-04 | 1.09E-04 | 2.69E-04 |
| **Er** | 4.20E-06 | 9.20E-07 | 7.92E-05 | 4.03E-04 | 8.81E-04 | 4.61E-04 | 3.89E-05 | 8.88E-05 | 2.13E-04 | 7.95E-05 | 5.30E-05 | 1.17E-04 |
| **Tm** | 6.10E-07 | 1.30E-07 | 5.72E-06 | 4.90E-05 | 1.16E-04 | 5.64E-05 | 1.82E-06 | 6.09E-06 | 2.05E-05 | 3.36E-06 | 3.11E-06 | 4.87E-06 |
| **Yb** | 3.60E-06 | 9.00E-07 | 2.45E-05 | 2.61E-04 | 6.55E-04 | 2.93E-04 | 4.53E-06 | 2.47E-05 | 1.02E-04 | 5.90E-06 | 7.49E-06 | 6.64E-06 |
| **Lu** | 6.40E-07 | 1.40E-07 | 6.20E-06 | 4.06E-05 | 9.87E-05 | 4.39E-05 | 2.59E-06 | 6.79E-06 | 1.93E-05 | 3.73E-06 | 3.23E-06 | 6.39E-06 |
| **Hf** | - | 7.00E-06 | 1.21E-05 | 6.39E-05 | 3.32E-05 | 1.88E-05 | 4.12E-06 | 7.78E-06 | 1.09E-05 | 9.14E-06 | 4.35E-06 | 1.10E-05 |
| **Re** | - | 4.00E-06 | 1.27E-05 | 6.85E-06 | 1.71E-05 | 3.94E-06 | 8.74E-06 | 1.42E-06 | 3.74E-05 | 0.00E+00 | 3.22E-06 | 1.42E-05 |
| **Pb** | 1.00E-03 | 2.00E-06 | 8.30E-04 | 1.25E-02 | 2.73E-02 | 1.15E-02 | 1.12E-04 | 8.79E-04 | 5.78E-03 | 2.58E-04 | 1.02E-04 | 1.10E-04 |
| **Th** | 1.00E-04 | 6.00E-08 | 9.96E-05 | 5.45E-04 | 4.98E-04 | 2.00E-04 | 1.21E-06 | 3.43E-05 | 6.48E-05 | 4.39E-06 | 5.39E-06 | 3.42E-06 |
| **U** | 4.00E-05 | 3.10E-03 | 1.74E-03 | 4.03E-04 | 9.52E-04 | 6.56E-04 | 3.70E-04 | 1.65E-03 | 2.50E-03 | 2.27E-03 | 1.45E-05 | 2.74E-03 |

Table III-7: Measured concentrations of trace elements in typical river water (Li, 1982; Martin *et al.*, 1976, as found in Taylor & McLennan, 1985), sea water (Broecker & Peng, 1982; Li, 1982, as found in Taylor & McLennan, 1985), and surface water samples from Arcachon Bay and the Gironde Estuary (this study). All values are in units of parts per million.

| | ΣREEs | Eu/Eu* | Th/Co | La/Sc | LaN/YbN | Th/Sc | Zr/Sc |
|---|---|---|---|---|---|---|---|
| **UCC** | 148.10 | - | 0.61 | 2.21 | 10.69 | 0.75 | 13.79 |
| **PAAS** | 171.50 | - | 0.73 | 2.39 | 9.17 | 0.91 | 13.13 |
| **G1-MD-GS** | 97.68 | 1.17 | 0.80 | 2.95 | 1.25 | 0.91 | 8.91 |
| **G1-MD-MT** | 110.04 | 1.08 | 0.86 | 3.53 | 1.45 | 1.02 | 8.72 |
| **G2-MD-GS** | 117.80 | 0.99 | 0.77 | 3.09 | 1.20 | 0.94 | 9.41 |
| **G2-MD-MT** | 153.22 | 0.94 | 0.81 | 3.31 | 1.28 | 0.97 | 10.09 |
| **G3-1** | 158.17 | 0.99 | 0.78 | 2.74 | 1.30 | 0.88 | 8.23 |
| **G3-2** | 155.29 | 0.90 | 0.83 | 2.68 | 1.26 | 0.90 | 7.52 |
| **G4** | 110.23 | 1.04 | 0.77 | 3.00 | 1.32 | 0.88 | 7.96 |
| **G5-MDX** | 142.16 | 0.86 | 0.79 | 2.86 | 1.16 | 0.91 | 9.65 |
| **G6** | 149.60 | 1.06 | 0.74 | 2.59 | 1.21 | 0.84 | 7.62 |
| **A3-MDX** | 134.67 | 0.97 | 0.90 | 2.56 | 1.45 | 0.81 | 6.15 |
| **A3-MD-1** | 124.08 | 1.07 | 0.80 | 2.95 | 1.22 | 0.90 | 6.94 |
| **A3-MD-2** | 94.88 | 1.12 | 0.97 | 2.95 | 1.22 | 0.89 | 7.30 |
| **A4** | 118.04 | 0.99 | 1.03 | 2.71 | 1.29 | 0.84 | 6.62 |
| **A4-MD** | 97.47 | 1.01 | 1.05 | 2.86 | 1.32 | 0.88 | 7.14 |

Table III-8: Sums of rare earth elements (∑REEs) in upper continental crust (UCC: Rudnick & Gao, 2014), post-Archean average shale (PAAS: Taylor & McLennan, 1985), and sediment samples from Arcachon Bay and the Gironde Estuary (this study). All values are calculated based on the values in Table III-6, and are in units of parts per million. Note that the ∑REEs values are calculated by adding the concentrations of La, Ce, Nd, Sm, Eu, Gd, Dy, Er, and Yb, as these are the only REEs for which data is available in the Arcachon Bay and Gironde Estuary sediment samples. The $La_N/Yb_N$ ratios and europium anomalies (Eu/Eu*) were calculated using published PAAS concentrations (Taylor & McLennan, 1985) and Equations III-1 and III-2, respectively.

| | ΣREEs |
|---|---|
| **River Water** | 1.92E-05 |
| **Sea Water** | 2.94E-06 |
| **G1-SW-C** | 6.49E-04 |
| **G2-SW-C** | 2.66E-03 |
| **G3-SW-C** | 5.91E-03 |
| **G4-SW-C** | 2.93E-03 |
| **G5-SW-C** | 2.96E-04 |
| **G6-SW-C** | 7.03E-04 |
| **A1-SW-C** | 1.60E-03 |
| **A2-SW-C** | 6.52E-04 |
| **A3-SW-C** | 3.55E-04 |
| **A4-SW-C** | 9.03E-04 |

Table III-9: Sums of rare earth elements (∑REEs) in typical river water (Li, 1982; Martin *et al.*, 1976, as found in Taylor & McLennan, 1985), sea water (Broecker & Peng, 1982; Li, 1982, as found in Taylor & McLennan, 1985), and surface water samples from Arcachon Bay and the Gironde Estuary (this study). All values are calculated based on the values in Table III-6, and are in units of parts per million. The $La_N/Yb_N$ ratios and europium anomalies (Eu/Eu*) were calculated using published PAAS concentrations (Taylor & McLennan, 1985) and Equations III-1 and III-2, respectively.

| | CIA | Weathering Stage |
|---|---|---|
| **UCC** | 52.76 | Early |
| **PAAS** | 70.38 | Intermediate |
| **G1-MD-GS** | 45.48 | Early* |
| **G1-MD-MT** | 59.91 | Early |
| **G2-MD-GS** | 65.55 | Intermediate |
| **G2-MD-MT** | 70.43 | Intermediate |
| **G3-1** | 69.01 | Intermediate |
| **G3-2** | 69.52 | Intermediate |
| **G4** | 63.01 | Intermediate |
| **G5-MDX** | 70.76 | Intermediate |
| **G6** | 62.48 | Intermediate |
| **A3-MD-X** | 58.56 | Early |
| **A3-MD-1** | 65.74 | Intermediate |
| **A3-MD-2** | 64.90 | Intermediate |
| **A4** | 58.58 | Early |
| **A4-MD** | 52.74 | Early |

Table III-10: Chemical indices of alteration (CIA) for typical upper continental crust (UCC: Rudnick & Gao, 2014), post-Archean average shale (PAAS: Taylor & McLennan, 1985), and the sediment samples collected from Arcachon Bay and the Gironde Estuary (this study). The CIA are calculated based upon the values in Table III-3, using Equations III-3 and III-4. The corresponding weathering stages for each sample are listed in the far-right column.

| Element | PAAS-RW | PAAS-SW | G1-A | G1-B | G2-A | G2-B | G3-A | G3-B | G4 | G5 | G6 | A3-A | A3-B | A3-C | A4-A | A4-B |
|---|---|---|---|---|---|---|---|---|---|---|---|---|---|---|---|---|
| **Sc** | 6.60 | 7.38 | 4.41 | 4.41 | 3.67 | 3.76 | 4.27 | 4.28 | 4.50 | 5.99 | 4.97 | 5.49 | 5.38 | 5.26 | 4.64 | 4.51 |
| **V** | 5.22 | 5.10 | 4.09 | 4.12 | 3.63 | 3.73 | 3.77 | 3.77 | 3.95 | 4.70 | 4.68 | 5.91 | 5.84 | 5.73 | 4.71 | 4.59 |
| **Cr** | 5.04 | 5.74 | 4.33 | 4.34 | 3.66 | 3.80 | 4.02 | 4.02 | 4.22 | 4.97 | 4.64 | 5.14 | 5.06 | 4.94 | 4.75 | 4.64 |
| **Co** | 5.36 | 7.06 | 4.14 | 4.15 | 3.36 | 3.44 | 3.39 | 3.37 | 3.56 | 5.24 | 4.60 | 5.49 | 5.48 | 5.27 | 5.00 | 4.89 |
| **Ni** | 5.26 | 5.04 | 3.70 | 3.71 | 3.49 | 3.59 | 3.66 | 3.68 | 3.70 | 4.10 | 4.03 | 4.18 | 4.04 | 3.90 | 3.74 | 3.62 |
| **Rb** | 5.20 | 3.12 | 2.93 | 2.91 | 3.62 | 3.64 | 3.55 | 3.51 | 3.69 | 4.73 | 3.13 | 4.37 | 4.16 | 3.99 | 2.74 | 2.58 |
| **Sr** | 3.46 | 1.42 | 1.31 | 1.31 | 3.10 | 3.11 | 1.85 | 1.86 | 2.08 | 3.01 | 1.34 | 2.92 | 2.74 | 2.66 | 0.93 | 1.06 |
| **Y** | 5.83 | 6.59 | 4.42 | 4.44 | 3.61 | 3.72 | 3.32 | 3.31 | 3.47 | 5.54 | 4.61 | 5.26 | 5.31 | 5.16 | 4.84 | 4.72 |
| **Zr** | - | 6.85 | 5.19 | 5.18 | 4.52 | 4.64 | 5.19 | 5.15 | 5.15 | 5.97 | 5.54 | 5.85 | 5.80 | 5.70 | 5.66 | 5.57 |
| **Ba** | 4.51 | 4.67 | 4.23 | 4.26 | 4.16 | 4.16 | 4.06 | 4.06 | 4.18 | 4.91 | 4.17 | 4.46 | 4.28 | 4.19 | 4.45 | 4.38 |
| **La** | 5.90 | 6.93 | 4.72 | 4.80 | 3.73 | 3.85 | 3.53 | 3.53 | 3.72 | 6.01 | 4.86 | 5.81 | 5.77 | 5.65 | 5.49 | 5.39 |
| **Ce** | 6.01 | 7.36 | 4.74 | 4.78 | 3.67 | 3.79 | 3.48 | 3.46 | 3.67 | 6.22 | 4.85 | 5.99 | 5.94 | 5.83 | 5.89 | 5.82 |
| **Nd** | 5.93 | 6.88 | 4.71 | 4.76 | 3.68 | 3.79 | 3.44 | 3.44 | 3.61 | 5.95 | 4.84 | 5.71 | 5.69 | 5.57 | 5.58 | 5.49 |
| **Sm** | 5.86 | 6.85 | 4.03 | 4.15 | 3.59 | 3.66 | 3.37 | 3.38 | 3.55 | 4.57 | 4.20 | 4.46 | 4.46 | 4.35 | 4.03 | 3.95 |
| **Eu** | 5.87 | 6.87 | 4.08 | 4.12 | 3.28 | 3.33 | 3.03 | 2.99 | 3.24 | 4.50 | 4.12 | 4.43 | 4.46 | 4.37 | 4.14 | 4.05 |
| **Gd** | 5.74 | 6.67 | 4.58 | 4.60 | 3.60 | 3.67 | 3.30 | 3.31 | 3.49 | 5.36 | 4.64 | 5.46 | 5.43 | 5.33 | 5.19 | 5.08 |
| **Dy** | 5.79 | 6.60 | 4.08 | 4.05 | 3.59 | 3.68 | 3.31 | 3.30 | 3.44 | 4.69 | 4.23 | 4.55 | 4.55 | 4.43 | 4.02 | 3.92 |
| **Er** | 5.84 | 6.50 | 4.20 | 4.23 | 3.53 | 3.66 | 3.36 | 3.18 | 3.41 | 4.63 | 4.41 | 4.53 | 4.53 | 4.44 | 3.97 | 3.91 |
| **Yb** | 5.89 | 6.49 | 4.71 | 4.72 | 3.79 | 3.88 | 3.49 | 3.50 | 3.67 | 5.64 | 4.91 | 5.31 | 5.34 | 5.22 | 5.36 | 5.25 |
| **Th** | 5.16 | 8.39 | 4.82 | 4.87 | 4.16 | 4.27 | 4.36 | 4.38 | 4.55 | 6.92 | 5.50 | 6.25 | 6.19 | 6.06 | 6.38 | 6.28 |

Table III-11: Logarithms of distribution coefficients of selected trace elements between sediment and surface water samples from Arcachon Bay and the Gironde estuary. Theoretical distribution coefficients of these trace elements between post-Archean Australian shale (PAAS) and river water, and PAAS and sea water are included for reference. Distribution coefficients in this table were calculated based on the measured concentrations in Table III-6 and Table III-7 of this paper, using Equation III-5. All values are presented as $\log(K_d)$.

# CHAPTER IV
# CONCLUSION

The work in this thesis examines the interactions between fine-grained sediments and their ambient waters under conditions representative of the continuum of sub-environments that comprise the freshwater to brackish-water transition zone. The intent of this research is to make direct observations of the factors controlling the geochemical signatures of fine-grained sediment deposits to enhance our understanding of sediment geochemistry in marginal marine environments. These observations engender many important considerations for the analysis of sedimentary successions, and have the potential to advance paleoenvironmental reconstructions and facies models.

Chapter II of this thesis describes two phases of controlled laboratory experiments that use illite, kaolinite, and montmorillonite clays to investigate the effects of mineralogy and water chemistry on element partitioning within systems. Caesium was evaluated for its potential to approximate salinity in mudstones by measuring its adsorption to each clay mineral at discrete solution ionic strength conditions. $Cs^+$ adsorption to each clay decreased as the solution ionic strength increased, most likely due to competition with Na cations for complexation sites on the clay surfaces and reaction with Cl anions in solution. At each ionic strength condition, illite adsorbed the most $Cs^+$, kaolinite adsorbed the least $Cs^+$, and montmorillonite adsorbed an intermediate amount of $Cs^+$. These results imply that the amount of Cs that can be partitioned into the fine sediment fraction is proportional to environmental salinity conditions. However, due to variable

sorption of $Cs^+$ between different clay minerals, the mineralogical compositions of sediments will need to be considered when comparing deposits spatially.

Fluvial and marine endmembers of marginal marine systems were modeled by equilibrating each of the three clay minerals with water samples from the North Saskatchewan River, Edmonton, Alberta, Canada, and English Bay, Vancouver, British Columbia, respectively. The proportions of clay and water in each suspension were varied to yield a range of suspended sediment load conditions. The partitioning of elements between the aqueous and particulate clay phases varied according to clay mineralogy, water chemistry, and sediment load conditions. In general, higher concentrations of clay corresponded to increased removal of aqueous species from solution. Each element analyzed displayed slightly different sorption signatures in river water systems as opposed to sea water systems. In virtually all trials, the clays adsorbed a greater proportion of the elements from river water than from sea water.

The results from the study outlined in Chapter II of this thesis are significant in that they highlight the potential of trace element geochemistry to provide insight to the depositional conditions of mudstones. This technique is especially interesting when applied to the estimation of syn-depositional salinity conditions, which have hitherto been relatively unexplored. This preliminary assessment of Cs as a potential salinity indicator suggests that comparing Cs abundance throughout the fine-grained fraction of sedimentary successions may be useful for approximating the freshwater to brackish water transition zone in the rock record. Further studies of Cs abundance in mud deposits in modern

estuaries and in ancient estuarine succession could help to refine this technique for future application. Examinations of element partitioning between natural water samples and suspended clay sediments show clear distinctions between fluvial and marine systems. These distinctions provide a premise for geochemical analyses of modern and ancient mud deposits to ascertain whether differences in element partitioning are preserved and can therefore be used as syn-depositional salinity proxies. However, before this technique can be applied to the interpretation of sedimentary successions, the relative influence of other environmental and depositional factors on sediment geochemistry should be determined through further laboratory- and field-based research. Similar experiments that examine element partitioning at various degrees of sediment heterogeneity, dissolved oxygen concentrations, organic matter content, and hydrodynamic energy would be valuable to the development of more realistic models of depositional conditions along the freshwater to brackish-water transition zone.

Chapter III of this thesis is an analysis of the major and trace element geochemistry in sediment and surface water samples collected from the modern Arcachon Bay and Gironde Estuary in southwestern France. The primary objective of this study was to describe the sediments in terms of their geochemistry and to make distinctions between fluvial, brackish, and marine sub-environments of these systems. These preliminary distinctions could be applied to the development of modern analogues for geochemical studies of ancient marginal marine systems.

The chemical differentiation indices of the sediment samples from both Arcachon Bay and the Gironde estuary suggest that the source of these sediments had a mixed felsic and mafic composition and was influenced by an active continental margin. The CIA values suggest a trend towards illitization and correspond to early- and intermediate-stage weathering. The total REE abundances, as well as the relative proportions of all trace elements in the sediment samples, did not vary spatially within either Arcachon Bay or the Gironde Estuary. As such, it is unlikely that spatially variable environmental parameters such as salinity, redox state, or mineralogy exert considerable control on sedimentary REE and trace element distributions. Although grain size does vary throughout both study areas, the samples discussed in this thesis were exclusively collected from mud beds, and so the effect of sediment grain size on REE and trace element enrichment is not observed. Mineralogical and grain size data were not available for the samples analyzed, and consequently these aspects of sediment heterogeneity could not be corrected for in this study. However, these analyses could present interesting avenues for future research that expands on the themes of this thesis. The relationship between trace element distributions and sub-environment conditions could be explored more thoroughly by means of sequential extraction experiments. Determining the proportions of REEs and trace elements that are adsorbed to the sediment surface, as opposed to substituted into the crystal lattice of the mineral, could allow for correlations between partitioned trace elements and sediment location within an estuary. However, within the scope of the data available in this study, REE and trace element variations

between sediment samples appear to be a function of of the organic matter content in the sediment. The assemblages of REEs and trace elements in these environments are derived from the source rock composition and tectonic setting, as well as the weathering and alteration processes operating in the system. Mineralogy and organic matter content most likely dictate how relative proportions of these elements in the sediments vary, and whether these variations are preserved in the rock record.

Extrapolating the results from Chapter III to the rock record, the trace element signature of sedimentary rocks is strongly influenced by the sediment source rock composition and sedimentary organic matter content, as opposed to the geochemical conditions at the time of deposition. The convolute geologic history and multi-lithic sediment source composition of Arcachon Bay and the Gironde Estuary contribute to the difficulty of attributing specific trace element signatures to particular causes. The variations in trace element signatures between locations may be correlated to sediment-associated organic matter. However, the exact types of organic matter are unknown, and their abundance is not distributed predictably or consistently throughout either estuary. Further geobiological analyses of the sediments could help to resolve this. However, other variables, such as climate, sediment source composition, chemical weathering processes, and the tectonic settings of sediment source and sink areas differ significantly between depositional systems. Some level of uncertainty is thus likely to be present in any modern depositional system. This uncertainty is exacerbated in the case of ancient sedimentary successions, where the relative influence of the

aforementioned environmental and depositional variables is difficult to unravel. As was demonstrated in Chapter II, syn-depositional geochemical conditions have the potential to affect the trace element signatures of sediments. However, the likelihood that these signatures are preserved, and the ability of researchers to distinguish these signatures in the rock record, is questionable. The case studies discussed in this thesis demonstrate the necessity of future research on a greater selection of environments and depositional parameters to define the interactions between sediment, water, and organic matter, and whether these can be distinguished in a variety of depositional periods and geological time periods.

# BIBLIOGRAPHY


Adamczyk, Z., & Warszyński, P. (1996). Role of electrostatic interactions in particle adsorption. *Advances in Colloid and Interface Science*, *63*, 41–149.

Adams, T. D., Haynes, J. R., & Walker, C. T. (1965). Boron in Holocene Illites of the Dovey Estuary, Wales, and Its Relationship To Palaeosalinity in Cyclothems. *Sedimentology*, *4*(3), 189–195.

Algeo, T. J. & Lyons, T. W. (2006). Mo-total organic carbon covariation in modern anoxic marine environments: Implications for analysis of paleoredox and paleohydrographic conditions. *Paleoceanography*, *21*(1), PA1016.

Allard, J., Chaumillon, E., & Féniès, H. (2009). A synthesis of morphological evolutions and Holocene stratigraphy of a wave-dominated estuary: The Arcachon lagoon, SW France. *Continental Shelf Research*, *29*(8), 957–969.

Allen, G. P. & Posamentier, H. W. (1993). Sequence stratigraphy and facies model of an incised valley fill: the Gironde Estuary, France. *Journal of Sedimentary Petrology*, *63*(3), 378–391.

Allen, G. P. (1991). Sedimentary processes and facies in the Gironde estuary: a recent model for macrotidal estuarine systems. *Clastic Tidal Sedimentology*, *16*, 29–40.

Allen, G. P., Salomon, J. C., Bassoullet, P., Du Penhoat, Y., & de Grandpré, C. (1980). Effects of tides on mixing and suspended sediment transport in macrotidal estuaries. *Sedimentary Geology*, *26*(1–3), 69–90.

Allen, K. A., Hönisch, B., Eggins, S. M., Haynes, L. L., Rosenthal, Y., & Yu, J. (2016). Trace element proxies for surface ocean conditions: A synthesis of culture calibrations with planktic foraminifera. *Geochimica et Cosmochimica Acta*, *193*, 197-221.

Anand, R. R., & Gilkes, R. J. (1984). Weathering of ilmenite in a lateritic pallid zone. *Clays and Clay Minerals*, *32*(5), 363-374.

Andrade, G. R. P., de Azevedo, A. C., Lepchak, J. K., & Assis, T. C. (2019). Weathering of Permian sedimentary rocks and soil clay minerals transformations under subtropical climate, southern Brazil (Paraná State). *Geoderma, 336*, 31–48.

Ayles, C. P. & Lapointe, M. F. (1996). Downvalley gradients in flow patterns, sediment transport and channel morphology in a small macrotidal estuary: Dipper Harbour Creek, New Brunswick, Canada. *Earth Surface Processes and Landforms, 21*(9), 829–842.

Balistrieri, L., Brewer, P. G., & Murray, J. W. (1981). Scavenging residence times of trace metals and surface chemistry of sinking particles in the deep ocean. *Deep Sea Research Part A, Oceanographic Research Papers*, *28*(2), 101–121.

Balls, P. W. (1989). The Partition of Trace Metals Between Dissolved and Particulate Phases. *Netherlands Journal of Sea Research*, *23*(1), 7–14.

Bhatia, M. R. & Crook, K. A. W. (1986). Mineralogy and Trace element characteristics of graywackes and tectonic setting discrimination of sedimentary basins. *Contributions to Mineralogy and Petrology*, *92*, 181–193.

Blanchet, H., Montaudouin, X. De, Chardy, P., & Bachelet, G. (2005). Structuring factors and recent changes in subtidal macrozoobenthic communities of a coastal lagoon, Arcachon Bay (France). *Estuarine, Coastal and Shelf Science*, *64*, 561–576.

Bohor, B. F., & Gluskoter, H. J. (1973). Boron in illite as an indicator of paleosalinity of Illinois
coals. *Journal of Sedimentary Research*, *43*(4).

Bohor, B. F. & Gluskoter, H. J. (1967). Clay minerals in Illinois coals. *Journal of Sedimentary Research*, *37*(1), 205–214.

Boillot, G. & Capdevila, R. (1977). The Pyrenees: Subduction and collision? *Earth and Planetary Science Letters*, *35*(1), 151–160.

Bouchet, J.-M. (1968). *Etude océanographique des chenaux du bassin d'Arcachon* (Doctoral Dissertation).

Boulegue, J., Lord III, C. J., & Church, T. M. (1982). Sulfur speciation and associated trace metals (Fe, Cu) in the pore waters of Great Marsh, Delaware. *Geochimica et Cosmochimica Acta*, *46*(3), 453-464.

Bowser, C. J. & Jones, B. F. (2002). Mineralogic controls on the composition of natural waters dominated by silicate hydrolysis. *American Journal of Science*, *302*(7), 582–662.

Branica, M. (1990). *Environmental research in aquatic systems, Volume 3.* Forschungszentrum Jülich.

Brewer, P. G., Spencer, D. W., & Robertson, D. E. (1972). Trace element profiles from the Geosecs-II test station in the Sargasso Sea. *Earth and Planetary Science Letters*, *16*(1), 111–116.

Broecker, W. S., & Peng, T.-H. (1982). *Tracers in the Sea.* Lamont-Doherty Geological Observatory, Palisades, New York.

Brouwer, E., Baeyens, B., Maes, A., & Cremers, A. (1983). Cesium and rubidium ion equilibriums in illite clay. *The Journal of Physical Chemistry*, *87*(7), 1213–1219.

Brumsack, H. J., & Gieskes, J. M. (1983). Interstitial water trace-metal chemistry of laminated sediments from the Gulf of California, Mexico. *Marine Chemistry*, *14*(1), 89-106.

Burton, J. D., Leatherland, T. M., & Liss, P. S. (1970). The Reactivity of Dissolved Silicon in Some Natural Waters. *Limnology and Oceanography*, *15*(3), 473–476.

Calvert, S. E., & Pedersen, T. F. (1993). Geochemistry of recent oxic and anoxic marine sediments: implications for the geological record. *Marine geology, 113*(1-2), 67-88.

Calvert, J. G. (1990). Glossary of Atmospheric Chemistry Terms (Recommendations 1990). *Pure and Applied Chemistry*, *62*(11), 2167–2219.

Campbell, A. C., Palmer, M. R., Klinkhammer, G. P., Bowers, T. S., Edmond, J. M., Lawrence, J. R., Casey, J. F., Thompson, G., Humphris, S., Rona, P., & Karson, J. A. (1988). Chemistry of hot springs on the Mid-Atlantic Ridge. *Nature*, *335*, 514–519.

Canfield, D. E. (1998). A new model for Proterozoic ocean chemistry. *Nature*, *396*(6710), 450.

Comans, R. N. J. & Hockley, D. E. (1992). Kinetics of cesium sorption on illite. *Geochimica et Cosmochimica Acta, 56*(3), 1157–1164.

Comans, R. N. J., Haller, M., & De Preter, P. (1991). Sorption of cesium on illite: Non-equilibrium behaviour and reversibility. *Geochimica et Cosmochimica Acta*, *55*(2), 433–440.

Condomines, M., Morand, P., Camus, G., & Duthou, L. (1982). Chronological and geochemical study of lavas from the Chaîne des Puys, Massif Central, France: Evidence for crustal contamination. *Contributions to Mineralogy and Petrology*, *81*(4), 296–303.

Cornell, R. M. (1993). Adsorption of cesium on minerals: A review. *Journal of Radioanalytical and Nuclear Chemistry Articles, 171*(2), 483–500.

Couch, E. L. (1971). Calculation of paleosalinities from boron and clay mineral data. *American Association of Petroleum Geologists Bulletin*, *55*(10), 1829–1837.

Crerar, E. E., & Arnott, R. W. C. (2007). Facies distribution and stratigraphic architecture of the lower Cretaceous McMurray Formation, Lewis property, northeastern Alberta. *Bulletin of Canadian Petroleum Geology, 55*(2), 99-124.

Dabrin, A., Schäfer, J., Blanc, G., Strady, E., Masson, M., Bossy, C., Castelle, S., Girardot, N., & Coynel, A. (2009). Improving estuarine net flux estimates for dissolved cadmium export at the annual timescale: Application to the Gironde Estuary. *Estuarine, Coastal and Shelf Science*, *84*(4), 429–439.

Dahl, T. W., Ruhl, M., Hammarlund, E. U., Canfield, D. E., Rosing, M. T., & Bjerrum, C. J. (2013). Tracing euxinia by molybdenum concentrations in sediments using handheld X-ray fluorescence spectroscopy (HHXRF). *Chemical Geology*, *360–361*, 241–251.

Dalrymple, R. W., Mackay, D.A., Ichaso, A. A., & Choi, K. S. (2012). Processes, Morphodynamics, and Facies of Tide-Dominated Estuaries. In Davis, Jr., R. A. & Dalrymple, R. W. (Eds.), *Principles of Tidal Sedimentology* (pp. 79–108). Springer Dordrecht.

Dashtgard, S. E., Venditti, J. G., Hill, P. R., Sisulak, C. F., Johnson, S. M., & La Croix, A. D. (2012). Sedimentation across the tidal-fluvial transition in the Lower Fraser River, Canada. *The Sedimentary Record*, *10*(4), 4–9.

Deborde, J., Anschutz, P., Auby, I., Glé, C., Commarieu, M. V., Maurer, D., Lecroart, P., & Abril, G. (2008). Role of tidal pumping on nutrient cycling in a temperate lagoon (Arcachon Bay, France). *Marine Chemistry*, *109*(1–2), 98–114.

Degens, E. T., Williams, E. G., & Keith, M. L. (1958). Environmental studies of Carboniferous sediments. Part II: Application of geochemical criteria. *AAPG Bulletin*, *42*(5), 981-997.

Degens, E. T., Williams, E. G., & Keith, M. L. (1957). Environmental studies of carboniferous sediments Part I: geochemical criteria for differentiating marine from fresh-water shales. *AAPG Bulletin*, *41*(11), 2427-2455.

Doxaran, D., Froidefond, J. M., Castaing, P., & Babin, M. (2009). Dynamics of the turbidity maximum zone in a macrotidal estuary (the Gironde, France): Observations from field and MODIS satellite data. *Estuarine, Coastal and Shelf Science*, *81*(3), 321–332.

Durrant, C. B., Begg, J. D., Kersting, A. B., & Zavarin, M. (2018). Cesium sorption reversibility and kinetics on illite, montmorillonite, and kaolinite. *Science of the Total Environment*, *610*, 511–520.

Dymond, J., Suess, E., & Lyle, M. (1992). Barium in Deep˜Sea Sediment: A Geochemical Proxy for Paleoproductivity. *Paleoceanography*, *7*(2), 163–181.

Eberl, D. D. (1980). Alkali Cation Selectivity and Fixation by Clay Minerals. Clays and Clay Minerals, 28(3), 161–172.

Egozy, Y. (1980). Adsorption of cadmium and cobalt on montmorillonite as a function of solution composition. *Clays and Clay Minerals*, *28*(4), 311–318.

Ekdale, A. A. (1985). Paleoecology of the marine endobenthos. *Palaeogeography, Palaeoclimatology, Palaeoecology*, *50*(1), 63–81.

Elbaz-Poulichet, F., Garnier, J., Guan, D., Martin, J., & Thomas, A. (1996). The conservative behaviour of trace metals (Cd, Cu, Ni and Pb) and as in the surface plume of stratified estuaries: example of the Rhône River (France). *Estuarine, Coastal and Shelf Science*, *42*, 289–310.

Fedo, C. M., Nesbitt, H. W., & Young, G. M. (1995). Unravelling the effects of potassium metasomatism in sedimentary rocks and paleosols, with implications for paleoweathering conditions and provenance. *Geology*, *23*(10), 921–924.

Fernandes, M. M., Scheinost, A. C., & Baeyens, B. (2016). Sorption of trivalent lanthanides and actinides onto montmorillonite: Macroscopic, thermodynamic and structural evidence for ternary hydroxo and carbonato surface complexes on multiple sorption sites. *Water Research, 99,* 74-82.

Filipek, L. H. & Owen, R. M. (1979). Geochemical associations and grain-size partitioning of heavy metals in lacustrine sediments. Chemical Geology, 26(1–2), 105–117.

Förstner, U., & Wittmann, G. T. W. (1979). Trace Metals in Water Purification Processes. *Metal Pollution in the Aquatic Environment*, 324–359. Springer, Berlin Heidelberg.

Frei, D., Liebscher, A., Franz, G., & Dulski, P. (2004). Trace element geochemistry of epidote minerals. *Reviews in Mineralogy and Geochemistry*, *56,* 553-605.

Freslon, N., Bayon, G., Toucanne, S., Bermell, S., Bollinger, C., Chéron, S., Etoubleau, J., Germain, Y., Khripounoff, A., Ponzevera, E., & Rouget, M. (2014). Rare earth elements and neodymium isotopes in sedimentary organic matter. *Geochimica and Cosmochimica Acta, 140*, 177–198.

Fu, X., Wang, J., Chen, W., Feng, X., Wang, D., Song, C., & Zeng, S. (2016). Elemental geochemistry of the early Jurassic black shales in the Qiangtang Basin, eastern Tethys: constraints for palaeoenvironment conditions. *Geological Journal*, *51*(3), 443-454.

Fuller, A. J., Shaw, S., Ward, M. B., Haigh, S. J., Mosselmans, J. F. W., Peacock, C. L., Stackhouse, S., Dent, A. J., Trivedi, D., & Burke, I. T. (2015). Caesium incorporation and retention in illite interlayers. *Applied Clay Science, 108,* 128-134.

Fuller, A. J., Shaw, S., Peacock, C. L., Trivedi, D., Small, J. S., Abrahamsen, L. G., & Burke, I. T. (2014). Ionic strength and pH dependent multi-site sorption of Cs onto a micaceous aquifer sediment. *Applied Geochemistry*, *40*, 32–42.

Gao, S. & Wedepohl, K. H. (1995). The negative Eu anomaly in Archean sedimentary rocks: Implications for decomposition, age and importance of their granitic sources. *Earth and Planetary Science Letters*, *133*(1–2), 81–94.

Garcia-Miragaya, J. & Page, A. L. (1976). Influence of Ionic Strength and Inorganic Complex Formation on the Sorption of Trace Amounts of Cd by Montmorillonite[1]. *Soil Science Society of America Journal*, *40*(5), 658–663.

Garrels, R. M. & Mackenzie, F. T. (1971). Gregor's Denudation of the Continents. *Nature*, *231*, 382–383.

Geyer, W. R., Beardsley, R. C., Lentz, S. J., Candela, J., Limeburner, R., Johns, W. E., Castro, B. E., & Soares, I. D. (1996). Physical oceanography of the Amazon shelf. *Continental Shelf Research*, *16*(5–6), 575–616.

Gibbs, R. J. (1983). Coagulation rates of clay minerals and natural sediments. *Journal of Sedimentary Research*, *53*(4), 1193–1203.

Gibbs, R. J. (1977). Transport phases of transition metals in the Amazon and Yukon Rivers. *Bulletin of the Geological Society of America, 88*(6), 829–843.

Gingras, M. K., MacEachern, J. A., Dashtgard, S. E., Ranger, M. J., Pemberton, S. G., & Hein, F. (2016). The significance of trace fossils in the McMurray Formation, Alberta, Canada. *Bulletin of Canadian Petroleum Geology*, *64*(2), 233-250.

Glé, C., Del Amo, Y., Sautour, B., Laborde, P., & Chardy, P. (2008). Variability of nutrients and phytoplankton primary production in a shallow macrotidal coastal ecosystem (Arcachon Bay, France). *Estuarine, Coastal and Shelf Science*, *76*, 642–656.

Goldberg, S. & J. Kabengi, N. (2010). Bromide Adsorption by Reference Minerals and Soils. *Vadose Zone Journal*, *9*(3), 780.

Goldschmidt, M. V. (1938). Geochemische Verteilungsgesetze der Elemente. IX. Die Mengenverhaltnisse der Elemente und der Atom - Arten. *Skrifter Norske Videnskaps - Akademi Oslo, I. Mat. - Naturv. Klasse*, *4*, 1–148.

Goldschmidt, V. M., Peters, C. L., & Hauptmann, H. (1932). Zur Geochemie des Bors. *Nachrichten von der Gesellschaft der Wissenschaften zu Göttingen, Mathematisch-Physikalische Klasse*, *1932*, 402-407.

Grim, R. E. (1968). *Clay Mineralogy*. McGraw-Hill, New York.
Grim, R. E. (1953). Clay Mineralogy. In *Encyclopedia of Ocean Sciences Second Edition, 2*, 563-571.

Guan, W. B., Kot, S. C., & Wolanski, E. (2005). 3-D fluid-mud dynamics in the Jiaojiang Estuary, China. *Estuarine, Coastal and Shelf Science*, *65*(4), 747–762.

Harkins, W. D. (1917). The evolution of the elements and the stability of complex atoms. I. A new periodic system which shows a relation between the abundance of the elements and the structure of the nuclei of atoms. *Journal of the American Chemical Society*, *39*(5), 856–879.

Haskin, L. A., Wildeman, T. R., Frey, F. A., Collins, K. A., Keedy, C. R., & Haskin, M. A. (1966). Rare Earths in Sediments. *Journal of Geophysical Research*, *71*(24).

Hauck, T. E., Dashtgard, S. E., Pemberton, S G., & Gingras, M. K. (2009). Brackish-Water Ichnological Trends in a Microtidal Barrier Island-Embayment System, Kouchibouguac National Park, New Brunswick, Canada. *Palaios*, *24*(8), 478–496.

Hensen, E. J. M., & Smit, B. (2002). Why clays swell. *Journal of Physical Chemistry, 106*(49), 12664–12667.

Hirst, D. M. (1962). The geochemistry of modern sediments from the Gulf of Paris-II The location and distribution of trace elements. *Geochimica et Cosmochimica Acta*, *26*(1962), 1147–1187.

Holland, H. D. (1978). *The Chemistry of the Atmosphere and Oceans*. John Wiley & Sons, New York.

Horowitz, A. (1985). A primer on trace metal- sediment chemistry. *U.S. Geological Survey Water-Supply Paper*, 2277.

Hu, X. F., Liu, Q. J., Liu, R., Sun, P. C., Hu, S. C., Meng, Q. T., & Liu, S. Y. (2012). Clay mineral and inorganic geochemical characteristics of Eocene Huadian formation in Huadian basin and their paleoenvironment implications. *Journal of China Coal Society*, *37*(3), 416-423.

Huang, J., Feng, L., Lu, D., Zhang, Q., Sun, T., & Chu, X. (2014). Multiple climate cooling prior to Sturtian glaciations: Evidence from chemical index of alteration of sediments in South China. *Nature: Scientific Reports, 4*(6868), 1–6.

Hubbard, S. M., Smith, D. G., Nielsen, H., Leckie, D. A., Fustic, M., Spencer, R. J., & Bloom, L. (2011). Seismic geomorphology and sedimentology of a tidally influenced river deposit, Lower Cretaceous Athabasca oil sands, Alberta, Canada. *AAPG bulletin*, *95*(7), 1123-1145.

Ingri, J., Widerlund, A., Suteerasak, T., Bauer, S., & Elming, S. Å. (2014). Changes in trace metal sedimentation during freshening of a coastal basin. *Marine Chemistry*, *167,* 2-12.

Jablonski, B. V., & Dalrymple, R. W. (2016). Recognition of strong seasonality and climatic cyclicity in an ancient, fluvially dominated, tidally influenced point bar: Middle McMurray Formation, Lower Steepbank River, north˜ eastern Alberta, Canada. *Sedimentology*, *63*(3), 552-585.

Jalón-Rojas, I., Schmidt, S., & Sottolichio, A. (2015). Turbidity in the fluvial Gironde Estuary (southwest France) based on 10-year continuous monitoring: Sensitivity to hydrological conditions. *Hydrology and Earth System Sciences*, *19*(6), 2805–2819.

Jenne, E. A., Kennedy, V. C., Burchard, J. M., & Ball, J. W. (1980). Sediment collection and processing for selective extraction and for total trace element analysis. *Contaminants and Sediments*, *2*, 169-191.

Jenne, E. A. (1968). Controls on Mn, Fe, Co, Ni, Cu and Zn concentrations in soils and waters: the significant role of hydrous Mn and Fe oxides. *Trace Inorganics in Water, Advanced Chemistry*, *73*, 337-387.

Johnson, K. R., Hu, C., Belshaw, N. S., & Henderson, G. M. (2006). Seasonal trace-element and stable-isotope variations in a Chinese speleothem: The potential for high-resolution paleomonsoon reconstruction. *Earth and Planetary Science Letters*, *244*(1–2), 394–407.

Jones, B. F., & Bowser, C. J. (1978). The mineralogy and related chemistry of lake sediments. In Lerman, A. (Ed.), *Lakes*, 179-235. Springer, New York, NY.

Jouanneau, J. M., & Latouche, C. (1981). The Gironde Estuary. In Fuchtbauer, H., Lisitzyn, A. P., Milliman, J. D., & Seibold, E. (Eds.) *Contributions to Sedimentology*, *10*. Schwiezerbart, Stuttgart.

Keene, A. F., Johnston, S. G., Bush, R. T., Burton, E. D., Sullivan, L. A., Dundon, M., McElnea, A. E., Smith, C. D., Ahern, C. R., Powell, B. (2014). Enrichment and heterogeneity of trace elements at the redox-interface of Fe-rich intertidal sediments. *Chemical Geology*, *383*, 1–12.

Kendall, B., Reinhard, C. T., Lyons, T. W., Kaufman, A. J., Poulton, S. W., & Anbar, A. D. (2010). Pervasive oxygenation along late Archaean ocean margins. *Nature Geoscience*, *3*(9), 647-652.

Khan, M. H. R., Liu, J., Liu, S., Seddique, A. A., Cao, L., & Rahman, A. (2019). Clay mineral compositions in surface sediments of the Ganges-Brahmaputra-Meghna river system of Bengal Basin, Bangladesh. *Marine Geology, 412*, 27–36.

Kraepiel, A. M. L., Chiffoleau, J. F., Martin, J. M., & Morel, F. M. M. (1997). Geochemistry of trace metals in the Gironde estuary. *Geochimica et Cosmochimica Acta*, *61*(7), 1421–1436.

Krauskopf, K. B., & Bird, D. K. (1995). *Introduction to geochemistry*. McGraw-Hill, New York.

Krauskopf, K. B. (1956). Factors controlling the concentrations of thirteen rare metals in sea-water. *Geochimica et Cosmochimica Acta, 9*, 1-32.

Kump, L. R. (2008). The rise of atmospheric oxygen. *Nature*, *451*, 277-278.

La Croix, A. D., & Dashtgard, S. E. (2014). Of sand and mud: sedimentological criteria for identifying the turbidity maximum zone in a tidally influenced river. *Sedimentology*, *61*(7), 1961-1981.

Lanceleur, L., Schäfer, J., Bossy, C., Coynel, A., Larrose, A., Masson, M., & Blanc, G. (2011). Silver fluxes to the Gironde Estuary - Eleven years (1999-2009) of monitoring at the watershed scale. *Applied Geochemistry*, *26*(5), 797–808.

Landergren, S. & Carvajal, M. C. (1969). Contribution to the geochemistry of boron, III. The relationship between boron concentration in marine clay sediments and the salinity of the depositional environments expressed as an adsorption isotherm. *Ark. Miner. o. Geol.*, *5*(2), 11–22.

Landergren, S., & Joensuu, O. (1963). Studies on trace element distribution in a sediment core from the Pacific Ocean. *Progress in Oceanography*, *3*, 179-189.

Lanoux, A., Etcheber, H., Schmidt, S., Sottolichio, A., Chabaud, G., Richard, M., & Abril, G. (2013). Factors contributing to hypoxia in a highly turbid, macrotidal estuary (the Gironde, France). *Environmental Sciences: Processes and Impacts*, *15*(3), 585–595.

Large, R. R., Halpin, J. A., Lounejeva, E., Danyushevsky, L. V., Maslennikov, V. V., Gregory, D., Sack, P. J., Haines, P. W., Long, J. A., Makoundi, C., & Stepanov, A. S. (2015). Cycles of nutrient trace elements in the Phanerozoic ocean. *Gondwana Research*, *28*(4), 1282-1293.

Large, R. R., Halpin, J. A., Danyushevsky, L. V., Maslennikov, V. V., Bull, S. W., Long, J. A., Gregory, D. D., Lounejeva, E., Lyons, T. W., Sack, P. J., McGoldrick, P. J., & Calver, C. R. (2014). Trace element content of sedimentary pyrite as a proxy for deep-time ocean-atmosphere evolution. *Earth and Planetary Science Letters, 389*, 209-220.

Lazure, P., Jégou, A., & Kerdreux, M. (2006). Analysis of salinity measurements near islands on the French continental shelf of the Bay of Biscay. *Scientia Marina*, *6*, 7–14.

Le Riche, H. H., & Weir, A. H. (1963). A method of studying trace elements in soil fractions. *Journal of Soil Science*, *14*(2), 225-235.

Lee, J., Park, S. M., Jeon, E. K., & Baek, K. (2017). Selective and irreversible adsorption mechanism of cesium on illite. *Applied Geochemistry*, *85,* 188-193.

Leontopoulou, G., Christidis, G. E., Geraga, M., Papatheodorou, G., & Koutsopoulou, E. (2019). A novel mineralogical approach for provenance analysis of late Quaternary marine sediments: The case of Myrtoon Basin and Cretan Sea, Aegean, Greece. *Sedimentary Geology, 384,* 70–84.

Levy, B. S., & Chambers, R. M. (1987). Bromide as a conservative tracer for soil and water studies. *Hydrological Processes*, *1*(4), 385–389.

Leybourne, M. I., & Johannesson, K. H. (2008). Rare earth elements (REE) and yttrium in stream waters, stream sediments, and Fe-Mn oxyhydroxides: Fractionation, speciation, and controls over REE + Y patterns in the surface environment. *Geochimica et Cosmochimica Acta*, *72*(24), 5962–5983.

Li, Y. H. (1982). A brief discussion on the mean oceanic residence time of elements. *Geochimica et Cosmochimica Acta*, *46*(12), 2671–2675.

Li, X., Li, H., & Yang, G. (2017). Electric fields within clay materials: How to affect the adsorption of metal ions. *Journal of Colloid and Interface Science, 501,* 54–59.

Liss, P. S., & Pointon, M. J. (1973). Removal of dissolved boron and silicon during estuarine mixing of sea and river waters. *Geochimica et Cosmochimica Acta*, *37*(6), 1493–1498.

Liu, X., Tian, R., Du, W., Li, R., Ding, W., & Li, H. (2019). A theory to determine the surface potentials of clay particles in electrolyte solutions. *Applied Clay Science, 169*, 112–119.

Liu, Y., Alessi, D. S., Flynn, S. L., Alam, M. S., Hao, W., Gingras, M., Zhao, H., & Konhauser, K. O. (2018). Acid-base properties of kaolinite, montmorillonite and illite at marine ionic strength. *Chemical Geology*, *483*, 191–200.

Manning, B. A. & Goldberg, S. (1996). Modeling arsenate competitive adsorption on kaolinite, montmorillonite, and illite. *Clays and Clay Minerals*, *44*(5), 609-623.

Marcus, Y. (1983). Ionic radii in aqueous solutions. *Journal of Solution Chemistry, 12*(4), 271-275.

Martin, J.-M., Høgdahl, O., & Philippot, J. C. (1976). Rare earth element supply to the Ocean. *Journal of Geophysical Research*, *81*(18), 3119–3124.

Matthiessen, J. (1995). Distribution patterns of dinoflagellate cysts and other organic-walled microfossils in recent Norwegian-Greenland Sea sediments. *Marine Micropaleontology*, *24*(3-4), 307-334.

Mazzucchelli, M., Rivalenti, G., Vannucci, R., Bottazzi, P., Ottolini, L., Hofman, A. W., & Parenti, M. (1992). Primary positive Eu anomaly in clinopyroxenes of low-crust gabbroic rocks. *Geochimica et Cosmochimica Acta*, *56*(6), 2363–2370.

Mclennan, S. M. (2001). Relationships between the trace element composition of sedimentary rocks and upper continental crust. *Geochemistry, Geophysics, Geosystems*, *2*(4), 2000GC000109.

McLennan, S. M., Hemming, S., McDaniel, D. K., & Hanson, G. N. (1993). Geochemical approaches to sedimentation, provenance, and tectonics. In Johnson, M. J. & Basu, A. (Eds.), *Processes Controlling the Composition of Clastic Sediments, Special Paper 284* (pp. 21-40). Geological Society of America.

McLennan, S. M., Taylor, S. R., McCulloch, M. T., & Maynard, J. B. (1990). Geochemical and Nd-Sr isotopic composition of deep-sea turbidites: Crustal evolution and plate tectonic associations. *Geochimica et Cosmochimica Acta*, *54*(7), 2015–2050.

Mikhailova, M. V. & Isupova, M. V. (2006). Water circulation, sediment dynamics, erosional and accumulative processes in the Gironde Estuary (France). *Water Resources, 33*(1), 10-23.

Milliman, J. D. (2001). River inputs. In Steele, J. H., Thorpe, S. A., & Turekian, K. K. (Eds.), *Elements of Physical Oceanography: A derivative of the Encyclopedia of Ocean Sciences* (pp. 457-464). Academic Press.

Milliman, J. D., & Meade, R. H. (1983). World-Wide Delivery of River Sediment to the Oceans. *The Journal of Geology*, *91*(1), 1–21.

Missana, T., Benedicto, A., García-Gutiérrez, M., & Alonso, U. (2014a). Modeling cesium retention onto Na-, K- and Ca-smectite: Effects of ionic

strength, exchange and competing cations on the determination of selectivity coefficients. *Geochimica et Cosmochimica Acta, 128,* 266-277.

Missana, T., García-Gutiérrez, M., Benedicto, A., Ayora, C., & De-Pourcq, K. (2014b). Modelling of Cs sorption in natural mixed-clays and the effects of ion competition. *Applied Geochemistry*, *49*, 95–102.

Mitchell, S. B., Lawler, D. M., West, J. R., & Couperthwaite, J. S. (2003). Use of continuous turbidity sensor in the prediction of fine sediment transport in the turbidity maximum of the Trent Estuary, UK. *Estuarine, Coastal and Shelf Science*, *58*(3), 645–652.

Mottl, M. J., & Holland, H. D. (1978). Chemical exchange during hydrothermal alteration of basalt by seawater-I. Experimental results for major and minor components of seawater. *Geochimica et Cosmochimica Acta*, *42*(8), 1103–1115.

Musial, G., Reynaud, J. Y., Gingras, M. K., Féniès, H., Labourdette, R., & Parize, O. (2012). Subsurface and outcrop characterization of large tidally influenced point bars of the Cretaceous McMurray Formation (Alberta, Canada). *Sedimentary Geology*, *279*, 156-172.

Nagata, T., Fukushi, K., & Takahashi, Y. (2009). Prediction of iodide adsorption on oxides by surface complexation modeling with spectroscopic confirmation. *Journal of Colloid and Interface Science*, *332*(2), 309–316.

Nakada, R., Shibuya, T., Suzuki, K., & Takahashi, Y. (2017). Europium anomaly variation under low-temperature water-rock interaction: A new thermometer. *Geochemistry International*, *55*(9), 822–832.

Nance, W. B. & Taylor, S. R. (1976). Rare earth element patterns and crustal sedimentary rocks-I. Australian post-Archean sedimentary rocks. *Geochimica et Cosmochimica Acta*, *40*, 1539–1551.

Nath, B. N., Kunzendorf, H., & Pluger, W. L. (2000). Influence of provenance, weathering, and sedimentary processes on the elemental ratios of the fine-grained fraction of the bedload sediments from the Vembanad Lake and the adjoining continental shelf, southwest coast of India. *Journal of Sedimentary Research*, *70*(5), 1081–1094.

Nesbitt, H. W. & Young, G. M. (1982). Early Proterozoic climates and plate motions inferred from major element chemistry of Intites. *Nature*, *299*, 715–717.

Newman, A. C. D. (1987). *Chemistry of clays and clay minerals*. Longman Scientific & Technical, 480.

Nomade, S., Pastre, J.-F., Nehlig, P., Guillou, H., Scao, V., & Scaillet, S. (2014). Tephrochronology of the Mont-Dore volcanic massif (Massif Central, France): new 40Ar/39Ar constraints on the Late Pliocene and Early Pleistocene activity. *Bulletin of Volcanology*, *76*(3), 1–17.

Oddo, G. (1914). Die Molekularstruktur der radioaktiven Atome. *Zeitschrift Fur Anorganische Chemie*, *87*(1), 253–268.

Pattan, J. N., Pearce, N. J. G., & Mislankar, P. G. (2005). Constraints in using Cerium-anomaly of bulk sediments as an indicator of paleo bottom water redox environment: A case study from the Central Indian Ocean Basin. *Chemical Geology*, *221*(3–4), 260–278.

Pemberton, S. G., Flach, P. D., & Mossop, G. D. (1982). Trace fossils from the Athabasca oil sands, Alberta, Canada. *Science*, *217*(4562), 825-827.

Plus, M., Dumas, F., Stanisière, J. Y., & Maurer, D. (2009). Hydrodynamic characterization of the Arcachon Bay, using model-derived descriptors. *Continental Shelf Research*, *29*(8), 1008–1013.

Poulton, S. W., & Canfield, D. E. (2005). Development of a sequential extraction procedure for iron: Implications for iron partitioning in continentally derived particulates. *Chemical Geology, 214*(3–4), 209–221.

Rajec, P., Sucha, V., Eberl, D. D., Srodon, J., Elsass, F. (1999). Effect of illite particle shape on cesium sorption. *Clays and Clay Minerals, 47*(6), 755–760.

Ranger, M. J., & Pemberton, S. G. (1997). Elements of a stratigraphic framework for the McMurray Formation in south Athabasca area, Alberta. *CSPG Special Publication: Petroleum Geology of the Cretaceous Mannville Group, Western Canada – Memoir 18*, 263-291.

Ranger, M. J., & Pemberton, S. G. (1988). Marine influence on the McMurray Formation in the Primrose area, Alberta. *CSPG Special Publication: Sequences, Stratigraphy, Sedimentology: Surface and Subsurface – Memoir 15,* 439-449.

Reardon, E. J. (1981). Kd's – Can they be used to describe reversible ion sorption reactions in contaminant migration? *Groundwater*, *19*(3), 279–286.

Regnier, P. & Wollast, R. (1993). Distribution of Trace-Metals in Suspended Matter of the Scheldt Estuary. *Marine Chemistry*, *43*(1–4), 3–19.

Rimmer, S. M. (2004). Geochemical paleoredox indicators in Devonian-Mississippian black shales, Central Appalachian Basin (USA). *Chemical Geology*, *206*(3–4), 373–391.

Rockwell Geyer, W., Beardsley, R. C., Lentz, S. J., Candela, J., Limeburner, R., Johns, W. E., Castro, B. M., & Dias Soares, I. (1996). Physical oceanography of the Amazon shelf. Continental Shelf Research, 16(5–6), 575–616.

Rudnick, R. L. & Gao, S. (2014). Composition of the Continental Crust. In *Treatise on Geochemistry: Second Edition*, *4*, (pp. 1–51). Elsevier.

Ruiz Pestana, L., Kolluri, K., Head-Gordon, T., & Lammers, L. N. (2017). Direct Exchange Mechanism for Interlayer Ions in Non-Swelling Clays. *Environmental Science and Technology, 51*(1).

Rutherford, J. C. & Bird, A. J. (2004). Metal-responsive transcription factors that regulate iron, zinc, and copper homeostasis in eukaryotic cells. *Eurkaryotic Cell*, *3*(1), 1–13.

Sadiq, M. (1992). *Toxic metal chemistry in marine environments*. Marcel Dekker, Inc., New York.

Salters, V. J. M., & Stracke, A. (2004). Composition of the depleted mantle. *Geochemistry, Geophysics, Geosystems*, *5*(5), Q05B07.

Sawhney, B. L. (1972). Selective sorption and fixation of cations by clay minerals. A review. *Clays and Clay Minerals*, *20*(2), 93–100.

Schieber, J. (1998). Developing a Sequence Stratigraphic Framework for the Late Devonian Chattanooga Shale of the southeastern US: Relevance for the Bakken Shale. *Eighth International Williston Basin Symposium*, 58–68.

Schieber, J. (1988). Redistribution of rare-earth elements during diagenesis of carbonate rocks from the Mid-Proterozoic Newland Formation, Montana, U.S.A. *Chemical Geology, 69,* 111-126.

Scott, C., Lyons, T. W., Bekker, A., Shen, Y. A., Poulton, S. W., Chu, X. L., & Anbar, A. D. (2008). Tracing the stepwise oxygenation of the Proterozoic ocean. *Nature, 452*(7186), 456-459.

Shchepetkina, A., Gingras, M. K., Zonneveld, J., & Pemberton, S. G. (2016). Sedimentary fabrics of the macrotidal, mud-dominated, inner estuary to fluvio-tidal transition zone, Petitcodiac River estuary, New Brunswick, Canada. *Sedimentary Geology*, *333*, 147–163.

Shi, Z. & Kirby, R. (2003). Observations of fine suspended sediment processes in the turbidity maximum at the North Passage of the Changjiang Estuary, China. *Journal of Coastal Research*, *19*(3), 529–540.

Singh, M. (2005). Weathering of the Ganga alluvial plain, northern India: Implications from fluvial geochemistry of the Gomati River. *Applied Geochemistry, 20*, 1–21.

Sinha, A. K. (2012). *Basement Tectonics 13: Proceedings of the Thirteenth International Conference on Basement Tectonics, held in Blacksburg, Virginia, USA, June 1997* (Vol. 7). Springer Science & Business Media.

Slack, J. F., Grenne, T., Bekker, A., Rouxel, O. J., & Lindberg, P. A. (2007). Suboxic deep seawater in the late Paleoproterozoic: evidence from hematitic chert and iron formation related to seafloor-hydrothermal sulfide deposits, central Arizona, USA. *Earth and Planetary Science Letters*, *255*(1-2), 243-256.

Smith, C. & Liu, X. (2018). Spatial and temporal distribution of rare earth elements in the Neuse River, North Carolina. *Chemical Geology*, *488*, 34–43.

Smith, K. S. (1999). Metal Sorption on Mineral Surfaces: An Overview with Examples Relating to Mineral Deposits. *Review in Economic Geology*, *6A–6B*, 161–182.

Sottolichio, A. & Castaing, P. (1999). A synthesis on seasonal dynamics of highly-concentrated structures in the Gironde estuary. *Comptes Rendus de l'Académie Des Sciences - Series IIA - Earth and Planetary Science*, *329*(11), 795–800.

Sposito, G., Skipper, N. T., Sutton, R., Park, S. H., Soper, A. K., & Greathouse, J. A. (1999). Surface geochemistry of the clay minerals. *Proceedings of the National Academy of Sciences*, *96*(7), 3358-3364.

Sposito, G. (1989). *The Chemistry of Soils* (1st ed.). Oxford Univeristy Press.

Stewart, A. D., & Parker, A. (1979). Palaeosalinity and environmental interpretation of red beds from the late Precambrian ('Torridonian') of Scotland. *Sedimentary Geology*, *22*(3-4), 229-241.

Sutherland, B. R., Barrett, K. J., & Gingras, M. K. (2015). Clay settling in fresh and salt water. *Environmental Fluid Mechanics*, *15*(1), 1–15.

Tachi, Y. & Yotsuji, K. (2014). Diffusion and sorption of Cs+, Na+, I- and HTO in compacted sodium montmorillonite as a function of porewater salinity: Integrated sorption and diffusion model. *Geochimica et Cosmochimica Acta*, *132*, 75–93.

Taylor, S. R., & McLennan, S. M. (1985). *The continental crust: Its composition and evolution*. Blackwell Scientific Publications, USA.

Teich-McGoldrick, S. L., Greathouse, J. A., Jové-Colón, C. F., & Cygan, R. T. (2015). Swelling Properties of Montmorillonite and Beidellite Clay Minerals from Molecular Simulation: Comparison of Temperature, Interlayer Cation, and Charge Location Effects. *Journal of Physical Chemistry C, 119*(36), 20880–20891.

Tertre, E., Hubert, F., Bruzac, S., Pacreau, M., Ferrage, E., & Prêt, D. (2013). Ion-exchange reactions on clay minerals coupled with advection/dispersion processes. Application to Na+/Ca2+ exchange on vermiculite: Reactive-transport modeling, batch and stirred flow-through reactor experiments. *Geochimica et Cosmochimica Acta*, *112*, 1–19.

Thorne, L. T. & Nickless, G. (1981). The relation between heavy metals and particle size fractions within the severn estuary (U.K.) inter-tidal sediments. *Science of The Total Environment, 19*(3), 207–213.

Tribovillard, N., Algeo, T. J., Lyons, T., & Riboulleau, A. (2006). Trace metals as paleoredox and paleoproductivity proxies: an update. *Chemical geology*, *232*(1-2), 12-32.

Turner, A. (1996). Trace-metal partitioning in estuaries: Importance of salinity and particle concentration. *Marine Chemistry, 54*, 27–39.

Turner, N. B., Ryan, J. N., & Saiers, J. E. (2006). Effect of desorption kinetics on colloid-facilitated transport of contaminants: cesium, strontium, and illite colloids. *Water Resources Research*, *42*(12), W12S09.

Virolle, M., Brigaud, B., Bourillot, R., Féniès, H., Portier, E., Duteil, T., Nouet, J., Patrier, P., & Beaufort, D. (2018). Detrital clay grain coats in estuarine clastic deposits: origin and spatial distribution within a modern sedimentary system, the Gironde Estuary (south-west France). *Sedimentology 66*, 859–894.

Wang, X., Dong, W., Li, Z., Du, J., & Tao, Z. (2000). Sorption and desorption of radiocesium on red earth and its solid components: Relative contribution and hysteresis. *Applied Radiation and Isotopes*, *52*(4), 813–819.

Weaver, C. E. (1967). Potassium, illite and the ocean. *Geochimica et Cosmochimica Acta*, *31*(11), 2181–2196.

Weaver, C. E. (1958). Geologic interpretation of argillaceous sediments Part I: Origin and significance of sedimentary material in argillaceous rocks. *Bulletin of the American Association of Petroleum Geologists, 42*(2), 254–271.

Wedepohl, B. K. H. (1971). Environmental influences on the chemical composition of shales and clays. *Physics and Chemistry of the Earth*, *8*, 307–333.

Wei, G., Liu, Y., Li, X. H., Shao, L., & Fang, D. (2004). Major and trace element variations of the sediments at ODP Site 1144, South China Sea, during the

last 230 ka and their paleoclimate implications. *Palaeogeography, Palaeoclimatology, Palaeoecology*, *212*(3–4), 331–342.

Whitehouse, U. G., Jeffrey, L. M., Debrecht, J. D. (1960). Differential settling tendencies of clay minerals in saline waters. *Clays and Clay Minerals,* 1-79.

Zhang, M., Liu, Z., Xu, S., Sun, P., & Hu, X. (2013). Element response to the ancient lake information and its evolution history of argillaceous source rocks in the Lucaogou Formation in Sangonghe area of southern margin of Junggar Basin. *Journal of Earth Science*, *24*(6), 987–996.

# APPENDIX A

# PH-DEPENDENT DESORPTION EXPERIMENTS

## 1.0 METHODS

Desorption experiment permutations are defined as unique combinations of sediment, basic reagent, and adjusted pH value. In each of the desorption experiments, 0.5 g of clay was suspended in 30 mL of deionized water in a 50 mL polypropylene tube. The pH of the resulting mixture was measured with a Mettler Toledo FiveEasy Plus pH probe. This pH was then adjusted to 3, 4, 5, 6, 7, or 8 with small aliquots of concentrated HCl, KOH, and NaOH, such that for each of the three clay-water combinations, there are six iterations, each with a different pH value (Table A-1). After a sufficient number of adjustments for the pH to remain stable at the target pH, each of the clay-water suspensions were mixed thoroughly using a Glas-Col Rugged Rotator for twenty-four hours, to ensure that equilibrium was reached. The samples were then prepared for ICP-MS analysis as described in Sec. II-2.5.

## 2.0 RESULTS

The geochemical data for the desorption experiments is represented in the form of scatter plots, in which the concentration of the element in solution is plotted as a function of the solution pH for six pH conditions: 3, 4, 5, 6, 7, and 8. Each of the elements analyzed, (see Tables A-1, A-2, and A-3) has a separate plot, on which the data series for the fluids equilibrated with each of the three clays are

distinguished by the colour scheme depicted in the legend. The exceptions are Cr, Se, Sr, and V, which were below the limit of detection for the instrument in the desorption fluids of all clays at all pH conditions, and were not plotted. As a result, plots were only made of the data for 24 elements, as opposed to the 28 elements that were analyzed. The measurements of each element were repeated between 3 and 5 times in each sample. Errors on the data points in Figures A-1, A-2, and A-3 were calculated by dividing the standard deviation of the repeated instrument measurements by their average, and multiplying this quotient by the concentration value. These calculated errors are displayed on the plot as error bars in units of ppm. Measured concentrations below the detection limit are plotted as 0. Due to the impossibility of calculating the standard deviation of a series of measurements below the threshold at which the element of interest can be detected, the errors on these data points cannot be accurately determined, and are consequently not plotted.

Al: The amount of Al desorbed from kaolinite is consistently very low, near 0 ppm, at all pH values tested (Fig. A-1; Table A-2). There is more variation in the amount of Al desorbed from the two-layer clay minerals, but the trends differ significantly: as the pH increases, the amount of Al desorbed from illite decreases, while the amount of Al desorbed from montmorillonite increases. At the relatively high pH values of 6, 7, and 8, the amount of any Al in the fluids in equilibrium with illite is below the instrument detection limit (Fig. A-1; Table A-1). The trend for the abundance of Al in fluids that are in equilibrium with montmorillonite is less consistent, and the change in concentration values

between pH conditions is less gradual than in the illite case. At the relatively low pH values of 3 and 4, Al is below the instrument detection limit in the desorption fluid associated with montmorillonite, and increases at the relatively basic pH values of 5, 6, 7, and 8 (Fig. A-1; Table A-3).

As: The amount of As that is desorbed from the clay is fairly consistently below the instrument detection limit for all three clay samples at all pH conditions. The notable exception to this trend is in the case of the fluids in equilibrium with montmorillonite at the relatively high pH values of 7 and 8, in which the abundance of As in solution is measurable (Fig. A-1; Table A-3).

B: The concentration of B in solution as a function of solution pH follows the most consistent trend in the case of kaolinite, with the amount of B in the equilibrium fluid decreasing with increasing pH, eventually reaching concentrations that are below the instrument detection limit at pH values of 7, 8, and 9 (Fig. A-1; Table A-2). The trend for fluids in equilibrium with montmorillonite is similar, in that the concentration of B in solution is consistently below the detection limit at the relatively high pH values of 6, 7, and 8, and is slightly higher at the lower pH values of 3, 4, and 5 (Fig. A-1; Table A-3). The concentration of B in solutions that are in equilibrium with illite is below the instrument detection limit at pH values of 7 and 8, but is consistently higher than the amount of B desorbed from either kaolinite or montmorillonite at pH values between 3 and 6. The amount of B in solution is fairly similar at pH values of 3, 5, and 6. The measured concentration of B in solution at a pH value of 4 is slightly lower (Fig. A-1; Table A-1).

Be: The amount of Be that is desorbed from all three clay minerals shows a clear dichotomy between the relatively low pH conditions and the relatively high pH conditions: there is more Be desorbed from the clays at more basic pH conditions. However, within each of the two pH "categories" – acidic and basic – there is little variation in the solution concentration of Be. The concentrations of Be in solution after the fluid equilibrated with the illite sample are noticeably lower at the relatively acidic pH values of 3, 4, and 5, respectively, than at the relatively basic pH values of 6, 7, and 8, respectively (Fig. A-1, Table A-1). Similarly, the concentrations of Be in solutions in equilibrium with kaolinite are lower at the pH conditions of 3, 4, and 5 than at the pH conditions of 6, 7, and 8 (Fig. A-1; Table A-2). The concentrations of Be in solutions equilibrated with montmorillonite are remarkably similar to those in solutions equilibrated with illite and kaolinite (Fig. A-1; Table A-3).

Br: The concentration of Br is below the instrument detection limit in solutions equilibrated with all three clay minerals, at all pH conditions, with one exception: at a pH of 3, the Br desorbed from illite amounts to a few ppm in solution (Fig. A-1; Tables A-1, A-2, and A-3).

Ca: In general, throughout the range of tested pH conditions, the amount of Ca desorbed from the clay samples is highest for illite, intermediate for montmorillonite, and lowest for kaolinite. For all three clay minerals, the solution concentration of Ca decreases in an approximately linear fashion as the solution pH increases from 3 to 5 (Fig. A-1; Tables A-1, A-2, and A-3). As the pH increases to 6, the concentration of Ca in fluids equilibrated with illite and

montmorillonite increased (Fig. A-1; Tables A-1 and A-3). By contrast, as the pH increases to 6, the concentration of Ca in fluids equilibrated with kaolinite decreased to a value below the instrument detection limit (Fig. A-1; Table A-2). At the higher pH values of 7 and 8, the solution concentrations of Ca in fluids equilibrated with illite decrease (Fig. A-1; Table A-1). In the case of the fluids equilibrated with montmorillonite, the concentration of Ca in solution increases linearly as the pH increases to 7 and 8 (Fig. A-1; Table A-3). At the pH 8 condition, the data series for illite and montmorillonite converge; this is the only point at which the concentration of Ca in the solutions in equilibrium with montmorillonite is greater than in the solutions in equilibrium with illite. The concentration of Ca in fluids equilibrated with kaolinite is below the instrument detection limit at pH values of both 7 and 8 (Fig. A-1; Table A-2).

Cd: The solution concentration of Cd was below the detection limit of the instrument in fluids equilibrated with illite at pH values of 4, 7, and 8, in fluids equilibrated with kaolinite at pH values of 7 and 8, and in fluids equilibrated with montmorillonite at pH values of 6, 7, and 8 (Fig. A-1; Tables A-1, A-2, and A-3). The amount of Cd in the fluids equilibrated with kaolinite is very consistent at the lower pH conditions of 3, 4, and 5, and increases slightly at the pH 6 condition (Fig. A-1; Table A-2). The concentrations of Cd in the fluids equilibrated with illite are comparable at the pH 3 and pH 5 conditions, and increased slightly at the pH 6 condition (Fig. A-1; Table A-1). In fluids equilibrated with montmorillonite, the concentration of Cd in solution is similar at pH values of 3, 4, and 5 (Fig. A-1; Table A-3).

Ce: The abundance of Ce in the fluids equilibrated with illite is similar at pH values of 3, 4, 5, and 6. At the higher pH values of 7 and 8, the concentration of Ce in solution is below the instrument detection limit (Fig. A-1; Table A-1). In the fluids that were equilibrated with kaolinite, the concentrations of Ce in solution at the relatively low pH values of 3, 4, and 5 were even more uniform, amounting to 0.214 ppm in all three cases. However, no Ce was detected in the fluids equilibrated with kaolinite at the relatively high pH values of 6, 7, and 8 (Fig. A-1; Table A-2). The trend for the fluids equilibrated with montmorillonite differs from those for the fluids equilibrated with either illite or kaolinite in that, in the case of the former, the concentration of Ce in solution increases incrementally as the solution pH increases (Fig. A-1; Table A-3).

Co: The concentration of Co in solution was below the instrument detection limit for nearly all of the samples, except for the fluid equilibrated with montmorillonite at a pH of 5, and in the fluids equilibrated with illite at the pH values of 3, 4, 5, and 6. In these latter samples, the concentration of Co was higher than in the montmorillonite system, and varied only slightly between samples (Fig. A-2; Tables A-1, A-2, and A-3).

Cr: Cr was not present in sufficient quantities for detection in any of the samples analyzed (Tables A-1, A-2, and A-3).

Cs: Each of the three data series – illite, kaolinite, and montmorillonite – display a trend in which the concentration of Cs decreases as the solution pH increases (Fig. A-2). This trend is one of exponential decay in the case of fluids equilibrated with illite. By contrast, the inverse proportionalities between Cs

concentration and pH in fluids equilibrated with kaolinite or montmorillonite are linear relationships, in which the concentration of Cs in fluids that were equilibrated with kaolinite is greater than that in fluids equilibrated with montmorillonite at almost every pH condition except for pH 6. At a pH of 6, the Cs concentration is greater in the fluid that was equilibrated with montmorillonite than in the fluid equilibrated with kaolinite (Table A-2; Table A-3), and this slight anomaly causes a minor aberration in the linear trend of the montmorillonite series.

Cu: The concentration of Cu in solution was below the instrument limit of detection for nearly all samples measured (Fig. A-2; Tables A-1, A-2, A-3). There are two exceptions: the fluids equilibrated with kaolinite at pH 3 and pH 4 (Table A-2).

Fe: Fe was not detected in any of the samples measured except for the fluids equilibrated with montmorillonite at pH values of 7 and 8 (Fig. A-2; Tables A-1, A-2, A-3).

K: K was not detected in the kaolinite- and montmorillonite-bearing samples at any of the tested pH conditions (Tables A-2, A-3). However, this element was relatively abundant in all of the illite-bearing samples (Table A-1). The concentration of K in the fluid equilibrated with illite at the pH 3 condition was significantly higher than at the pH 4 condition. The highest concentration of K was measured in the fluid equilibrated with illite at a pH of 5; as the solution pH increases from 5 to 8, there is a steady decrease in the concentration of K (Fig. A-2).

Li: The only sample in which Li was abundant enough to be detected by the instrument was the fluid equilibrated with montmorillonite at a pH of 3 (Fig. A-2; Tables A-1, A-2, A-3).

Mg: At nearly every pH condition, Mg is most abundant in the fluids that were in equilibrium with illite, present in intermediate abundance in the fluids that were in equilibrium with montmorillonite, and is the least abundant in the fluids that were in equilibrium with kaolinite (Fig. A-2; Tables A-1, A-2, A-3). At the pH 8 condition, there is a minor exception to this succession: the concentration of Mg in the montmorillonite-equilibrated fluid surpasses that of the illite-equilibrated fluid. In the lower range of pH values the concentration of Mg in the fluids equilibrated with all three clay minerals is observed to decrease as the pH increases from 3 to 5. In the montmorillonite case, the trend is similar, albeit with slightly lower concentrations of Mg. The fluids in equilibrium with kaolinite follow a different trajectory along this same pH range: the solution Mg concentration decreases subtly from the pH 3 condition to the pH 4 condition, and suddenly declines to some value below the instrument detection limit at the pH 5 condition (Fig. A-2). No significant quantities of Mg are detected are detected in the fluids equilibrated with kaolinite at the higher pH values of 6, 7, or 8 (Table A-2). This observation is in distinct contrast to those of the fluids in equilibrium with either illite or montmorillonite, both of which exhibit a sharp increase in the Mg concentration at pH 6. In the former case, this is followed by a gradual decrease in the Mg concentrations as the pH increases to 8. In the fluids that were

equilibrated with montmorillonite, the concentration of Mg in solution increases as the pH increases to 8 in a somewhat linear fashion (Fig. A-2).

Mn: For the greater part of the range of pH values studied, the concentration of Mn is highest in the fluids equilibrated with illite, lower in the fluids equilibrated with montmorillonite, and below the instrument detection limit in all of the fluids equilibrated with kaolinite (Tables A-1, A-2, A-3). The fluids in equilibrium with illite exhibit a linear decrease in the Mn concentration as the pH increases from 3 to 8, crossing over the montmorillonite series at a pH of 7, and crossing over the kaolinite series at a pH of 8, at which the solution concentration of Mn is below the instrument detection limit. In the case of the fluids equilibrated with montmorillonite, the concentration of Mn decreases as the pH increases from 3 to 5, but then begins to increase as the pH increases from 5 to 8 (Fig. A-2).

Na: On the plot of Na desorption, all three of the data series have the same morphology; the points for the illite and kaolinite series are nearly coincident with each other, while the points for the montmorillonite series are suprajacent to the aforementioned series for the other two clays as a result of their significantly higher concentration values (Fig. A-3). The concentrations of Na in the fluids equilibrated with illite and kaolinite are higher in the relatively low pH range of 3 to 5 than in the relatively high pH range of 6 to 8. In the latter pH range, the Na concentration was below the instrument limit of detection for all fluid samples that have been equilibrated with either illite or kaolinite. Within the former pH range, there is little variation in the measured concentrations of Na (Fig. A-3;

Tables A-1 and A-2). This pattern is also observed, *sensu lato,* in the montmorillonite data series, although the measured concentration of Na at the pH 6 condition is intermediate between the average values at the pH 3, 4, and 5 conditions and the average values at the pH 7 and 8 conditions, so there is more of a gradual transition in Na concentration as the pH increases (Fig. A-3; Table A-3).

Ni: The concentration of Ni is below the instrument detection limit for the fluids equilibrated with kaolinite and montmorillonite at all of the pH conditions studied, and for the fluids equilibrated with illite at the relatively high pH values of 6, 7, and 8 (Fig. A-3; Tables A-1, A-2, and A-3).

P: No appreciable amounts of P were detected in any of the fluids that were equilibrated with kaolinite (Fig. A-3; Table A-2). The same observation holds true for the fluids equilibrated with illite and montmorillonite, except for the pH 3 condition (Fig. A-3; Tables A-1 and A-2).

Pb: In each of the three data series, the concentration of Pb increases marginally as the solution pH increases (Fig. A-3). The fluids equilibrated with illite at a pH value of 8, and those equilibrated with kaolinite at pH values of 7 and 8, deviate from this pattern in that their Pb concentrations are below the instrument detection limits (Fig. A-3; Tables A-1 and A-2).

S: No S was detected in the fluids that were in equilibrium with either the illite or kaolinite at any of the pH conditions studied (Fig. A-3; Tables A-1 and A-2). In the fluids equilibrated with montmorillonite, the concentration of S in solution was variable (Fig. A-3; Table A-3).

Se: The concentration of Se was below the instrument detection limit in all of the samples analyzed. However, it should be noted that, relative to the measured Se concentration values, the errors are quite high for the high-pH range of 6 to 8 (Tables A-1, A-2, and A-3).

Si: No Si was detected in any of the fluid samples that were in equilibrium with kaolinite at any of the pH values analyzed (Fig. A-3; Table A-2). In the case of the illite data series, the data points follow a linear trend in which the concentration of Si in solution decreases as the pH increases (Fig. A-3; Table A-1). With respect to the montmorillonite series, the pattern is less distinct, although the highest concentration of Si is measured at the highest pH (Fig. A-3; Table A-3).

Sr: The concentration of Sr was below the instrument detection limit in all of the samples analyzed (Tables A-1, A-2, and A-3). However, it should be noted that, relative to the measured Sr concentration values, the errors are extremely high for the kaolinite data series (Table A-2).

U: The solution concentrations of U in fluids that were equilibrated with illite, kaolinite, and montmorillonite are nearly all within the range of 0.270 ppm to 0.280 ppm (Fig. A-3; Tables A-1, A-2, and A-3). The exceptions to this observation are the fluids in equilibrium with kaolinite at the relatively high pH values of 6, 7, and 8, in which no appreciable amounts of U were detected (Fig. A-3; Table A-2).

V: In all of the fluid samples analyzed, V was not present in sufficient quantities to be detected by the instrument (Tables A-1, A-2, and A-3).

Zn: The concentration of Zn is below the instrument limit of detection in all of the fluid samples equilibrated with illite, in the fluid samples equilibrated with kaolinite at pH values of 3, 4, 5, and 7, and in the fluid samples equilibrated with montmorillonite at pH values of 4 and 5 (Fig. A-3; Tables A-1, A-2, and A-3). At the pH 6 and pH 8 conditions in the kaolinite data series, the two samples for which Zn can be detected contain similar concentrations (Fig. A-3; Table A-2). Within the montmorillonite data series, the Zn concentrations are slightly more variable (Fig. A-3; Table A-3).

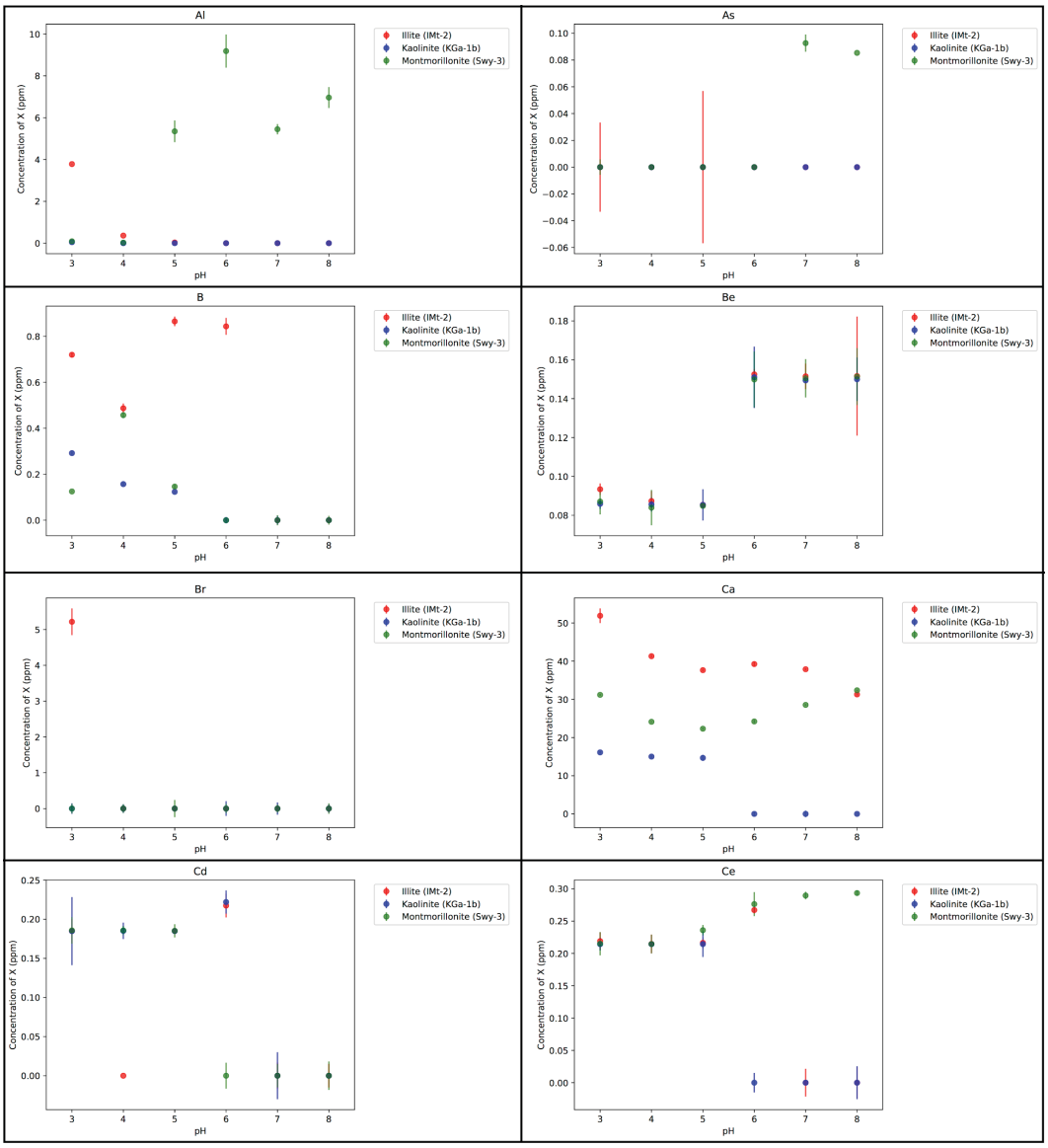
Al
As
B
Be
Br
Ca
Cd
Ce
Illite (IMt-2)
Kaolinite (KGa-1b)
Montmorillonite (Swy-3)
Concentration of X (ppm)
pH

Figure A-1: Compiled plots of selected results from the desorption experiments as described in Appendix A. Each plot shows the solution concentrations of Al, As, B, Be, Br, Ca, Cd, or Ce measured in deionized water after equilibration with illite (IMt-2), kaolinite (KGa-1b), or montmorillonite (Swy-3) at pH conditions ranging from 3 to 8. The pH conditions of each experiment (3, 4, 5, 6, 7, and 8) are located along the x-axis. The concentrations of each of the elements analyzed are located along the y-axis and are plotted in units of ppm. The values of all data points and errors are given in Tables A-1, A-2, and A-3.

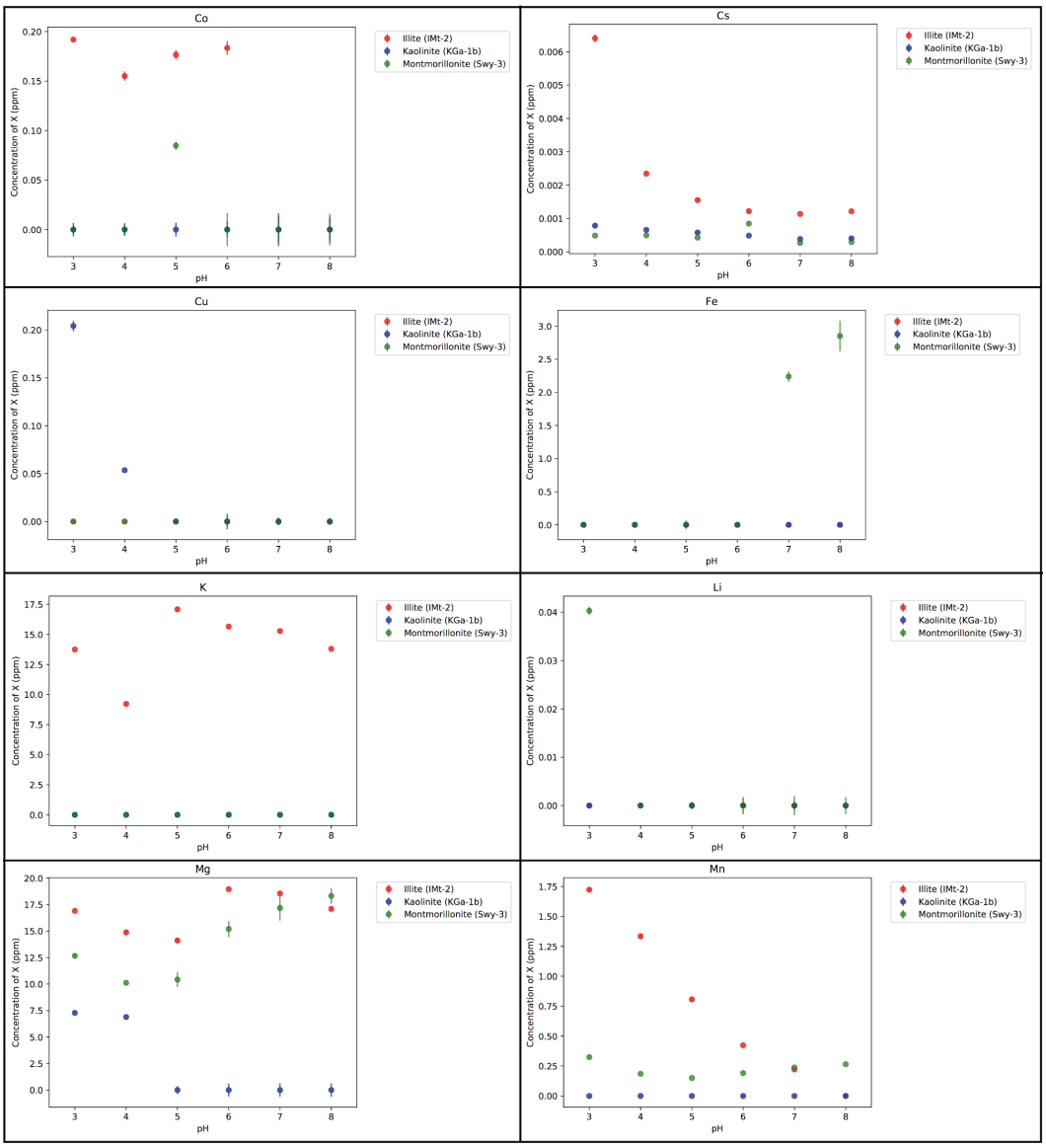
Co
Cs
Cu
Fe
K
Li
Mg
Mn
Illite (IMt-2)
Kaolinite (KGa-1b)
Montmorillonite (Swy-3)
Concentration of X (ppm)
pH

Figure A-2: Compiled plots of selected results from the desorption experiments as described in Appendix A. Each plot shows the solution concentrations of Co, Cs, Cu, Fe, K, Li, Mg, or Mn measured in deionized water after equilibration with illite (IMt-2), kaolinite (KGa-1b), or montmorillonite (Swy-3) at pH conditions ranging from 3 to 8. The pH conditions of each experiment (3, 4, 5, 6, 7, and 8) are located along the x-axis. The concentrations of each of the elements analyzed are located along the y-axis and are plotted in units of ppm. The values of all data points and errors are given in Tables A-1, A-2, and A-3.

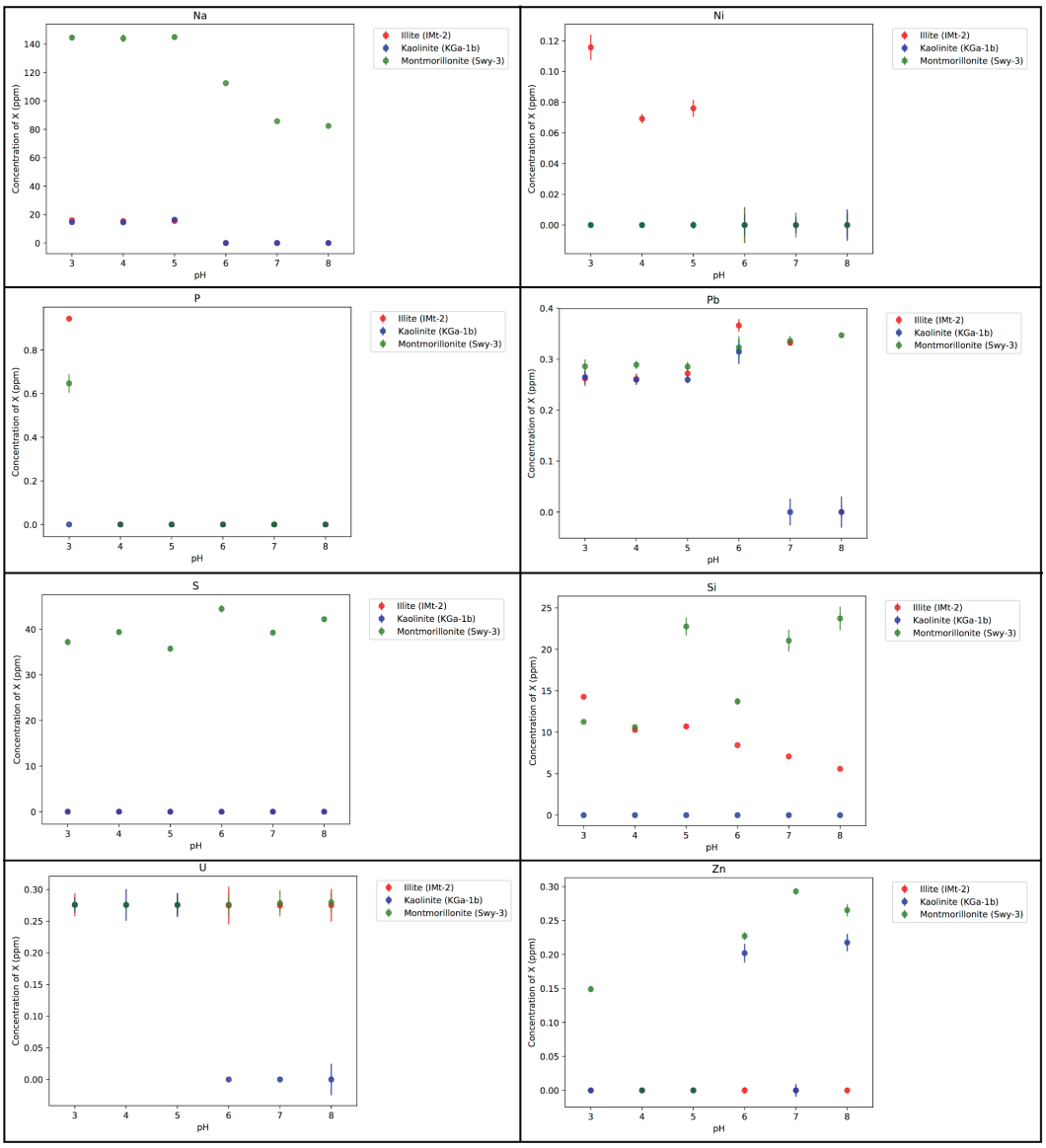
Na
Ni
P
Pb
S
Si
U
Zn
Illite (IMt-2)
Kaolinite (KGa-1b)
Montmorillonite (Swy-3)
Concentration of X (ppm)
pH

Figure A-3: Compiled plots of selected results from the desorption experiments as described in Appendix A. Each plot shows the solution concentrations of Na, Ni, P, Pb, S, Si, U, or Zn measured in deionized water after equilibration with illite (IMt-2), kaolinite (KGa-1b), or montmorillonite (Swy-3) at pH conditions ranging from 3 to 8. The pH conditions of each experiment (3, 4, 5, 6, 7, and 8) are located along the x-axis. The concentrations of each of the elements analyzed are located along the y-axis and are plotted in units of ppm. The values of all data points and errors are given in Tables A-1, A-2, and A-3.

| | I-3 | | I-4 | | I-5 | | I-6 | | I-7 | | I-8 | |
|---|---|---|---|---|---|---|---|---|---|---|---|---|
| | [X] (ppm) | σ (ppm) | [X] (ppm) | σ (ppm) | [X] (ppm) | σ (ppm) | [X] (ppm) | σ (ppm) | [X] (ppm) | σ (ppm) | [X] (ppm) | σ (ppm) |
| **Li** | 0.0000 | 0.0003 | 0.0000 | -0.0004 | 0.0000 | -0.0003 | 0.0000 | 0.0015 | 0.0000 | 0.0010 | 0.0000 | 0.0006 |
| **Be** | 0.0934 | 0.0030 | 0.0873 | 0.0051 | 0.0854 | 0.0000 | 0.1525 | 0.0028 | 0.1515 | 0.0065 | 0.1516 | 0.0306 |
| **B** | 0.7198 | 0.0119 | 0.4871 | 0.0210 | 0.8650 | 0.0211 | 0.8432 | 0.0369 | 0.0000 | 0.0098 | 0.0000 | 0.0124 |
| **Na** | 16.0852 | 0.0922 | 15.4170 | 0.1750 | 15.4745 | 0.1555 | 0.0000 | -0.0631 | 0.0000 | -0.0455 | 0.0000 | -0.0559 |
| **Mg** | 16.9102 | 0.1067 | 14.8833 | 0.2254 | 14.1121 | 0.2656 | 18.9618 | 0.0833 | 18.5543 | 0.0823 | 17.0988 | 0.1471 |
| **Al** | 3.7818 | 0.0129 | 0.3623 | 0.0063 | 0.0326 | 0.0014 | 0.0000 | 0.0025 | 0.0000 | 0.0021 | 0.0000 | 0.0014 |
| **Si** | 14.2773 | 0.0943 | 10.2866 | 0.1529 | 10.7053 | 0.2325 | 8.4481 | 0.0349 | 7.0867 | 0.0401 | 5.5888 | 0.0438 |
| **P** | 0.9435 | 0.0052 | 0.0000 | 0.0000 | 0.0000 | 0.0000 | 0.0000 | -0.0035 | 0.0000 | -0.0010 | 0.0000 | -0.0040 |
| **S** | 0.0000 | -0.1697 | 0.0000 | -0.1348 | 0.0000 | -0.1315 | 0.0000 | -0.0153 | 0.0000 | -0.2018 | 0.0000 | -0.1604 |
| **K** | 13.7496 | 0.0440 | 9.2240 | 0.1006 | 17.0872 | 0.2262 | 15.6587 | 0.1126 | 15.2884 | 0.1061 | 13.8002 | 0.0709 |
| **Ca** | 51.8934 | 1.9212 | 41.3017 | 0.3474 | 37.6439 | 0.3606 | 39.2446 | 0.5369 | 37.8830 | 0.2928 | 31.2856 | 0.2822 |
| **V** | 0.0000 | -0.0034 | 0.0000 | -0.0024 | 0.0000 | -0.0032 | 0.0000 | -0.0010 | 0.0000 | -0.0007 | 0.0000 | -0.0002 |
| **Cr** | 0.0000 | 0.0008 | 0.0000 | 0.0002 | 0.0000 | 0.0006 | 0.0000 | 0.0059 | 0.0000 | 0.0073 | 0.0000 | 0.0054 |
| **Mn** | 1.7239 | 0.0128 | 1.3346 | 0.0210 | 0.8073 | 0.0191 | 0.4235 | 0.0038 | 0.2212 | 0.0033 | 0.0000 | 0.0039 |
| **Fe** | 0.0000 | 0.0078 | 0.0000 | -0.0003 | 0.0000 | 0.0032 | 0.0000 | 0.0005 | 0.0000 | -0.0001 | 0.0000 | 0.0001 |
| **Co** | 0.1919 | 0.0020 | 0.1550 | 0.0047 | 0.1766 | 0.0048 | 0.1834 | 0.0071 | 0.0000 | 0.0168 | 0.0000 | 0.0159 |
| **Ni** | 0.1157 | 0.0083 | 0.0693 | 0.0031 | 0.0760 | 0.0055 | 0.0000 | 0.0118 | 0.0000 | 0.0035 | 0.0000 | 0.0077 |
| **Cu** | 0.0000 | 0.0005 | 0.0000 | 0.0004 | 0.0000 | 0.0010 | 0.0000 | 0.0040 | 0.0000 | 0.0029 | 0.0000 | 0.0029 |
| **Zn** | 0.0000 | 0.0020 | 0.0000 | 0.0028 | 0.0000 | 0.0031 | 0.0000 | 0.0049 | 0.0000 | 0.0063 | 0.0000 | 0.0030 |
| **As** | 0.0000 | -0.0333 | 0.0000 | 0.0000 | 0.0000 | -0.0568 | 0.0000 | 0.0000 | 0.0000 | 0.0000 | 0.0000 | 0.0000 |
| **Se** | 0.0000 | 0.0000 | 0.0000 | 0.0000 | 0.0000 | 0.0000 | 0.0000 | 0.0059 | 0.0000 | 0.0025 | 0.0000 | 0.0024 |
| **Br** | 5.2163 | 0.3729 | 0.0000 | -0.0285 | 0.0000 | -0.0645 | 0.0000 | -0.0225 | 0.0000 | -0.0736 | 0.0000 | -0.0996 |
| **Sr** | 0.0000 | -0.0953 | 0.0000 | -0.0904 | 0.0000 | -0.1001 | 0.0000 | -0.0639 | 0.0000 | -0.1578 | 0.0000 | -0.1561 |
| **Cd** | 0.1850 | 0.0154 | 0.0000 | 0.0000 | 0.1850 | 0.0000 | 0.2174 | 0.0152 | 0.0000 | 0.0168 | 0.0000 | 0.0151 |
| **Cs** | 0.0064 | 0.0001 | 0.0023 | 0.0000 | 0.0016 | 0.0001 | 0.0012 | 0.0001 | 0.0011 | 0.0000 | 0.0012 | 0.0000 |
| **Ce** | 0.2190 | 0.0135 | 0.2147 | 0.0144 | 0.2163 | 0.0084 | 0.2670 | 0.0052 | 0.0000 | 0.0215 | 0.0000 | 0.0243 |
| **Pb** | 0.2624 | 0.0154 | 0.2610 | 0.0110 | 0.2719 | 0.0165 | 0.3662 | 0.0125 | 0.3322 | 0.0046 | 0.0000 | 0.0132 |
| **U** | 0.2759 | 0.0182 | 0.2757 | 0.0043 | 0.2756 | 0.0174 | 0.2747 | 0.0299 | 0.2748 | 0.0095 | 0.2752 | 0.0258 |

Table A-1: Tabulated results from the desorption experiments with illite (IMt-2), described in Appendix A. Data include: [X], the concentrations of selected elements in deionized waters that have been equilibrated with illite at a range of pH conditions, as well as ˜, the error on each concentration, as a concentration standard deviation. All values are in units of ppm. Each of the 28 elements analyzed is listed in the leftmost column. The experiments are identified by a two-digit code in which the first digit, I, denotes the clay as illite, and the second digit is a number between 3 and 8 which denotes the pH condition of that experiment. Measurements were obtained via ICP-MS analysis, as described in Chapter II.

| | K-3 | | K-4 | | K-5 | | K-6 | | K-7 | | K-8 | |
|---|---|---|---|---|---|---|---|---|---|---|---|---|
| | [X] (ppm) | σ (ppm) | [X] (ppm) | σ (ppm) | [X] (ppm) | σ (ppm) | [X] (ppm) | σ (ppm) | [X] (ppm) | σ (ppm) | [X] (ppm) | σ (ppm) |
| **Li** | 0.0000 | -0.0004 | 0.0000 | -0.0006 | 0.0000 | -0.0004 | 0.0000 | 0.0003 | 0.0000 | 0.0004 | 0.0000 | 0.0007 |
| **Be** | 0.0859 | 0.0027 | 0.0856 | 0.0037 | 0.0854 | 0.0080 | 0.1510 | 0.0158 | 0.1494 | 0.0000 | 0.1500 | 0.0112 |
| **B** | 0.2919 | 0.0083 | 0.1570 | 0.0070 | 0.1235 | 0.0029 | 0.0000 | 0.0138 | 0.0000 | 0.0184 | 0.0000 | 0.0091 |
| **Na** | 14.6401 | 0.1220 | 14.5157 | 0.0970 | 16.3915 | 0.1800 | 0.0000 | -0.0820 | 0.0000 | -0.0535 | 0.0000 | -0.1264 |
| **Mg** | 7.2812 | 0.2118 | 6.8924 | 0.2005 | 0.0000 | 0.3669 | 0.0000 | 0.6173 | 0.0000 | 0.6328 | 0.0000 | 0.6245 |
| **Al** | 0.0461 | 0.0016 | 0.0000 | 0.0001 | 0.0000 | -0.0002 | 0.0000 | 0.0036 | 0.0000 | 0.0024 | 0.0000 | 0.0035 |
| **Si** | 0.0000 | 0.0038 | 0.0000 | 0.0052 | 0.0000 | 0.0048 | 0.0000 | 0.0060 | 0.0000 | 0.0060 | 0.0000 | 0.0033 |
| **P** | 0.0000 | 0.0000 | 0.0000 | 0.0000 | 0.0000 | 0.0000 | 0.0000 | -0.0068 | 0.0000 | -0.0039 | 0.0000 | -0.0049 |
| **S** | 0.0000 | -0.1431 | 0.0000 | -0.1270 | 0.0000 | -0.3050 | 0.0000 | -0.4434 | 0.0000 | -0.4363 | 0.0000 | -0.0001 |
| **K** | 0.0000 | -0.0258 | 0.0000 | -0.0251 | 0.0000 | -0.0180 | 0.0000 | 0.0087 | 0.0000 | 0.0201 | 0.0000 | 0.0185 |
| **Ca** | 16.1103 | 0.3173 | 15.0049 | 0.3501 | 14.6688 | 0.7976 | 0.0000 | 0.5347 | 0.0000 | 0.8549 | 0.0000 | 0.2383 |
| **V** | 0.0000 | -0.0014 | 0.0000 | -0.0024 | 0.0000 | -0.0016 | 0.0000 | -0.0010 | 0.0000 | -0.0005 | 0.0000 | -0.0005 |
| **Cr** | 0.0000 | 0.0009 | 0.0000 | 0.0005 | 0.0000 | 0.0002 | 0.0000 | 0.0056 | 0.0000 | 0.0081 | 0.0000 | 0.0077 |
| **Mn** | 0.0000 | 0.0010 | 0.0000 | 0.0021 | 0.0000 | 0.0005 | 0.0000 | 0.0067 | 0.0000 | 0.0018 | 0.0000 | 0.0061 |
| **Fe** | 0.0000 | -0.0002 | 0.0000 | -0.0002 | 0.0000 | -0.0002 | 0.0000 | 0.0001 | 0.0000 | 0.0001 | 0.0000 | 0.0000 |
| **Co** | 0.0000 | 0.0069 | 0.0000 | 0.0065 | 0.0000 | 0.0069 | 0.0000 | 0.0079 | 0.0000 | 0.0135 | 0.0000 | 0.0112 |
| **Ni** | 0.0000 | 0.0000 | 0.0000 | 0.0016 | 0.0000 | 0.0019 | 0.0000 | 0.0069 | 0.0000 | 0.0054 | 0.0000 | 0.0102 |
| **Cu** | 0.2042 | 0.0056 | 0.0536 | 0.0007 | 0.0000 | 0.0005 | 0.0000 | 0.0080 | 0.0000 | 0.0041 | 0.0000 | 0.0017 |
| **Zn** | 0.0000 | 0.0023 | 0.0000 | 0.0030 | 0.0000 | 0.0023 | 0.2020 | 0.0138 | 0.0000 | 0.0094 | 0.2176 | 0.0128 |
| **As** | 0.0000 | 0.0000 | 0.0000 | 0.0000 | 0.0000 | 0.0000 | 0.0000 | 0.0000 | 0.0000 | 0.0000 | 0.0000 | 0.0000 |
| **Se** | 0.0000 | 0.0000 | 0.0000 | 0.0000 | 0.0000 | 0.0000 | 0.0000 | 0.0044 | 0.0000 | 0.0009 | 0.0000 | 0.0024 |
| **Br** | 0.0000 | -0.1470 | 0.0000 | -0.1197 | 0.0000 | -0.0881 | 0.0000 | -0.2063 | 0.0000 | -0.1718 | 0.0000 | -0.1118 |
| **Sr** | 0.0000 | -0.2260 | 0.0000 | -0.3593 | 0.0000 | -0.1345 | 0.0000 | -0.7582 | 0.0000 | -0.7489 | 0.0000 | -0.3898 |
| **Cd** | 0.1848 | 0.0435 | 0.1852 | 0.0105 | 0.1849 | 0.0000 | 0.2220 | 0.0148 | 0.0000 | 0.0300 | 0.0000 | 0.0000 |
| **Cs** | 0.0008 | 0.0001 | 0.0007 | 0.0000 | 0.0006 | 0.0000 | 0.0005 | 0.0000 | 0.0004 | 0.0000 | 0.0004 | 0.0000 |
| **Ce** | 0.2144 | 0.0098 | 0.2144 | 0.0000 | 0.2144 | 0.0200 | 0.0000 | 0.0151 | 0.0000 | 0.0000 | 0.0000 | 0.0255 |
| **Pb** | 0.2647 | 0.0126 | 0.2597 | 0.0101 | 0.2597 | 0.0069 | 0.3147 | 0.0241 | 0.0000 | 0.0262 | 0.0000 | 0.0307 |
| **U** | 0.2757 | 0.0120 | 0.2757 | 0.0250 | 0.2756 | 0.0190 | 0.0000 | 0.0000 | 0.0000 | 0.0000 | 0.0000 | 0.0250 |

Table A-2: Tabulated results from the desorption experiments with kaolinite (KGa-1b), described in Appendix A. Data include: [X], the concentrations of selected elements in deionized waters that have been equilibrated with illite at a range of pH conditions, as well as ˜, the error on each concentration, as a concentration standard deviation. All values are in units of ppm. Each of the 28 elements analyzed is listed in the leftmost column. The experiments are identified by a two-digit code in which the first digit, K, denotes the clay as kaolinite, and the second digit is a number between 3 and 8 which denotes the pH condition of that experiment. Measurements were obtained via ICP-MS analysis, as described in Chapter II.

| | M-3 | | M-4 | | M-5 | | M-6 | | M-7 | | M-8 | |
|---|---|---|---|---|---|---|---|---|---|---|---|---|
| | [X] (ppm) | σ (ppm) | [X] (ppm) | σ (ppm) | [X] (ppm) | σ (ppm) | [X] (ppm) | σ (ppm) | [X] (ppm) | σ (ppm) | [X] (ppm) | σ (ppm) |
| **Li** | 0.0403 | 0.0009 | 0.0000 | 0.0005 | 0.0000 | 0.0008 | 0.0000 | 0.0018 | 0.0000 | 0.0020 | 0.0000 | 0.0018 |
| **Be** | 0.0871 | 0.0066 | 0.0839 | 0.0091 | 0.0848 | 0.0000 | 0.1499 | 0.0144 | 0.1505 | 0.0099 | 0.1514 | 0.0146 |
| **B** | 0.1251 | 0.0019 | 0.4571 | 0.0131 | 0.1463 | 0.0089 | 0.0000 | 0.0038 | 0.0000 | 0.0220 | 0.0000 | 0.0192 |
| **Na** | 144.5616 | 1.6901 | 143.9863 | 2.7013 | 144.9044 | 1.7032 | 112.5110 | 0.3214 | 85.6857 | 0.1942 | 82.3688 | 0.3495 |
| **Mg** | 12.6660 | 0.1873 | 10.1220 | 0.0638 | 10.4310 | 0.7104 | 15.2045 | 0.7603 | 17.1895 | 1.1995 | 18.3179 | 0.7399 |
| **Al** | 0.0894 | 0.0010 | 0.0278 | 0.0005 | 5.3487 | 0.5196 | 9.1837 | 0.7932 | 5.4476 | 0.2475 | 6.9622 | 0.5012 |
| **Si** | 11.2620 | 0.0929 | 10.6283 | 0.1754 | 22.7638 | 1.0826 | 13.7216 | 0.4147 | 21.0573 | 1.3119 | 23.7309 | 1.4257 |
| **P** | 0.6469 | 0.0424 | 0.0000 | 0.0000 | 0.0000 | 0.0000 | 0.0000 | -0.0065 | 0.0000 | -0.0034 | 0.0000 | -0.0079 |
| **S** | 37.2201 | 0.7194 | 39.3923 | 0.6575 | 35.7504 | 0.6846 | 44.4935 | 0.8102 | 39.2651 | 0.4256 | 42.2077 | 0.5310 |
| **K** | 0.0000 | -0.0081 | 0.0000 | 0.0081 | 0.0000 | -0.0296 | 0.0000 | 0.0320 | 0.0000 | 0.0371 | 0.0000 | 0.0352 |
| **Ca** | 31.1776 | 0.2501 | 24.1219 | 0.1342 | 22.3108 | 0.2581 | 24.2121 | 0.4141 | 28.5476 | 0.1977 | 32.3643 | 0.1818 |
| **V** | 0.0000 | -0.0022 | 0.0000 | -0.0189 | 0.0000 | -0.0030 | 0.0000 | -0.0011 | 0.0000 | -0.0009 | 0.0000 | -0.0006 |
| **Cr** | 0.0000 | 0.0006 | 0.0000 | 0.0005 | 0.0000 | 0.0005 | 0.0000 | 0.0036 | 0.0000 | 0.0071 | 0.0000 | 0.0049 |
| **Mn** | 0.3243 | 0.0046 | 0.1854 | 0.0015 | 0.1504 | 0.0007 | 0.1909 | 0.0033 | 0.2373 | 0.0030 | 0.2655 | 0.0032 |
| **Fe** | 0.0000 | 0.0092 | 0.0000 | 0.0079 | 0.0000 | 0.0665 | 0.0000 | 0.0146 | 2.2396 | 0.0788 | 2.8514 | 0.2322 |
| **Co** | 0.0000 | 0.0049 | 0.0000 | 0.0055 | 0.0847 | 0.0042 | 0.0000 | 0.0168 | 0.0000 | 0.0158 | 0.0000 | 0.0134 |
| **Ni** | 0.0000 | 0.0014 | 0.0000 | 0.0019 | 0.0000 | 0.0025 | 0.0000 | 0.0114 | 0.0000 | 0.0081 | 0.0000 | 0.0069 |
| **Cu** | 0.0000 | 0.0003 | 0.0000 | 0.0003 | 0.0000 | 0.0005 | 0.0000 | 0.0060 | 0.0000 | 0.0015 | 0.0000 | 0.0039 |
| **Zn** | 0.1490 | 0.0045 | 0.0000 | 0.0021 | 0.0000 | 0.0026 | 0.2271 | 0.0059 | 0.2929 | 0.0048 | 0.2653 | 0.0092 |
| **As** | 0.0000 | -0.0058 | 0.0000 | 0.0000 | 0.0000 | 0.0000 | 0.0000 | 0.0000 | 0.0926 | 0.0064 | 0.0854 | 0.0000 |
| **Se** | 0.0000 | 0.0000 | 0.0000 | 0.0000 | 0.0000 | 0.0000 | 0.0000 | 0.0021 | 0.0000 | 0.0010 | 0.0000 | 0.0014 |
| **Br** | 0.0000 | -0.1388 | 0.0000 | -0.1233 | 0.0000 | -0.2399 | 0.0000 | -0.1307 | 0.0000 | -0.1194 | 0.0000 | -0.1463 |
| **Sr** | 0.0000 | -0.0385 | 0.0000 | -0.0706 | 0.0000 | -0.0843 | 0.0000 | -0.0594 | 0.0000 | -0.0438 | 0.0000 | -0.0913 |
| **Cd** | 0.1857 | 0.0171 | 0.1856 | 0.0058 | 0.1852 | 0.0084 | 0.0000 | 0.0166 | 0.0000 | 0.0150 | 0.0000 | 0.0182 |
| **Cs** | 0.0005 | 0.0000 | 0.0005 | 0.0000 | 0.0004 | 0.0000 | 0.0008 | 0.0000 | 0.0003 | 0.0000 | 0.0003 | 0.0000 |
| **Ce** | 0.2150 | 0.0180 | 0.2145 | 0.0146 | 0.2359 | 0.0081 | 0.2763 | 0.0186 | 0.2895 | 0.0058 | 0.2934 | 0.0040 |
| **Pb** | 0.2859 | 0.0137 | 0.2889 | 0.0081 | 0.2853 | 0.0096 | 0.3230 | 0.0223 | 0.3359 | 0.0098 | 0.3470 | 0.0050 |
| **U** | 0.2761 | 0.0082 | 0.2758 | 0.0065 | 0.2759 | 0.0133 | 0.2761 | 0.0177 | 0.2783 | 0.0207 | 0.2798 | 0.0145 |

Table A-3: Tabulated results from the desorption experiments with montmorillonite (Swy-3), described in Appendix A. Data include: [X], the concentrations of selected elements in deionized waters that have been equilibrated with illite at a range of pH conditions, as well as ˜, the error on each concentration, as a concentration standard deviation. All values are in units of ppm. Each of the 28 elements analyzed is listed in the leftmost column. The experiments are identified by a two-digit code in which the first digit, M, denotes the clay as montmorillonite, and the second digit is a number between 3 and 8 which denotes the pH condition of that experiment. Measurements were obtained via ICP-MS analysis, as described in Chapter II.

# APPENDIX B

## SPECIATION MODELLING OF MAJOR IONS IN NATURAL RIVER WATER AND SEA WATER SAMPLES

The major elements initially measured in North Saskatchewan River Water (NSRW) and English Bay Sea Water (EBSW) (Table II-4) were input into Hydra software to define the chemical system of each of these two water samples prior to equilibration with the clays. The speciation of each component in EBSW and NSRW was modelled using Medusa software to make fraction diagrams (Fig. B-1 and Fig. B-2, respectively). C and Cl and could not be analyzed by the ICP-MS used in this study. Hence, the model input molalities for C and Cl are published average values for river water and sea water (Holland, 1978). The ionic strengths of the NSRW system and the EBSW system were calculated using Equation B-1.1 and Equation B-1.2, respectively, and used as model inputs.

$$I_{RW} = \frac{1}{2}\sum_{i=1}^{n} m_i \cdot z_i^2 \quad \text{(B-1.1)}$$

$$m_i = initial\ molality\ of\ component\ i\ in\ NSRW$$
$$= concentration\ measured\ in\ NSRW\ prior\ to\ equilibration\ with\ clays\ (Table\ II-4)$$

$$m_{Br^-} = 0.0001\ \frac{mol}{L}$$

$$m_{Ca^{2+}} = 0.0014\ \frac{mol}{L}$$

$$m_{Cl^-} = 0.0002\ \frac{mol}{L}$$

$$m_{HCO_3^-} = 0.0009\ \frac{mol}{L}$$

$$m_{K^+} = 0.0000\ \frac{mol}{L} \text{(BDL)}$$

$$m_{Mg^{2+}} = 0.0017\ \frac{mol}{L}$$

$$m_{Na^+} = 0.0000\ \frac{mol}{L}\text{(BDL)}$$
$$m_{SO_4^{2-}} = 0.0006\ \frac{mol}{L}$$
$$m_{\mathrm{Si(OH)_4}} = 0.0001\ \frac{mol}{L}$$
$$m_{Sr^{2+}} = 0.0000\ \frac{mol}{L}\text{(BDL)}$$

$$z_i = charge\ on\ ion\ of\ species\ i\ in\ NSRW$$
$$z_{Br^-} = -1$$
$$z_{Ca^{2+}} = +2$$
$$z_{Cl^-} = -1$$
$$z_{HCO_3^-} = -1$$
$$z_{K^+} = +1$$
$$z_{Mg^{2+}} = +2$$
$$z_{Na^+} = +1$$
$$z_{SO_4^{2-}} = -2$$
$$z_{\mathrm{Si(OH)_4}} = 0$$
$$z_{Sr^{2+}} = +2$$

$$I_{RW} = 8.0 \times 10^{-3}$$

$$I_{SW} = \frac{1}{2}\sum_{i=1}^{n} m_i \cdot z_i^2 \qquad \text{(B-1.2)}$$

$$m_i = initial\ molality\ of\ component\ i\ in\ EBSW$$
$$= concentration\ measured\ in\ EBSW\ prior\ to\ equilibration\ with\ clays\ (Table\ II-4)$$
$$m_{Br^-} = 0.0003\ \frac{mol}{L}$$
$$m_{Ca^{2+}} = 0.0040\ \frac{mol}{L}$$
$$m_{Cl^-} = 0.5460\ \frac{mol}{L}$$
$$m_{HCO_3^-} = 0.0024\ \frac{mol}{L}$$
$$m_{K^+} = 0.0041\ \frac{mol}{L}$$
$$m_{Mg^{2+}} = 0.0211\ \frac{mol}{L}$$

$$m_{Na^+} = 0.0199\ \frac{mol}{L}$$
$$m_{SO_4^{2-}} = 0.0017\ \frac{mol}{L}$$
$$m_{\mathrm{Si(OH)_4}} = 0.0000\ \frac{mol}{L}\text{(BDL)}$$
$$m_{Sr^{2+}} = 0.0000\ \frac{mol}{L}\text{(BDL)}$$

$$z_i = charge\ on\ ion\ of\ species\ i\ in\ EBSW$$
$$z_{Br^-} = -1$$
$$z_{Ca^{2+}} = +2$$
$$z_{Cl^-} = -1$$
$$z_{HCO_3^-} = -1$$
$$z_{K^+} = +1$$
$$z_{Mg^{2+}} = +2$$
$$z_{Na^+} = +1$$
$$z_{SO_4^{2-}} = -2$$
$$z_{\mathrm{Si(OH)_4}} = 0$$
$$z_{Sr^{2+}} = +2$$

$$I_{SW} = 3.4 \times 10^{-1}$$

The redox potentials of the NSRW system and the EBSW system were calculated as pe using published average redox potential (Eh) values (Krauskopf & Bird, 1995) for river water and sea water in Equation B-2.1 and Equation B-2.2, respectively. These calculated pe values were input into each model.

$$pe = \frac{Eh_{RW}}{0.05916} = 6.8 \qquad \text{(B-2.1)}$$

$$Eh_{RW} = typical\ redox\ potential\ of\ river\ water\ = 0.4\ V$$

$$pe = \frac{Eh_{SW}}{0.05916} = 5.1 \qquad \text{(B-2.2)}$$

$$Eh_{SW} = typical\ redox\ potential\ of\ sea\ water\ = 0.3\ V$$

The pH of each water sample was measured upon collection and used as model inputs:

$$pH_{RW} = 6.8$$

$$pH_{SW} = 7.0$$

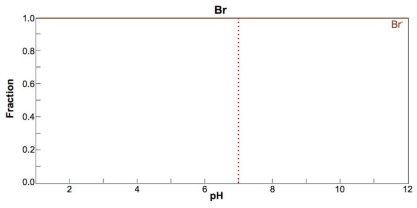
Br
Br⁻
Fraction
pH

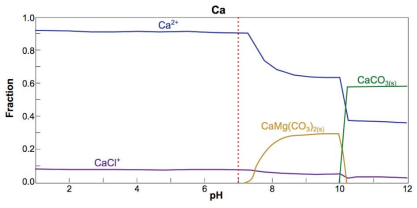
Ca
Ca2+
CaCO3(s)
CaMg(CO3)2(s)
CaCl+
Fraction
pH

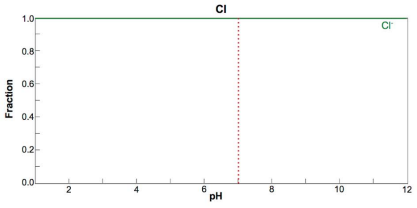
Cl
Cl⁻
Fraction
pH

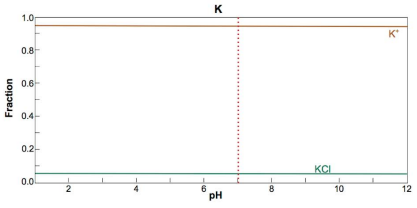
K
K+
KCl
Fraction
pH

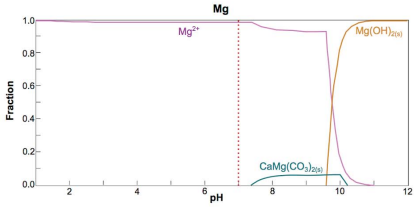
Mg
Mg2+
Mg(OH)2(s)
CaMg(CO3)2(s)
Fraction
pH

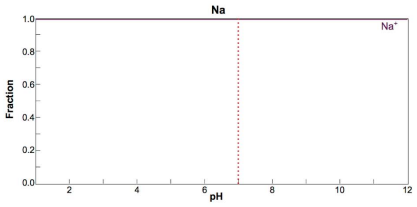
Na
Na+
Fraction
pH

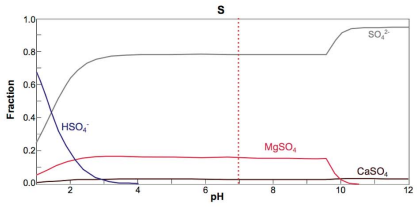
S
SO4 2-
HSO4-
MgSO4
CaSO4
Fraction
pH

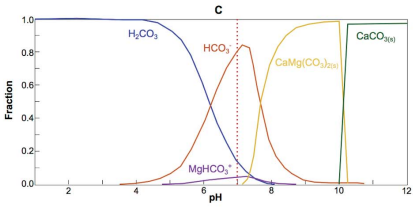
C
H2CO3
HCO3-
CaMg(CO3)2(s)
CaCO3(s)
MgHCO3+
Fraction
pH

Figure B-1: Compiled speciation diagrams of the major elements detected in the English Bay Sea Water (EBSW) sample. Model input molalities for Br, Ca, K, Mg, Na, and S are the initial concentrations of these elements in the water sample prior to equilibration with the clays, in Table II-4. The model input molalities for C and Cl are published average values for sea water (Holland, 1978). This system was modeled at an ionic strength (I) of $3.4 \times 10^{-1}$ and a redox potential (pe) of 5.1. The pH of this water sample at the time of collection was measured as 7.00 and is denoted by the red dashed line on each diagram.

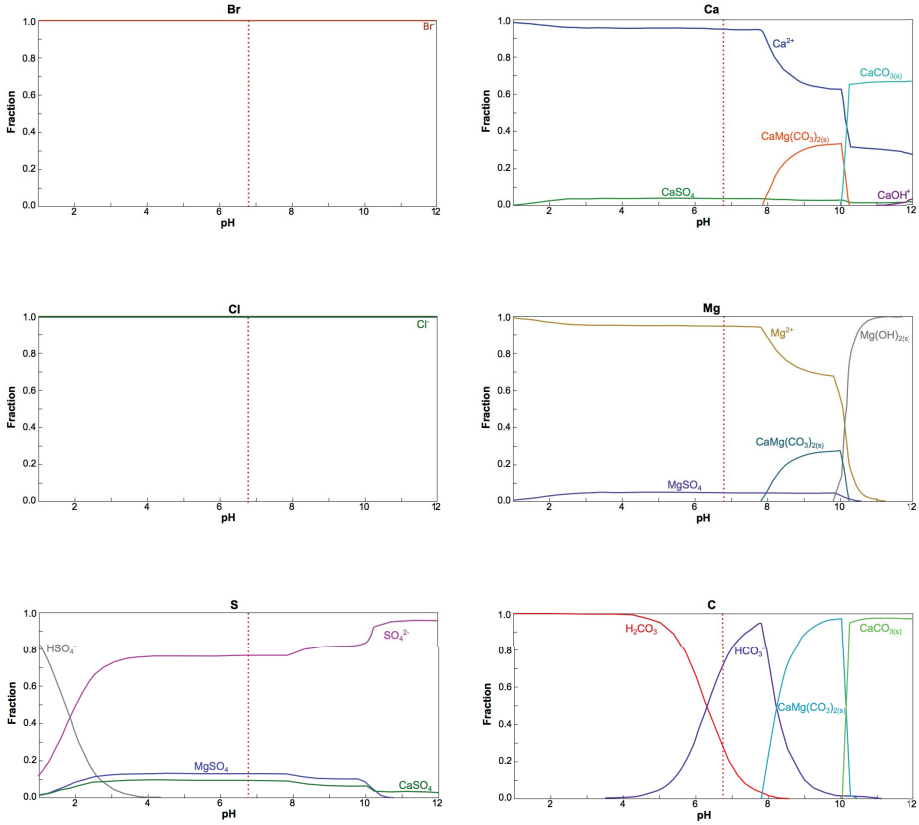
Br
Br⁻
Ca
Ca²⁺
CaCO3(s)
CaMg(CO3)2(s)
CaSO4
CaOH⁺
Cl
Cl⁻
Mg
Mg²⁺
Mg(OH)2(s)
CaMg(CO3)2(s)
MgSO4
S
HSO4⁻
SO4²⁻
MgSO4
CaSO4
C
H2CO3
HCO3⁻
CaMg(CO3)2(s)
CaCO3(s)
Fraction
pH

Figure B-2: Compiled speciation diagrams of the major elements detected in the North Saskatchewan River Water (NSRW) sample. Model input molalities for Br, Ca, Mg, and S are the initial concentrations of these elements in the water sample prior to equilibration with the clays, in Table II-4. The model input molalities for C and Cl are published average values for river water (Holland, 1978). This system was modeled at an ionic strength (I) of $8.0 \times 10^{-3}$ and a redox potential (pe) of 6.8. The pH of this water sample at the time of collection was measured as 6.80 and is denoted by the red dashed line on each diagram.

# APPENDIX C

# ENRICHMENT FACTORS OF MAJOR AND TRACE ELEMENTS IN SEDIMENTS AND SURFACE WATERS FROM ARCACHON BAY AND THE GIRONDE ESTUARY

## 1.0 BACKGROUND ON ENRICHMENT FACTORS

It is often necessary to normalize measured element concentrations to conservative elements in order to determine the proportion of the element of interest that is detrital as opposed to chemically partitioned. The normalized value, $X_N$, of the concentration of a specific element of interest, X, can be calculated as a simple ratio of the raw concentration value, $X_R$, to the concentration of the conservative element, C, as in Equation C-1:

$$X_N = \frac{X_R}{C} \qquad \text{(C-1)}$$

The most commonly used conservative elements are Al and Ti. These elements are relatively abundant in granitic rocks (e.g. Taylor & McLennan, 1985; McLennan, 2001; Rudnick & Gao, 2014), almost entirely terrigenous in origin, and their flux to sediments is relatively constant over time, making them useful proxies for detrital sediment input (e.g. Calvert & Pederson, 1993). Al is a major structural component of the crystal lattice in both primary (e.g. feldspar) and secondary (e.g. clay) aluminosilicate minerals. Al is usually not mobilized by diagenesis, and it is widely considered to be a proxy for the proportion of the sediment that is comprised of aluminosilicate minerals. The mobility of Ti in natural

environments tends to be very low, as this element is relatively insoluble (Le Riche & Weir, 1963) and Ti-bearing minerals, such as ilmenite and rutile, tend to be extremely resistant to weathering (Anand & Gilkes, 1984). However, the concentration of Ti in natural waters is much lower than that of Al. As this research analyzes the major and trace element content of both sediment and water samples, Al is the conservative element used.

The interpretation of element concentrations in siliciclastic sediments is complicated by variable distributions of organic matter and mineral phases, such as carbonate and apatite, between different samples. Therefore, to aid the interpretation of Al-normalized element concentration data, in this paper we calculate the enrichment factor of a trace element in the sample of interest relative to a reference standard (Equation C-2).

$$EF_X = \frac{[X]_{sample}}{[Al]_{sample}} \times \frac{[Al]_{reference\ standard}}{[X]_{reference\ standard}} \qquad \text{(C-2)}$$

*X = element of interest*

*$EF_X$ = enrichment factor of X*

If the enrichment factor of some element of interest, X, is less than 0.95, then element X is depleted relative to the reference standard. If the enrichment factor of an element of interest is greater than 1.05, then element X is enriched relative to the reference standard. Enrichment factors between 0.95 and 1.05 are considered to be close enough to 1 to assume minimal enrichment or depletion.

The type of reference standard used in these calculations depends upon the research objective. When applying the trace element data to the reconstruction of palaeoproductivity and palaeoredox conditions, the sample may be compared to an average shale (e.g. Wedepohl, 1971). However, in this study, enrichment factors are being used to inform our understanding of the provenance and weathering history of the sediments of interest. Consequently, the sediment and water samples presented here are compared to the average upper continental crust (Rudnick & Gao, 2014). Major and trace element abundances of the average upper continental crust (Rudnick & Gao, 2014) are compiled in Table III-4 and Table III-6.

# 2.0 RESULTS

## 2.1 ENRICHMENT FACTORS OF MAJOR ELEMENTS IN SEDIMENT SAMPLES

The enrichment factors calculated for the major elements in the sediment samples (Table C-1) indicate consistent enrichment of K and P in all sediments analyzed. The majority of the other major elements are depleted in these sediment samples, with the exception of Si, which is enriched in both of the sediment samples from Location G1, one of the two sediment samples from Location G2, the sediment sample from Location G4, two of the three sediment samples from Location A3, and both of the sediment samples from Location A4 (Table C-1). The

enrichment factors of Si in one of the sediment samples from Location G2 and the sediment sample from Location G5 are sufficiently close to 1 to indicate minimal variation from UCC values (Table C-1). Although Ca is depleted in the majority of the sediment samples analyzed, it has similar abundance to that in UCC in one of the sediment samples from Location G1 (Table C-1).

## 2.2 ENRICHMENT FACTORS OF TRACE ELEMENTS IN SEDIMENT SAMPLES

Of the trace elements analyzed, nearly all are depleted in the Arcachon and Gironde sediment samples, with few exceptions. In one of the sediment samples from Location G1, Rb is neither enriched nor depleted, but is proportional to the Rb content of UCC (Table C-2). Similar behaviours can be seen in the case of Nb in the sediment sample from Location G5 and in one of the two sediment samples from Location A4, and in the case of V, Sm, and Gd in one of the sediment samples from Location A3 (Table C-2). The only trace element that appears to be enriched relative to UCC is Eu in one of the two sediment samples from Location A3 (Table C-2).

## 2.3 ENRICHMENT FACTORS OF MAJOR ELEMENTS IN SURFACE WATER SAMPLES

All of the water samples analyzed in this study resemble the river water standard in that they are enriched in Fe while being depleted in Ti (Table C-3). The values of enrichment factors for all other major elements in the Arcachon Bay and Gironde Estuary water samples indicate enrichment, with the exception of Mg, which is depleted in the surface water sample from Location G2 (Table C-3). There is no data available for Si in any of the surface water samples, or for Na and K in the surface water sample from Location A3.

## 2.4 ENRICHMENT FACTORS OF TRACE ELEMENTS IN SURFACE WATER SAMPLES

The values of the trace element enrichment factors in the surface water samples collected from Arcachon Bay and the Gironde Estuary are significantly more variable than the values for the corresponding sediments. Similar to the river water standard, the surface water samples from Locations G2, G3, G4, and A1 are depleted in Sc, while the surface water sample from Location G1 is neither enriched nor depleted in Sc (Table C-4). Cr and Ni are both depleted in the surface water sample from Location G2 (Table C-4). Zr is depleted in all of the surface water samples analyzed, except for those from Locations G5 and A4, in which this element is neither enriched nor depleted (Table C-4). Ba is depleted in the

surface water samples from Locations G2, G3, and A1(Table C-4). La is depleted in the surface water samples from Locations G1 and G2 (Table C-4). Ce, Pr, and Nd are depleted in the surface water sample from Location G1 and are neither enriched nor depleted in the surface water sample from Location G2 (Table C-4). The surface water sample from Location G2 is neither enriched nor depleted in Er. Tm and Lu are neither enriched nor depleted in the surface water from Location G1, but are depleted in that from Location G2 (Table C-4). Yb is depleted in the surface water samples from both Locations G1 and G2 (Table C-4). The surface water samples at Locations G1, G2, G3, G4, G6, and A1 are all depleted with respect to Hf (Table C-4). Re is extremely depleted in the surface water sample collected from Location A2 (Table C-4). Th is depleted in all of the surface water samples collected, except for that from Location A3 (Table C-4).

| | PAAS | G1-MD-GS | G1-MD-MT | G2-MD-GS | G2-MD-MT | G3-1 | G3-2 | G4 | G5-MDX | G6 | A3-MD-X | A3-MD-1 | A3-MD-2 | A4 | A4-MD |
|---|---|---|---|---|---|---|---|---|---|---|---|---|---|---|---|
| **Si** | 0.65 | 1.28 | 1.26 | 1.19 | 0.98 | 0.76 | 0.72 | 1.25 | 0.97 | 0.76 | 0.85 | 1.30 | 1.95 | 1.10 | 1.53 |
| **Ti** | 0.65 | 0.61 | 0.60 | 0.65 | 0.71 | 0.65 | 0.61 | 0.63 | 0.71 | 0.62 | 0.57 | 0.60 | 0.61 | 0.59 | 0.61 |
| **Fe** | 0.54 | 0.52 | 0.52 | 0.52 | 0.58 | 0.61 | 0.59 | 0.53 | 0.58 | 0.59 | 0.62 | 0.81 | 0.79 | 0.65 | 0.63 |
| **Mn** | 0.64 | 0.68 | 0.69 | 0.84 | 0.84 | 0.70 | 0.70 | 0.74 | 0.91 | 0.59 | 0.30 | 0.27 | 0.23 | 0.27 | 0.51 |
| **Mg** | 0.37 | 0.44 | 0.38 | 0.38 | 0.38 | 0.42 | 0.42 | 0.37 | 0.39 | 0.42 | 0.38 | 0.36 | 0.38 | 0.40 | 0.41 |
| **Ca*** | 0.22 | 1.00 | 0.44 | 0.30 | 0.22 | 0.27 | 0.26 | 0.36 | 0.22 | 0.43 | 0.44 | 0.09 | 0.09 | 0.24 | 0.72 |
| **Na** | 0.15 | 0.68 | 0.30 | 0.20 | 0.15 | 0.18 | 0.18 | 0.24 | 0.15 | 0.29 | 0.42 | 0.43 | 0.44 | 0.54 | 0.49 |
| **K** | 1.17 | 1.49 | 1.43 | 1.36 | 1.17 | 1.09 | 1.06 | 1.39 | 1.13 | 1.11 | 1.17 | 1.03 | 1.09 | 1.23 | 1.26 |
| **P** | 1.77 | 2.43 | 2.37 | 2.56 | 3.03 | 2.13 | 2.21 | 2.48 | 2.72 | 2.27 | 1.64 | 2.50 | 3.23 | 2.24 | 2.49 |

Table C-1: Enrichment factors of the major elements in post-Archean average shale (Taylor & McLennan, 1985) and sediment samples from Arcachon Bay and the Gironde Estuary (this study). Values are calculated from the major element concentrations listed in Table III-4, using Equation C-2.

| | PAAS | G1-MD-GS | G1-MD-MT | G2-MD-GS | G2-MD-MT | G3-1 | G3-2 | G4 | G5-MDX | G6 | A3-MD-X | A3-MD-1 | A3-MD-2 | A4 | A4-MD |
|---|---|---|---|---|---|---|---|---|---|---|---|---|---|---|---|
| **Sc** | 0.55 | 0.47 | 0.45 | 0.49 | 0.52 | 0.53 | 0.52 | 0.49 | 0.54 | 0.53 | 0.51 | 0.56 | 0.60 | 0.52 | 0.54 |
| **V** | 0.74 | 0.63 | 0.65 | 0.60 | 0.66 | 0.66 | 0.64 | 0.62 | 0.64 | 0.68 | 0.77 | 0.93 | 1.01 | 0.83 | 0.86 |
| **Cr** | 0.57 | 0.50 | 0.50 | 0.52 | 0.61 | 0.56 | 0.54 | 0.49 | 0.56 | 0.55 | 0.54 | 0.62 | 0.67 | 0.57 | 0.61 |
| **Co** | 0.64 | 0.43 | 0.43 | 0.49 | 0.50 | 0.48 | 0.45 | 0.45 | 0.51 | 0.49 | 0.37 | 0.51 | 0.44 | 0.34 | 0.36 |
| **Ni** | 0.56 | 0.41 | 0.40 | 0.43 | 0.46 | 0.45 | 0.45 | 0.41 | 0.43 | 0.46 | 0.42 | 0.43 | 0.45 | 0.40 | 0.40 |
| **Rb** | 0.91 | 1.01 | 0.93 | 0.89 | 0.79 | 0.81 | 0.72 | 0.93 | 0.75 | 0.84 | 0.86 | 0.74 | 0.71 | 0.88 | 0.83 |
| **Sr** | 0.30 | 0.46 | 0.44 | 0.31 | 0.28 | 0.25 | 0.24 | 0.34 | 0.29 | 0.27 | 0.25 | 0.23 | 0.27 | 0.27 | 0.49 |
| **Y** | 0.62 | 0.62 | 0.63 | 0.69 | 0.75 | 0.62 | 0.60 | 0.62 | 0.71 | 0.61 | 0.50 | 0.78 | 0.79 | 0.59 | 0.62 |
| **Zr** | 0.52 | 0.30 | 0.28 | 0.34 | 0.38 | 0.31 | 0.28 | 0.28 | 0.38 | 0.29 | 0.23 | 0.28 | 0.32 | 0.25 | 0.28 |
| **Nb** | 0.76 | 0.83 | 0.87 | 0.88 | 0.94 | 0.84 | 0.79 | 0.94 | 0.95 | 0.81 | 0.79 | 0.80 | 0.86 | 0.84 | 0.95 |
| **Ba** | 0.50 | 0.52 | 0.54 | 0.54 | 0.46 | 0.35 | 0.35 | 0.55 | 0.44 | 0.37 | 0.34 | 0.31 | 0.36 | 0.39 | 0.45 |
| **La** | 0.59 | 0.62 | 0.71 | 0.69 | 0.78 | 0.65 | 0.63 | 0.66 | 0.70 | 0.62 | 0.59 | 0.74 | 0.79 | 0.64 | 0.69 |
| **Ce** | 0.61 | 0.62 | 0.65 | 0.67 | 0.75 | 0.64 | 0.60 | 0.66 | 0.70 | 0.62 | 0.59 | 0.73 | 0.80 | 0.61 | 0.71 |
| **Nd** | 0.57 | 0.66 | 0.72 | 0.72 | 0.78 | 0.66 | 0.63 | 0.66 | 0.72 | 0.63 | 0.59 | 0.78 | 0.83 | 0.66 | 0.72 |
| **Sm** | 0.57 | 0.69 | 0.88 | 0.85 | 0.86 | 0.77 | 0.75 | 0.86 | 0.89 | 0.72 | 0.67 | 0.93 | 1.03 | 0.80 | 0.90 |
| **Eu** | 0.53 | 0.82 | 0.85 | 0.81 | 0.77 | 0.71 | 0.64 | 0.81 | 0.71 | 0.70 | 0.63 | 0.93 | 1.07 | 0.73 | 0.81 |
| **Gd** | 0.56 | 0.82 | 0.82 | 0.91 | 0.92 | 0.78 | 0.77 | 0.82 | 0.88 | 0.70 | 0.72 | 0.92 | 1.03 | 0.79 | 0.83 |
| **Dy** | 0.54 | 0.63 | 0.56 | 0.66 | 0.70 | 0.59 | 0.56 | 0.58 | 0.69 | 0.58 | 0.51 | 0.71 | 0.75 | 0.58 | 0.62 |
| **Er** | 0.60 | 0.49 | 0.51 | 0.48 | 0.55 | 0.50 | 0.32 | 0.43 | 0.50 | 0.57 | 0.48 | 0.66 | 0.76 | 0.35 | 0.41 |
| **Yb** | 0.69 | 0.58 | 0.57 | 0.67 | 0.71 | 0.58 | 0.58 | 0.58 | 0.70 | 0.59 | 0.47 | 0.71 | 0.76 | 0.57 | 0.61 |
| **Th** | 0.67 | 0.57 | 0.61 | 0.62 | 0.68 | 0.62 | 0.62 | 0.57 | 0.66 | 0.59 | 0.55 | 0.67 | 0.71 | 0.58 | 0.63 |

Table C-2: Enrichment factors of the trace elements in post-Archean average shale (Taylor & McLennan, 1985) and sediment samples from Arcachon Bay and the Gironde Estuary (this study). Values are calculated from the major element concentrations listed in Table III-6, using Equation C-2.

| | River Water | Sea Water | G1-SW-C | G2-SW-C | G3-SW-C | G4-SW-C | G6-SW-C | A1-SW-C | A2-SW-C | A3-SW-C | A4-SW-C |
|---|---|---|---|---|---|---|---|---|---|---|---|
| **Si** | 17.02 | 458.16 | - | - | - | - | - | - | - | - | - |
| **Ti** | 0.51 | 10.18 | 0.31 | 0.92 | 0.20 | 0.15 | 0.26 | 0.47 | 0.27 | 0.16 | 0.39 |
| **Fe** | 1.48 | 0.14 | 2.68 | 2.31 | 5.04 | 6.24 | 3.35 | 7.05 | 2.04 | 8.91 | 5.98 |
| **Mn** | 7.37 | 19.73 | 7.55 | 3.09 | 16.00 | 30.83 | 7.20 | 2.98 | 7.41 | 10.71 | 3.59 |
| **Mg** | 90.06 | 1771015.53 | 1260.59 | 0.81 | 135.28 | 182.27 | 2932.00 | 845.36 | 33189.55 | 2536.27 | 47713.35 |
| **Ca** | 476.51 | 819997.40 | 679.88 | 18.33 | 105.79 | 194.16 | 1625.70 | 430.74 | 16822.90 | 378.19 | 24139.18 |
| **Na** | 131.19 | 14056260.89 | 13142.94 | 109.87 | 1411.36 | 1219.50 | 28586.36 | 7787.37 | 325824.72 | - | 434934.08 |
| **K** | 161.31 | 1748985.75 | 1480.29 | 7.06 | 153.40 | 228.73 | 3368.70 | 965.00 | 37027.20 | - | 54438.55 |
| **P** | 141.38 | 31369.15 | 70.81 | 13.19 | 77.88 | 126.24 | 208.85 | 51.27 | 1444.98 | 968.86 | 1599.49 |

Table C-3: Enrichment factors of the major elements in typical river water (Li, 1982; Martin *et al.*, 1976, as found in Taylor & McLennan, 1985), sea water (Broecker & Peng, 1982; Li, 1982, as found in Taylor & McLennan, 1985), and surface water samples from Arcachon Bay and the Gironde Estuary (this study). Values are calculated from the major element concentrations listed in Table III-5, using Equation C-2.

| | River Water | Sea Water | G1-SW-C | G2-SW-C | G3-SW-C | G4-SW-C | G5-SW-C | G6-SW-C | A1-SW-C | A2-SW-C | A3-SW-C | A4-SW-C |
|---|---|---|---|---|---|---|---|---|---|---|---|---|
| **Li** | 82.87 | 293511.56 | 466.96 | 2.89 | 33.13 | 51.28 | 273.04 | 1095.41 | 441.99 | 13416.39 | 646.21 | 28706.29 |
| **Sc** | 0.19 | 1.98 | 1.02 | 0.71 | 0.70 | 0.71 | 1.42 | 1.24 | 0.52 | 10.57 | 8.02 | 22.28 |
| **V** | 6.15 | 512.62 | 2.85 | 0.95 | 2.75 | 3.25 | 32.30 | 3.13 | 6.33 | 44.89 | 4.63 | 29.73 |
| **Cr** | 7.21 | 90.08 | 1.32 | 0.75 | 1.32 | 1.37 | 15.48 | 2.79 | 1.81 | 10.74 | 18.85 | 18.86 |
| **Co** | 3.83 | 4.79 | 1.76 | 1.42 | 4.87 | 5.77 | 7.51 | 2.68 | 2.04 | 20.19 | 5.84 | 6.40 |
| **Ni** | 4.23 | 440.82 | 4.54 | 0.92 | 2.44 | 3.77 | 86.35 | 9.38 | 3.62 | 72.09 | 136.77 | 132.98 |
| **Cu** | 165.75 | 443.97 | 15.40 | 1.36 | 8.09 | 14.12 | 107.82 | 12.79 | 5.59 | 95.48 | 75.67 | 85.87 |
| **Zn** | 197.91 | 247.38 | 9.84 | 3.96 | 31.37 | 38.27 | 331.24 | 12.72 | 10.34 | 5300.08 | 110.02 | 108.11 |
| **As** | 276.25 | 14675.58 | 38.69 | 14.46 | 37.79 | 80.50 | 957.03 | 72.30 | 50.65 | 498.47 | 125.78 | 597.80 |
| **Se** | 441.99 | 59853.34 | 10963.26 | 845.18 | 3677.39 | 6009.09 | 312502.37 | 18322.44 | 5434.32 | 227864.11 | 538429.51 | 328959.36 |
| **Rb** | 7.89 | 59195.61 | 66.64 | 1.42 | 5.65 | 8.89 | 35.59 | 137.37 | 56.45 | 1715.58 | 178.97 | 2992.27 |
| **Sr** | 145.03 | 984127.01 | 1256.79 | 1.67 | 86.83 | 132.61 | 726.05 | 2662.48 | 980.13 | 32363.31 | 1462.59 | 58121.74 |
| **Y** | 1.26 | 13.81 | 1.32 | 1.13 | 7.44 | 9.80 | 5.25 | 3.27 | 2.87 | 10.28 | 13.32 | 16.05 |
| **Zr** | - | 6.44 | 0.11 | 0.07 | 0.05 | 0.09 | 1.04 | 0.19 | 0.03 | 0.71 | 1.55 | 1.01 |
| **Mo** | 361.63 | 414369.27 | 2610.47 | 3.91 | 173.84 | 226.65 | 5957.25 | 5998.59 | 3009.35 | 83082.13 | 2567.29 | 178695.30 |
| **Cd** | 73.67 | 36832.82 | 114.91 | 4.93 | 45.85 | 114.75 | 422.66 | 201.46 | 43.04 | 658.58 | 1017.29 | 1390.64 |
| **Ba** | 21.11 | 923.75 | 1.72 | 0.25 | 0.76 | 1.69 | 13.86 | 5.47 | 0.50 | 17.15 | 57.33 | 25.50 |
| **La** | 1.03 | 6.02 | 0.66 | 0.86 | 4.74 | 5.90 | 1.76 | 1.87 | 1.57 | 2.83 | 4.41 | 3.83 |
| **Ce** | 0.83 | 2.30 | 0.63 | 0.96 | 5.26 | 6.50 | 1.08 | 1.94 | 1.81 | 1.52 | 2.91 | 1.46 |
| **Pr** | 0.68 | 5.84 | 0.93 | 0.99 | 5.29 | 7.12 | 6.56 | 2.58 | 2.02 | 8.27 | 12.75 | 13.49 |
| **Nd** | 0.93 | 6.45 | 0.72 | 1.00 | 5.91 | 7.54 | 2.06 | 1.99 | 1.94 | 1.56 | 5.55 | 3.19 |
| **Sm** | 1.10 | 7.05 | 3.62 | 1.46 | 8.07 | 11.27 | 61.58 | 10.12 | 4.11 | 60.72 | 113.33 | 138.47 |
| **Eu** | 0.99 | 6.22 | 3.79 | 2.83 | 16.41 | 21.51 | 56.64 | 11.69 | 6.59 | 52.25 | 112.59 | 98.50 |
| **Gd** | 1.41 | 10.36 | 1.20 | 1.54 | 9.68 | 12.19 | 9.76 | 3.51 | 2.82 | 4.69 | 11.93 | 9.49 |
| **Tb** | 1.14 | 10.06 | 9.82 | 1.76 | 9.22 | 14.56 | 172.09 | 26.14 | 10.00 | 254.98 | 364.10 | 502.68 |
| **Dy** | 1.22 | 11.69 | 2.91 | 1.13 | 7.17 | 9.76 | 36.57 | 7.47 | 3.61 | 58.89 | 69.15 | 101.39 |
| **Ho** | 1.12 | 13.98 | 9.69 | 1.50 | 7.62 | 13.27 | 209.69 | 25.96 | 7.60 | 205.74 | 385.37 | 446.61 |
| **Er** | 1.21 | 16.57 | 1.74 | 0.95 | 5.39 | 7.81 | 30.29 | 4.93 | 2.42 | 32.46 | 67.95 | 69.88 |
| **Tm** | 1.35 | 17.96 | 0.96 | 0.89 | 5.45 | 7.33 | 10.86 | 2.60 | 1.79 | 10.53 | 30.54 | 22.40 |
| **Yb** | 1.22 | 19.03 | 0.63 | 0.73 | 4.70 | 5.83 | 4.13 | 1.61 | 1.37 | 2.83 | 11.27 | 4.67 |
| **Lu** | 1.37 | 18.71 | 1.01 | 0.71 | 4.48 | 5.52 | 14.96 | 2.80 | 1.63 | 11.28 | 30.73 | 28.42 |
| **Hf** | - | 54.73 | 0.11 | 0.07 | 0.09 | 0.14 | 1.39 | 0.19 | 0.05 | 1.62 | 2.42 | 2.86 |
| **Re** | - | 837109.63 | 3226.96 | 188.62 | 1214.96 | 775.57 | 78962.35 | 917.97 | 4951.24 | 0.00 | 47893.00 | 98724.38 |
| **Pb** | 39.00 | 4.87 | 2.46 | 4.02 | 22.58 | 26.39 | 11.78 | 6.61 | 8.90 | 14.22 | 17.70 | 8.92 |
| **Th** | 6.31 | 0.24 | 0.48 | 0.28 | 0.67 | 0.74 | 0.21 | 0.42 | 0.16 | 0.39 | 1.51 | 0.45 |
| **U** | 9.82 | 47575.73 | 32.37 | 0.81 | 4.96 | 9.47 | 244.85 | 78.20 | 24.24 | 789.69 | 15.84 | 1399.76 |

Table C-4: Enrichment factors of the trace elements in typical river water (Li, 1982; Martin *et al.*, 1976, as found in Taylor & McLennan, 1985), sea water (Broecker & Peng, 1982; Li, 1982, as found in Taylor & McLennan, 1985), and surface water samples from Arcachon Bay and the Gironde Estuary (this study). Values are calculated from the major element concentrations listed in Table III-7, using Equation C-2.